

Dynamic behaviour of a
propulsion plant and its
controller
with Hardware In the Loop
R.J. Roberti

Technische Universiteit Delft

Dynamic behaviour of a propulsion plant and its controller with Hardware In the Loop

by

R.J. Roberti

to obtain the degree of Master of Science in Maritime Technology
at the Delft University of Technology,
to be defended publicly on Thursday September 23, 2021 at 14:00.

Student number: 4281543
Project number: SDPO.21.026.m
Project duration: November 9, 2020 – September 23, 2021
Thesis committee: Rear-Admiral (ME) ret. ir. K. Visser, TU Delft, Chairman
Prof. dr. ir. T.J.C. van Terwisga, TU Delft
Cdr (ME) dr. ir. R.D. Geertsma, TU Delft, Supervisor
Dr. ir. S.P. Mulders, TU Delft,
Lt Cdr (ME) ir. J.W. Reurings, Defence Materiel Organisation

An electronic version of this thesis is available at <http://repository.tudelft.nl/>.

The photo on the cover is taken by the author near Somalia. HNLMS Tromp is sailing towards a tanker to replenish oil at sea. This air defence and command frigate has a combined diesel and gas (CODAG) with a controllable pitch propeller. Therefore, the control system studied in this thesis can be implemented on this ship.

Summary

Everything should be made as simple as possible, but not simpler.

Albert Einstein

Due to legislation, the shipping industry is forced to reduce its emissions and underwater radiated noise in order to decrease the impact on the environment and limit global warming. Moreover, do Navy ships have another motivation to reduce their noise. When there is a submarine or mine threat, it can be lifesaving to be as quiet as possible. To operate in these circumstances, a navy frigate wants to be flexible due to its complex operational profile. A propulsion plant that can contribute to flexibility is a diesel engine with a controllable pitch propeller (CPP).

A way to reduce emissions and noise is by improving the control strategy of the propulsion plant. Often a strategy is tested with numerical models. However, these models often do not include all the hydrodynamic effects that can occur. With Hardware In the Loop (HIL), a part of the model is replaced by a hardware element. In this thesis, this is the CPP. However, this model is scaled and is therefore introducing scaling effects. A feasibility study is performed to determine whether it is possible to perform open water HIL experiments and determine the dynamic behaviour of a propulsion plant and its controller. It is also studied if the results of a HIL experiment can be used to improve numerical models.

The control strategy that is used is Adaptive Pitch Control (APC). This control system requires no fixed rotational speed and pitch of the propeller. But based on the required virtual shaft speed, the inflow of the CPP, speed and charge pressure of the diesel engine and the actual propeller pitch the required pitch and rotational speed are determined.

APC can deliver the requested virtual shaft speed, prevent cavitation, minimise fuel consumption, maintain engine air excess ratio and prevent under- and overspeed. Cavitation is prevented by maintaining the optimal inflow in the CPP. However, in waves, this inflow is constantly fluctuating, and as a result, the pitch is also continuously changing. Current actuation systems of CPP's are not able to keep up with this constantly adjusting pitch setting. Moreover, high-frequency pitch actuation can lead to increased wear of the propeller hub. Thus, class regulations require an overhaul of a CPP system designed for regular use after 10^7 pitch actuations. Therefore, the last objective of this thesis is to determine whether it is possible to reduce the pitch actuations and determine how that influences the dynamic performance of the propulsion plant.

Full-scale simulations of an Ocean-going Patrol Vessel (OPV) with APC showed that implementing a tuned Kalman filter for the inflow estimation with a deadband can reduce the pitch actuations. Simulations are performed with regular and irregular waves. In regular waves, it is possible to achieve zero actuations during constant speed. However, in irregular waves, there are some actuations at a constant speed because bigger waves are encountered after a certain amount of time. An actuation reduction of 92 per cent can be achieved at sea state four and 60 per cent at sea state five. Reducing the pitch actuations has no significant effects on the control objectives of APC. However, due to slower pitch settings, irregular waves at sea state four and five the propeller operates approximately 25 per cent extra time outside the cavitation bucket.

As mentioned before, an objective is to determine whether it is possible to simulate the dynamic behaviour with the scaled open water HIL setup. By implementing Froude scaling, it is assumed that comparing full and model scale results is valid. Therefore, the in and output to the hardware CPP are Froude scaled. However, in the controller, Froude time scaling must be applied in the integral gain, torque limiters and Kalman uncertainties. Also, the delays of the pitch actuation, fuel rack and exhaust filling are time scaled. Finally, the thrust and torque coefficients are scaled to compensate for drag differences. It is shown that with the correct scaling, it is possible to compare the similarities in full free sailing and model scale HIL simulations. The difference in the measured parameters are minor. Thus, the dynamic behaviour in both simulations is similar.

The similarity between the full and model scale simulations is desired. It shows that it is possible to simulate the dynamics of a propulsion plant with the open water HIL setup at constant speed. In other research, an open water HIL setup is used to study the effects of propeller ventilation. However, other scaling effects

due likely occur even when Froude scaling is applied. For example, in model scale, it can be assumed that air is incompressible, while in full-scale, this is not true. To prove the added value of HIL in ventilation requires, therefore, more research. Nevertheless, it is possible to force an oblique inflow in the propeller with the open water HIL setup. It is expected that APC can provide a steady angle of attack during a turn. With the HIL setup it is possible to assess this in a controlled environment. The results can provide extra information to improve numerical models and control strategies.

However, the propeller open water HIL setup at the TU Delft is currently unsuitable for testing novel control strategies. The high backlash in the CPP blades and the low sample rate of the pitch makes it impossible to test novel control strategies and simulate realistic dynamic behaviour properly. Also, due to Froude dissimilarity in the acceleration speed of the towing car, it is not possible to perform dynamic acceleration runs with the HIL setup. These issues need to be solved before conducting HIL experiments with novel control strategies.

This research proposed to add a Kalman filter and deadband to the APC strategy to reduce pitch actuations. A trade-off is that the propeller cavitates 25 per cent more. However, the other control objectives of the dynamic performance of the propulsion plant are hardly influenced. By correctly implementing scale effects, it is possible to study the dynamic behaviour of the plant with the open water HIL setup. Still, in waves, HIL experiments are expected to provide little extra information compared to numerical models. Nevertheless, oblique inflow can be forced in controlled conditions and give new insights to improve numerical models and control strategies, thus investigating the behaviour in turns. These improvements can lead to emission and noise reduction to decrease the environmental impact and prevent detection of naval vessels under threat.

Samenvatting

De scheepvaart moet zijn uitstoot en onderwater geluid reduceren door nieuwe regelgeving. Het doel is om de klimaatverandering tegen te gaan. Bovendien hebben marineschepen nog een andere motivatie om het onderwatergeluid te reduceren. Het kan namelijk van levensbelang zijn in het geval van onderzeeboot of mijnen dreiging. Fregatten moeten complexe taken uitvoeren. Een voortstuwingsrelin die daar bij uitstek geschikt voor is, is een voortstuwingsdiesel met een verstelbare schroef.

Om emissies en geluid van de voortstuwingsrelin te reduceren kan de regeltechniek aangepast worden. Vaak wordt een nieuwe regelmethode getest met numerieke modellen, echter, deze modellen hebben hun beperkingen. Vaak zijn hydrodynamische effect versimpeld. Met "Hardware In the Loop" (HIL) is het mogelijk om een onderdeel uit het model te vervangen door een fysiek component. In dit onderzoek is de verstelbare schroef dit component en die neemt de hydrodynamische effecten mee. Maar een kleine schroef zorgt voor schaal effecten. Om deze reden is er een haalbaarheidsstudie gedaan om te bepalen of het mogelijk is om met een open water HIL-opstelling het dynamisch gedrag van de voortstuwingsrelin en de regelstrategie te bepalen. Het uiteindelijke doel is om te bepalen of HIL-experimenten kunnen bijdragen aan het verbeteren van numerieke modellen en regelstrategieën.

Het regelsysteem dat gebruikt wordt in dit onderzoek is de adaptieve schroefspoed regeling. In tegenstelling tot een traditioneel regelsysteem, heeft de regeling geen vaste draaisnelheid en pitch van de schroef bij een vaartinstelling. Maar op basis de aanstroom hoek, huidige spoed en draaisnelheid van de schroef en turbo druk wordt bepaald wat de gewenste draaisnelheid en spoed moet worden.

De adaptieve schroefspoed regeling kan de gewenste vaartinstelling leveren, cavitatie voorkomen, brandstof verbruik verminderen, luchtvermaat boven een gestelde grens te houden, en voorkomt dat de motor te snel of te langzaam gaat draaien. Omdat de regeling de aanstroom-hoek van de schroef constant wil houden, zal de spoedhoek continue aangepast worden als het schip in golven vaart. Huidige verstelbare spoed installaties (VSI) zijn niet in staat om met de juiste snelheid de spoed aan te passen. Daarnaast zorgen vele spoedverstellingen voor slijtage, om die reden geven klasse bureaus aan dat na een bepaalde hoeveelheid spoedhoek veranderingen de schroef overhaalt moet worden. Daarom wordt in deze studie onderzocht of het mogelijk is om het aantal spoed veranderingen te reduceren en te bepalen wat het effect op het dynamisch gedrag van de voortstuwingsrelin is.

Simulaties op ware grote met een patrouilleschip met adaptieve schroefspoed regeling hebben laten zien dat het implementeren van een Kalman filter met een dode band het aantal spoekhoek bewegingen kan verminderen. In regelmatige golven op constante snelheid zijn de spoed veranderingen te reduceren tot nul. Met onregelmatige golven komt het schip incidenteel een grotere golf tegen, als gevolg hiervan wordt dan wel de spoed veranderd. Desondanks is een reductie van 92 procent in sea state vier gerealiseerd en van 60 procent in sea state vijf. Het verminderen van de spoed bewegingen zorgt voor iets meer cavitatie, maar de overige parameters voor dynamisch gedrag worden nauwelijks aangetast. Door het filter zal de propeller ongeveer 25 procent tijd extra buiten de cavitatie bucket opereren.

Om te bepalen of het mogelijk om met de open water HIL-opstelling het dynamisch gedrag te simuleren wordt Froude schaling toegepast. De in- en uitvoer naar de schroef wordt geschaald. Maar ook de integraal constante van de snelheidsregeling, de koppel beperking, Kalman constanten, tijdconstanten van de spoed, vulsnelheid van de uitlaat en brandstofinspuiting. Ten slotte, zijn ook de koppel en stuwkracht coëfficiënten geschaald om het verschil in wrijving te compenseren. Na het juist toepassen van de schaling hebben simulaties laten zien dat het dynamisch gedrag op ware grote en op model schaal zeer goed overeenkomen op constante snelheid.

Deze overeenkomst is noodzakelijk om te HIL-opstelling te gebruiken voor verder onderzoek. Een dergelijke opstelling is gebruikt in andere studies om ventilatie effecten op de propeller te onderzoeken. Maar bij propeller ventilatie op model schaal kan aangenomen worden dat lucht onsamendrukbaar is, terwijl dit op ware grote niet het geval is. Het gevolg is dat er andere schalingeffecten kunnen plaats vinden die niet opgelost worden door het toepassen van Froude schaling. Maar een schuine instroom in de schroef kan wel onderzocht worden met de opstelling. Hiermee kan gesimuleerd worden dat een schip een bocht maakt. Het is te verwachten dat de adaptieve spoedhoek regeling in staat is om de instroomhoek constant te houden

tijdens een bocht. Het is mogelijk om deze stelling te verifiëren met een HIL-experiment. Resultaten van een dergelijk experimenten kunnen wel gebruikt worden om numerieke modellen te verbeteren.

De open water HIL-opstelling van de TU delft is op dit moment nog niet geschikt om dergelijke experimenten mee uit te voeren. De speling in de schroeven is te groot en de bemonsteringsfrequentie voor het uitlezen van de pitch te laag. Het is hierdoor niet mogelijk om moderne regelsystemen te testen en realistisch dynamisch gedrag te simuleren. Daarnaast is het door Froude ongelijkheid van de versnelling van de sleepwagen niet mogelijk om dynamische versnelling runs uit te voeren.

Samengevat is er een Kalman filter met dode band toegevoegd aan de adaptieve schroefspoed regeling. Dit heeft als effect dat de spoed veranderingen gereduceerd worden. Echter gaat de schroef wel meer caviteren. Daarnaast is geconstateerd dat met het correct toepassen van Froude schaling het mogelijk is om met de open water HIL-opstelling het dynamisch gedrag van een voorstuwingstrein te simuleren. Echter, extra informatie ten opzichte van numerieke modellen wordt hier niet door verkregen in regelmatige en onregelmatige golven. Mogelijk kan er wel extra informatie worden verkregen door een schuine instroom op de schroef te forceren. Deze metingen kunnen mogelijk gebruikt worden om numerieke modellen en regelstrategieën te verbeteren. Hiermee kunnen emissies en geluid gereduceerd worden en wordt ook voorkomen dat marine fregatten eerder gedetecteerd worden.

Preface

My academic growth began in 2006 when I started with my bachelor at the Royal Netherlands Naval College. After completion in 2010, my operational adventure started on HNLMS Amsterdam and HNLMS Tromp. After almost ten years of working, in 2019, the navy allowed me to continue my academic growth and follow the master of Maritime Technology at the Delft University of Technology. The transition from an operational life to an academic life did not come naturally. Coming up to speed on the desired math, writing, and academic thinking level took a few months. Nevertheless, I can say that I have enjoyed the last two years and learned a lot.

The final stage of the master is this thesis. I am grateful that it was possible to study a subject that is useful for the Defence Material Organisation. It is good to see that academic work can contribute to an operational navy ship. However, it was not possible to do this research without the assistance of talented and helpful people. I want to start to thank Rinze Geertsma. The time you have spent on feedback and critical questions is highly appreciated. My gratitude also goes to Jeroen Reurings, whom I could always call if I had struggles. I would also like to express my thanks to Lode Huijgens. At the start of my research, he helped me to understand the Hardware In the Loop setup. And even though he started a new career in Norway, he found the time to provide me with answers to several questions.

The initial plan was to perform HIL experiments in the towing tank. Frits Sterk and Pascal Taudin put much effort into improving the setup. I can't thank you enough for your creative help, and I sincerely hope that the setup can be used soon. There are more people I want to express my gratitude to. Will van Geest and Peter Valk for their assistance in programming. Peter Poot and Jennifer Rodrigues Monteiro preparing the towing tank. And finally, Michail Drakoulas for a very inspiring discussion.

I am looking forward to sailing on board HNLMS De Zeven Provinciën after graduation to enlarge my operational experience. This adventure will be combined with my academic experience to improve ship design in the near future.

Ronald Roberti
Sneek, 8 September 2021

Contents

Summary	iii
Samenvatting	v
Preface	vii
1 Introduction	1
1.1 Literature review	1
1.2 Research objective and questions	2
1.3 Aim and contribution	4
1.4 Thesis outline	5
2 Methodology	7
2.1 Proposed approach	7
2.2 Adaptive pitch control	9
2.2.1 Inflow estimation	10
2.2.2 Kalman filter	11
2.3 HIL setup	12
2.3.1 Physical description	13
2.3.2 Numerical model	14
2.4 Summary	15
3 Free Sailing Simulation Results	17
3.1 Kalman filter	18
3.1.1 Dependency uncertainties with sea state	22
3.2 Deadband	24
3.3 Kalman filter and deadband	26
3.4 Gain scheduling	29
3.5 Irregular waves	31
3.6 Summary	33
4 Open water HIL setup simulation results	35
4.1 Towing tank and full-scale simulations	35
4.2 Preparation of HIL experiments	39
4.2.1 Dynamic acceleration comparison	39
4.2.2 Hardware CPP	40
4.2.3 Discussion	42
4.3 Summary	42
5 Conclusions and recommendations	45
5.1 Answer to research questions	45
5.2 Additional conclusions	46
5.3 Recommendations	46
5.3.1 Regarding the HIL setup	46
5.3.2 APC with Kalman filter and deadband	47
5.3.3 Improving numerical models and control strategies	47
5.4 Closing summary	47

A	Theoretical background	49
A.1	Scale effects	49
A.2	Adaptive Pitch Control Strategy	53
A.3	Diesel Engine	57
A.4	Propeller model	60
A.5	Matching	61
A.6	Irregular wave model	62
B	Manual HIL setup	65
C	Paper	79
	References	91
	Nomenclature	93
	List of Figures	95
	List of Tables	97

1

Introduction

A man without a goal is like a ship without a rudder

Thomas Carlyle

The shipping industry is obliged to reduce their emission and radiated noise in order to decrease the impact on the environment and limit global warming (IMO [2020]). Moreover, do navy ships have another motivation to reduce their noise. During a submarine or mine threat it can be lifesaving to be quiet. One way of improving fuel consumption and noise is with novel control strategies. These strategies aim to achieve the best effective inflow of the propeller. The control strategy that is studied is the novel adaptive pitch control that regulates the effective angle of attack.

1.1. Literature review

A method to determine the dynamic behaviour of a diesel engine with a CPP is with numerical models. This can be relatively simple with a transfer function; however, these models often do not consider dynamics (Vrijdag [2009], Huijgens [2021]). On the other hand, a Mean Value First Principle (MVFP) model does take these into account and is, therefore, suitable to determine the dynamic behaviour of a propulsion plant (Schulten [2005], Geertsma [2019]).

A downside of numerical models is that hydrodynamic effects, such as ventilation and free surface effects, are often simplified (White [2008], Niklas and Pruszko [2019], Kozłowska et al. [2020]). However, in a towing tank, these effects can be taken into account with scaling effects (Journee and Massie [2001]). It is assumed that keeping the Froude number the same for the model and full-scale ship, it is possible to increase the results of the model to full scale, i.e. the forces can directly be scaled between the model and the full-scale ship. Nevertheless, building a scaled diesel engine with the same dynamic behaviour as a full-scale diesel is impossible.

Full-scale trials do not have scale effects; however, they are time-consuming and complex to organize. Also, it is hard to compare results due to changing environmental conditions (van Terwisga et al. [2004], Vrijdag [2009]). However, the main advantage of full-scale trials is that all the simulation uncertainties are eliminated, and the effect of a novel control strategy can be determined with more certainty.

Hardware in The Loop (HIL) can combine the hydrodynamics in the towing tank and engine behaviour of a numerical model. In a HIL setup, a software model is replaced by a hardware component. In this study, a hardware CPP is used. Huijgens [2021] demonstrated that it is possible to study propulsion plant behaviour with the open water HIL setup and linear propulsion model. Therefore, the present study has implemented a validated non-linear MVFP diesel engine model with turbocharger dynamics and adaptive pitch control strategy.

The foundation of APC has been researched by Vrijdag [2009]. He concluded that effective angle of attack control reduces cavitation. A thrust sensor on the shaft is used to determine the effective angle of attack. However, the focus of this study was not on the behaviour of the diesel engine. Therefore, Geertsma [2019] filled this gap by studying the dynamic behaviour of the engine. Also, an improvement in the control system

was implemented by adding slow integrating speed control. Moreover, he assumed that the angle of attack was known, where Vrijdag [2009] demonstrated how this could be established with a thrust sensor. Thus, an improvement would be to measure the thrust to determine the angle of attack and study whether the APC with slow integrating speed control gets the same results. However, a full-scale trial such as Vrijdag [2009] is costly and complex to set up. Hence, Hardware-In-the-Loop could be a solution to combine the previous two studies.

Table 1.1: Most relevant literature

Author	Year	Focus	Finding	Future research
Vrijdag	2009	New controller to reduce cavitation	Effective angle of attack control reduces cavitation	Behaviour diesel engine must be studied further
Geertsma	2019	Adaptive pitch control (APC) with slow integrating speed control	APC improves dynamic behaviour and improves manoeuvrability.	Assumed that the effective inflow is known
Huijgens	2021	Propeller-Engine interaction with Open Water HIL setup	It is possible to use an open water setup with an electric motor to simulate diesel engine-propeller interaction	Nonlinear diesel model for better dynamics and CPP

1.2. Research objective and questions

To be able to better assess novel control strategies of ship propulsion plants, the research objective is:

to improve control strategies of ship propulsion systems and the numerical models to evaluate them in dynamic conditions by using Hardware-In-the-Loop in an open water setup.

The objective of this study is comprehensive. Therefore, a case study is used to demonstrate how HIL can be used to improve control strategies and numerical models. The propulsion system in this case study is a diesel engine with a turbocharger and CPP of an Ocean-going Patrol Vessel (OPV) of the Dutch Navy. The control strategy that is studied is APC. This strategy actuates the pitch at every wave, resulting in less time between maintenance periods. The case study allows to extract the following sub-objectives from the primary research objective:

- Sub-objective 1: reduce the movements of CPP blades controlled by adaptive pitch control while maintaining the dynamic performance of the propulsion plant.
- Sub-objective 2: implement a dynamic propulsion model and a hardware controllable pitch propeller in the HIL setup.
- Sub-objective 3: determine if numerical models of propulsion systems with CPP and its control strategy can be improved with HIL experiments.

To be able to achieve the objective, the following research question is formulated:

How can Hardware-In-the-Loop experiments improve control strategies of ship propulsion systems and the numerical models?

The sub-questions that have been formulated to answer the main question are also focussed on the case study:

- Sub-question 1: How can adaptive pitch control be improved by reducing pitch actuations while maintaining its performance?
- Sub-question 2: How can a full-scale diesel engine model with turbocharger dynamics and a model scale hardware controllable pitch propeller be implemented in an open water HIL setup?

- Sub-question 3: How can the results of HIL experiments be used to improve numerical models of a ships propulsion system and its control strategy?

Sub-question one is answered with simulations of a full-scale model of an OPV. The answer for sub-question two is given with simulations of the open water HIL setup. The final answer combines both simulation results, followed by a discussion. The methodology is further elaborated in chapter 2.

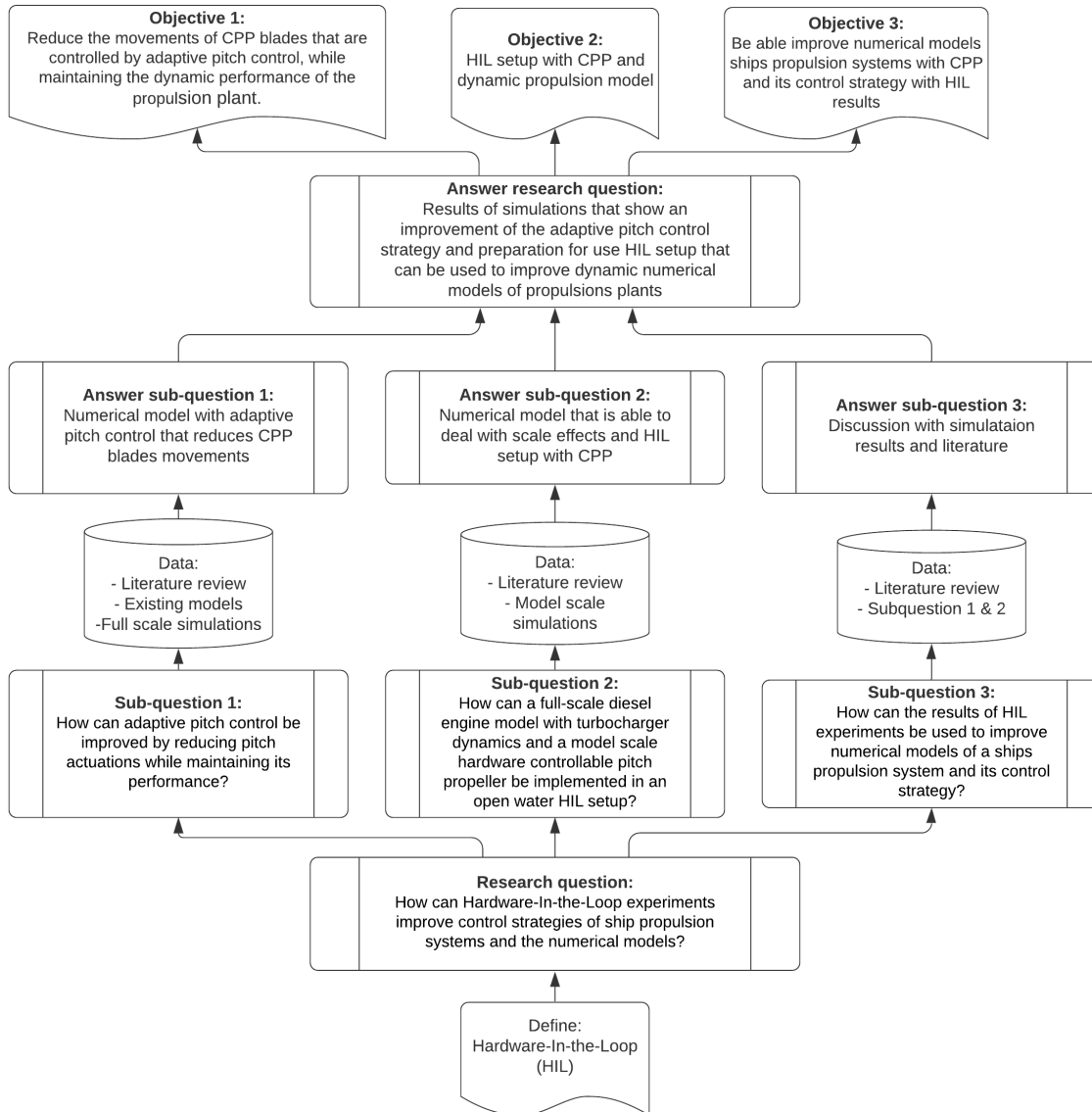


Figure 1.1: Structure master thesis

1.3. Aim and contribution

APC with slow integrating speed control continuously changes the pitch settings in waves to achieve the desired flow inflow. Geertsma [2019] showed that this would result in less cavitation and fuel consumption. However, high-frequency pitch actuation can lead to increased wear of the propeller hub. Thus, class regulations require an overhaul of a CPP system designed for regular use after 10^7 pitch actuations (DNV). A control strategy that results in more actuations reduces the lifetime of the CPP and results in more maintenance.

Another reason to reduce propeller blade movements is that current pitch actuation is too slow to follow wake speed fluctuations (Vrijdag et al. [2010], Geertsma [2019]). This could be solved by faster actuations mechanisms. However, this would increase the number of movements instead of reducing it. So instead of increasing the speed of the actuations, it is worthwhile to study the effects of reducing movements and studying the effects on the performance of the propulsion plant.

The foundation for this master thesis are three studies by Vrijdag [2009], Geertsma [2019] and Huijgens [2021]. First, Vrijdag studied the effective angle of attack control and concluded that this significantly reduced cavitation. Second, Geertsma added a slow integrating speed control for diesel engine fuel injection. In the former, the thrust and rotational speed were measured to determine the inflow. However, the inflow was extracted from the propeller model in the latter. Third, Huijgens studied if it is possible to simulate diesel engine behaviour with an open water HIL setup where a fixed-pitch propeller is driven by a permanent magnet synchronous motor (PMSM). By adding a virtual flywheel and friction torque compensation, the PMSM can behave like a diesel engine.

The contribution of this study is threefold: First, the three earlier mentioned dissertations are combined, making it possible to simulate a diesel engine with turbocharger dynamics and CPP in the open water HIL setup. The added value is to determine whether it is possible to study a novel control strategy based on the angle of attack estimation with scale effects in the HIL setup. HIL experiments could be used to improve numerical models; however, they could also reduce time in full-scale trials. Secondly, a Kalman filter with deadband is implemented in the adaptive pitch control strategy to reduce pitch actuations. The effects of this filter on the performance are studied. The added value is that reduction in actuations can increase the time between maintenance. Finally, the performance of APC with Kalman filter and deadband is studied in irregular waves. Currently, APC is only simulated in regular waves. However, in irregular waves, a ship encounters different wave heights and frequencies. This can provide valuable information about the APC in a more realistic simulated environment.

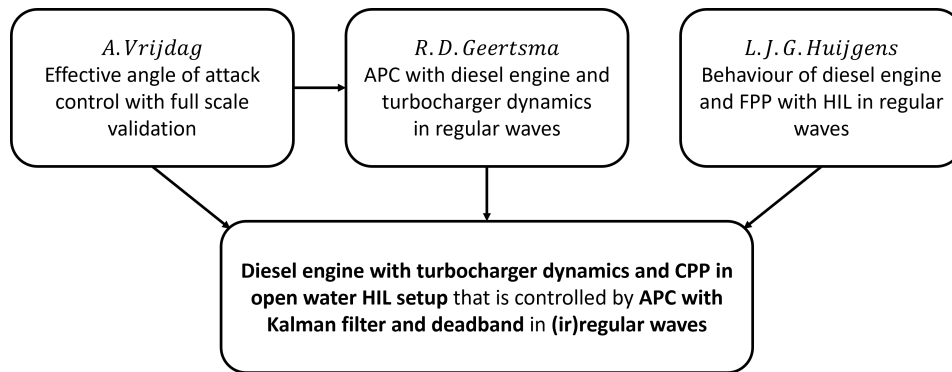


Figure 1.2: Schematic representation of combining three studies

1.4. Thesis outline

This master thesis has five chapters required to answer the three sub-questions and the research question. Chapter 2 elaborates the methodology that is used and a summary of the theoretical background of APC. Additionally, a brief explanation is given of how the inflow of the propeller can be determined with the pitch, rotational speed and thrust measurements of the HIL setup. This inflow estimation is processed with a Kalman filter to reduce the disturbance caused by waves. This filter is also clarified.

With the problem, methodology and theoretical background known, it is possible to elaborate on the full-scale simulations where the pitch actuations are reduced by the Kalman filter. In chapter 3, the dynamic behaviour of the propulsion plant is discussed. First will the altered APC strategy tested regular waves, followed by results in irregular waves.

With the full-scale behaviour known, it is studied if the scaled setup can give the same results in chapter 4. By implementing Froude scaling, it is shown that full and model scale simulations show similar dynamic effects. Finally, the added value of the HIL setup is discussed.

When all the sub-questions are answered, the main research question is answered in chapter 5. Followed by some recommendations in the use of adaptive pitch control. Also, some proposals are given to improve the open water HIL setup allowing to improve studies in novel control strategies.

2

Methodology

He who love practice without theory is like the sailor who board ship without a rudder and compass and never know where he may cast

Leonardo da Vinci

Two methods are used to improve and evaluate the novel adaptive pitch control strategy during dynamic conditions, such as acceleration and sailing in waves. The first model is a full-scale representation of an ocean-going patrol vessel's (OPV) hull and propulsion plant, see figure 2.1. The second is an open water HIL setup that can simulate the behaviour of the propulsion plant with a scaled hardware propeller, see figure 2.2. The models are elaborated, followed by a short description of APC and the HIL setup. Complete explanations are given by Geertsma [2019] and Huijgens [2021].



Figure 2.1: Ocean-going patrol vessel

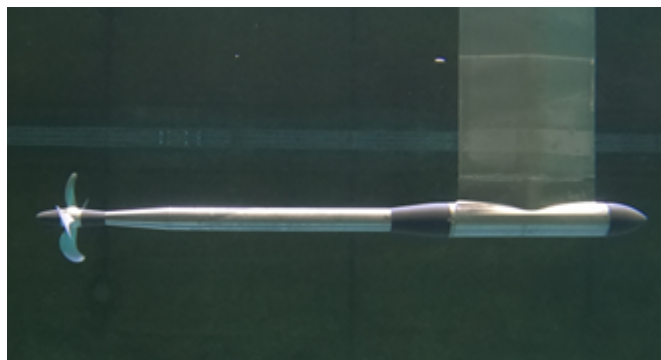


Figure 2.2: HIL setup [Huijgens [2021]]

2.1. Proposed approach

The validated full-scale model is schematically depicted in figure 2.3, it is also used by Geertsma [2019]. However, three changes are implemented. First, the adaptive pitch controller can estimate and filter the flow angle. Second, the wave model can simulate irregular waves and finally, the propeller model is a C4-40 instead of a C5-60. This is done because the hardware CPP of the open water HIL setup is also a C4-40. The propeller is matched to the diesel engine to achieve the best performance of the propulsion plant (see Appendix A.5). Due to the matching process, the gearbox reduction ratio is altered. A few assumptions are taken into account with the model. The first one is the validation of the model still holds with a C4-40 propeller. Secondly, the ship model experiences no pitch angle due to waves. This is valid for moderate seas as long as the propeller stays submerged. So if ventilation occurs, this model is not accurate.

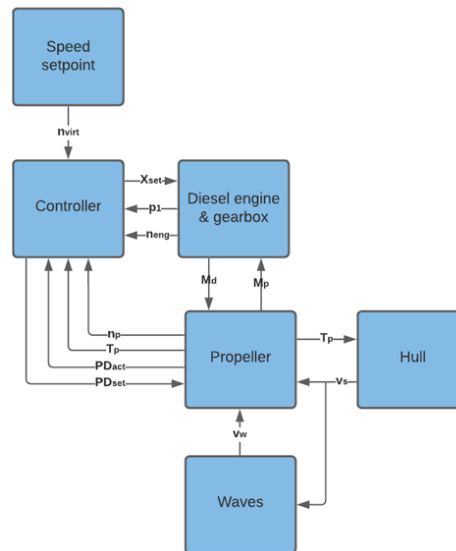


Figure 2.3: Scheme for the MATLAB Simulink model

With full-scale free sailing simulations, the dynamic behaviour of the propulsion plant with the adaptive pitch control with Kalman filter and deadband is studied. This is done by evaluating the pitch actuations and the five measures performance measures used by Geertsma [2019]. It is desirable that the filter and deadband do not have negative influence on the dynamic performance.

The model scale simulations represent the open water HIL setup. It is applied to evaluate the use of the HIL setup to investigate the propulsion plant's dynamic behaviour. The main difference is that the scaling effects of the model basin should be taken into account. But also, the drive that controls the propeller and the towing car are implemented in the model. In figure 2.4, a schematic overview can be seen. The blue blocks are similar to the blocks in figure 2.3. The yellow blocks are implemented to be able to simulate an open water HIL setup.

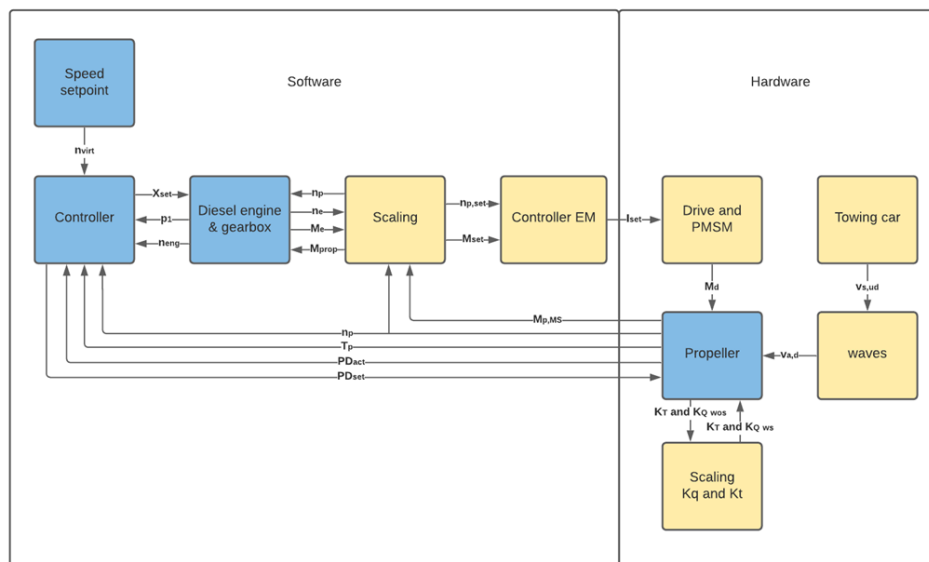


Figure 2.4: Scheme Open Water HIL Simulink model

The rotational speed and torque are scaled from full to model scale in the scaling block and vice versa. Scaling is done according to Froude's law with a geometric scale factor (λ) of 9.697. In the speed controller of the diesel engine, the integrator gain in the PID controller must be time scale to achieve Froude similarity.

In the controller EM (Electric Motor) block, the scaled torque is converted to a current. This current goes to the drive that controls the Permanent Magnetic Synchronous Motors (PMSM). In the model, it is assumed that the set current is the actual current. Huijgens [2021] has proven that the wave encounter frequencies this assumption is valid. In the hardware drive, there is a close electric loop that controls the current.

The propeller model in the HIL model is the same as in the free sailing model. However, the propeller in the HIL has a diameter of 0.33 meter and not 3.2 meters. This results in scaling effects due to drag, which accounts for the scaling block for K_Q and K_T .

A difference between the free sailing model and the open water model is the towing car. The hull in the free sailing model is propelled by the propeller that delivers a thrust. However, the towing car has its own propulsion. It can move forward at a constant speed and with an acceleration between 0.3 and 0.9 m/s^2 . This speed is not realistic with a real ship in Froude similarity.

A comparison is made between the two models to determine whether the HIL setup can simulate the non-linear dynamic behaviour of a propulsion plant. Suppose there is a similarity between the full and model scale simulations. In that case, it can be concluded that setup can be used to study the dynamic behaviour of a ships propulsion plant. The next step is to prepare the actual HIL experiments in the towing tank.

For the preparation of the experiments, the runs are first simulated with the second model. The physical limitations of the setup, such as backlash, the sample rate of the pitch and acceleration speed, gave some interesting insights, and it is concluded that it is not worthwhile to perform experiments at this moment. Nevertheless, it is possible to give recommendations on how to improve the setup and how it can be used to improve numerical models and control strategies for future research.

2.2. Adaptive pitch control

The interaction between the diesel engine and the CPP is controlled by adaptive pitch control (APC). The performance of the propulsion plant with this control strategy is determined with Measures of Performance (MOP's) as proposed by Geertsma [2019]:

- Provide requested virtual shaft speed.
- Maintain operation within cavitation bucket for the broadest possible operating conditions.
- Minimise fuel consumption across the ship speed profile and for all operating conditions.
- Maintain engine air excess ratio within predefined limits.
- Prevent engine over and under-speed.

The virtual shaft speed is often used on navy frigates because it has almost a linear relationship with the ship speed. In contrast to a combinator curve control strategy, APC requires no fixed rotational speed and pitch of the propeller. As a result, a lower engine speed and higher pitch can result in the same virtual shaft speed as a higher engine speed with a small pitch.

The cavitation bucket represents the operating area of the propeller in which the risk of cavitation is limited in the two-dimensional plane of cavitation number and angle of attack. The former is a non-dimensional pressure at mean shaft immersion; the rotational speed of the propeller mainly influences this variable. The latter is dependent on the advance speed and the pitch of the propeller.

Two assumptions are made. The first is that the advance speed is homogeneous, which is well a well accepted method if a open water diagram is used. The second is that when the propeller is operating in the bucket no cavitation occurs. However, in reality, due to waves, or oblique inflow cavitation might occur. Nevertheless, the assumption holds for acceleration as is demonstrated by Vrijdag [2009]. On the left side of the bucket, pressure side cavitation can be observed, and on the right side, suction side cavitation as is illustrated in figure 2.5.

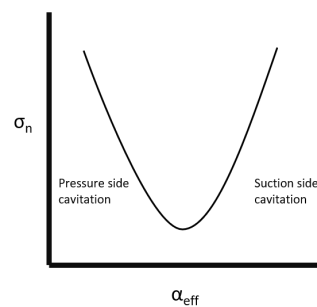


Figure 2.5: Cavitation bucket

In figure 2.6, a schematic representation of the Adaptive Pitch Controller is shown. The combinator curve, speed and pitch control are the three blocks that are the foundation of the controller. In addition, the inflow estimation and Kalman filter are implemented in this thesis.

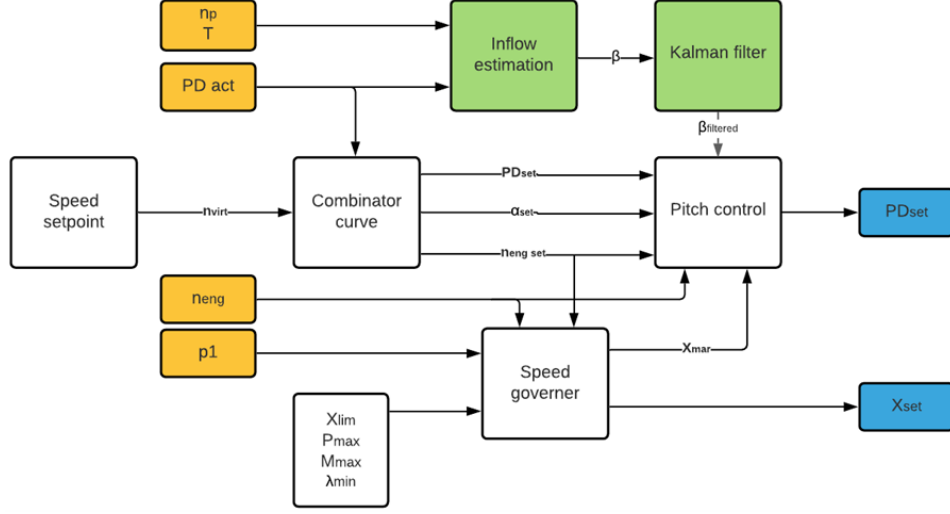


Figure 2.6: Adaptive pitch control

The virtual shaft speed is an input for the speed setpoint that is determined in the combinator curve block. The output of this block is the pitch, angle of attack and engine speed setpoint. The latter is determined with equation 2.1;

$$n_{e,set}(t) = \frac{P_{pd,nom} - P_{pd,0}}{P_{pd}(t) - P_{pd,0}} n_{virt,set}(t) \quad (2.1)$$

The pitch setting is determined with equation 2.2;

$$PD_{set}(t) = \frac{n_{virt,set}(t)}{n_{min}} \quad (2.2)$$

The desired angle of attack is predefined in a lookup table.

The speed governor controls the fuel rack. In this block is a PID controller that has a torque, fuel injection and speed constraint. If the former is reached a fuel injection margin ($X_{mar}(t)$) is activated, and pitch reduction ($\theta_{red}(t)$) is enabled in the pitch control.

The pitch control block set the pitch control setpoint to achieve the desired angle of attack and uses the following two equations:

$$P_{pd,set}^*(t) = \frac{0.7\pi \tan(\theta_{set}(t) - \theta_{red}(t)) + P_{pd,0}}{P_{pd,nom} - P_{pd,0}} \quad (2.3)$$

$$\theta_{set}(t) = \alpha_{eff,set} + \alpha_i + \text{atan}(c_1 \tan(\beta(t))) \quad (2.4)$$

Where $P_{pd,set}^*$ is the normalized pitch, θ_{set} the pitch angle setpoint, $P_{pd,0}$ pitch at zero thrust, $P_{pd,nom}$ the nominal pitch, $\alpha_{eff,set}$ the effective angle of attack setpoint, α_i the shock free-angle at the leading edge, β the hydrodynamic pitch angle and c_1 the Vrijdag coefficient that can be used for calibrating the $\alpha_{eff,set}$ in such a way that the cavitation buckets overlap for different pitch settings (Vrijdag [2009], pp 116 - 120).

Geertsma [2019] already implemented the previously described blocks, and a detailed explanation can be found in Geertsma [2019] page 116 - 124. In addition, a summary is given in Appendix A.

2.2.1. Inflow estimation

This study determines the hydrodynamic pitch angle with parameters that are measured on the hardware propeller. These are the shaft speed n_p , thrust (T), and the actual pitch (PD_{act}). The added value of this thesis is to estimate flow angle (β) to determine the effective angle of attack (α_{eff}). In equation 2.5, the

equation for the angle of attack is repeated. By rearranging the formula, it can be concluded, that advance ratio (J) and PD ratio are the two variables that influence this parameter.

$$\alpha_{eff} = \theta - \beta - \alpha_i \quad (2.5)$$

$$\alpha_{eff} = \text{atan}\left(\frac{P_{0.7R}}{0.7\pi D}\right) - \text{atan}\left(\frac{c_1 v_a}{0.7\pi n D}\right) - \alpha_i \quad (2.6)$$

$$\alpha_{eff} = \text{atan}\left(\frac{P_{0.7R}}{0.7\pi D}\right) - \text{atan}\left(\frac{c_1}{0.7\pi} J\right) - \alpha_i \quad (2.7)$$

The advance ratio is dependent on the advance speed. Unfortunately, it is impossible to measure this speed; therefore, a thrust or torque measurement is used to determine the advance ratio. Pivano et al. [2007] was the first to apply this method. Vrijdag [2009] also implemented a thrust measurement to determine the advance ratio. The thrust measurement is used to determine the K_T with the following equation:

$$K_T = \frac{T}{\rho n_p^2 D_p^4} \quad (2.8)$$

With the PD ratio, thrust and torque coefficient known, it is possible to determine the advance ratio using an open water diagram. In the model used in this thesis, only the first quadrant is implemented, as is depicted in figure 2.7. A consequence is that the estimation of J can only be performed in normal forward operation of the propeller.

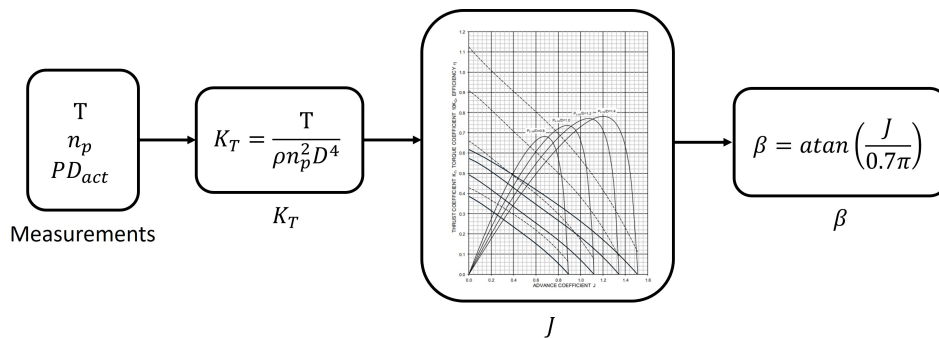


Figure 2.7: Inflow estimation

The advance ratio is used to determine the effective angle of attack. The adaptive pitch control strategy tries to achieve the desired effective angle of attack of 10.5 degrees by changing the PD ratio. It is assumed that this angle is within the cavitation bucket.

In the model, thrust is used to determine the effective angle of attack. A thrust sensor measures the thrust delivered by the propeller. However, a torque sensor can measure a different torque than was delivered by the propeller. For example, if it is measured near the gearbox, a different value is measured than directly in front of the propeller due to friction of the shaft bearings.

2.2.2. Kalman filter

Especially in waves, the measured thrust is continuously fluctuating. This results in a constant changing pitch to be able to keep the desired effective angle of attack. In this study, a Kalman filter is implemented to reduce the fluctuations of the estimated flow angle (β). By filtering this value, the pitch settings have smaller changes. A Kalman filter can filter out noise that is Gaussian distributed. Although, regular waves have this distribution, it is also assumed that irregular waves follow the Gaussian distribution (Journee and Massie [2001], page 9-36).

A Kalman filter can estimate the state of a process (\hat{x}_k). The Kalman gain performs the filtering (g_k). This is a weight factor that determines whether the one time step older prediction (\hat{x}_{k-1}) or the actual measurement (z_k) is trusted more. A high Kalman gain (close to 1) will result in an estimation close to the measurement. On

the other hand, a low Kalman gain (close to 0) results in an estimation close to the previous estimation. To filter out the fluctuations of the waves, the Kalman gain in the APC controller must be close to zero ([14],[15]). This process is done by the state update equation of the Kalman filter:

$$\hat{x}_k = \hat{x}_{k-1} + g_k(z_k - \hat{x}_{k-1}) \quad (2.9)$$

The following equations give the Kalman gain and estimate uncertainty equations:

$$g_k = p_k(p_k + r)^{-1} \quad (2.10)$$

$$p_k = p_{k-1} + q \quad (2.11)$$

Where p_k is the estimate uncertainty, r the measurement uncertainty and q the process uncertainty. The effects of the measurement and process uncertainty (r and q) on the adaptive pitch control are elaborated in the next chapter. In figure 2.8, the flow diagram of the Kalman filter is depicted.

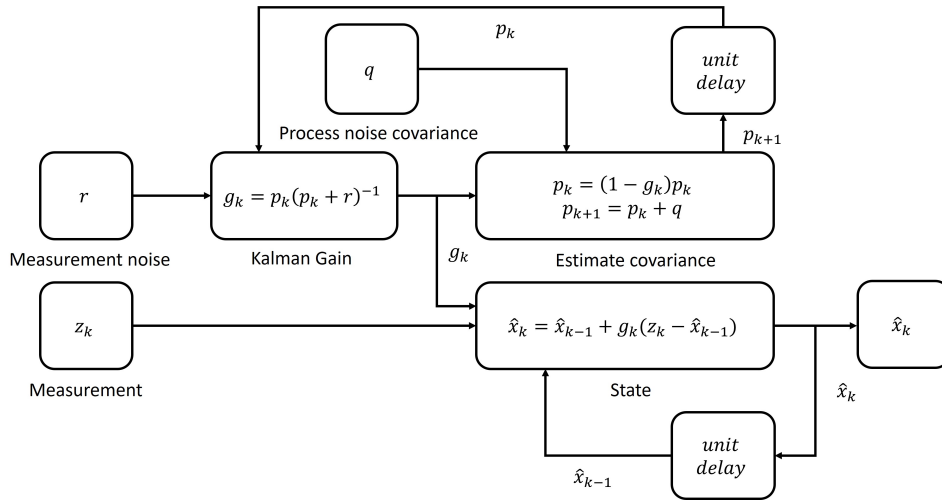


Figure 2.8: Kalman filter

2.3. HIL setup

The open water HIL setup can combine the benefits of towing tank experiments and numerical simulations. Hydrodynamic effects are taken into account in the towing tank with the hardware CPP. In numerical models, these effects are often simplified. An example is the free surface effects, Kozłowska et al. [2020] showed that this is complex to consider in a numerical model.

The proposed use of the HIL setup is to perform acceleration, and constant speed runs in the towing tank with waves. The goal is to validate the simulation results of the model scaled open water HIL simulations by making a comparison with validated full scale simulations. After validation, the setup can be used in situations in which the propeller's numerical model is no longer valid due to inaccurate hydrodynamic effects. Usually, full-scale trials need to be performed to study these effects. However, the HIL setup takes these effects into account. Therefore, the HIL setup can reduce the necessity to perform these time consuming and expensive trials.

The towing tank of the TU Delft has a limitation. The acceleration is restricted between 0.3 and 0.9 m/s². This means that if acceleration runs are performed, the acceleration doesn't have Froude similarity with full scale runs. Nevertheless, a comparison is made between the full scale and model scale acceleration to confirm that the HIL setup can not be used to perform acceleration runs without Froude similarity in acceleration. Also, to be able to make a fair comparison, the differences at a constant speed are compared.

The hardware CPP also has a few limitations. The first is the backlash in the blades of five degrees. The second is the low sample rate of the pitch measurements. Simulations with the open water HIL model with these limitations showed that it is not useful to perform experiments with these known limitations.

Nevertheless, it is still worthwhile to study if the HIL setup can simulate the dynamic behaviour of a ships propulsion plant. Therefore, a comparison is made between a full-scale free sailing ship and an open water propeller HIL setup with scaling effects. The simulations results are compared to decide whether the dynamic effects have similarities between the full and model scale.

2.3.1. Physical description

The TU Delft has its own propeller open water HIL setup and consists out of the following elements:

- Interface computer
- Simulator
- Motor controller
- Electric Motor
- Thrust and torque sensor
- Controllable pitch propeller
- Towing carriage

All these elements, except the interface computer, can be seen in figure 2.9. The interface computer runs MATLAB-Simulink and can be used to monitor and control the simulator. A copy of the Simulink model is duplicated on the simulator and runs real-time. This model is the software part that is illustrated in figure 2.4. The simulator converts the scaled drive torque to a current setpoint and sends this value to the motor controller. This motor controller governs the current. Note that this is not the adaptive pitch controller because this is implemented in the software model. The motor controller's current drives the PMSM electric motor, which runs the shaft. The feedback signals that are required for the APC strategy are the measured the shaft speed, the torque- and the pitch-measurement. The whole setup is built on the towing carriage, making it possible to sail through the towing tank.

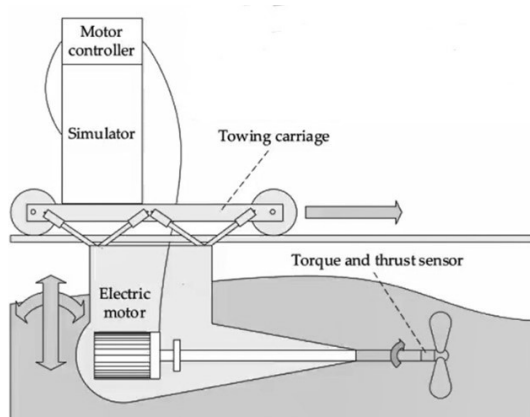


Figure 2.9: Open water HIL setup (Huijgens [2021])

The electric motor, torque and thrust sensor are enclosed by a gondola. This part of the setup is designed, manufactured and assembled by Maritiem Research Instituut Nederland (MARIN). The gondola is designed in such a way that it does not disturb the inflow in the propeller. It is mounted with a hexapod which allows it to move in six degrees of freedom.

The CPP propeller is a design by the TU Delft [16]. It is based on a C4-40 design. The diameter ratio of the hub is higher than a traditional Wageningen C4-40 propeller. It is a rightward turning propeller; this is done because it can easily be switched with an FPP propeller. An electric motor is built in the propeller to change the pitch, as shown in figure 2.10.

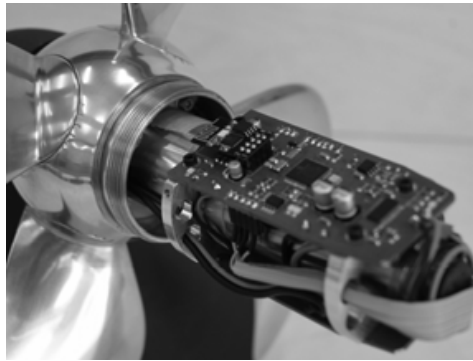


Figure 2.10: Servo motor of hardware CPP

For this study, the control signal to the servomotor is improved. In the first design, this was a Wi-Fi signal. However, this doesn't work correctly under water. Therefore a wired solution was desired. A challenge was that there was no room for extra wires. The solution is to send the TCP/IP signal over the power cable of the servomotor. A downside is that there is a limited amount of bites that can be sent per second. Due to this reason, it is only possible to send and receive a signal three times per second. The effects of this low sample rate are shown with simulation results and are discussed in section 4.2.2.

2.3.2. Numerical model

Two crucial requirements must be met in the numerical model for it to be used in a HIL setup. The first is that it must be able to run the model in real-time. The second is that the required sensor parameters of the propulsion plant are accurate to determine the dynamics between the propeller and the engine. Examples of these parameters are torque and engine speed.

The fastest way to do real-time simulations is by using transfer functions, a fuel rack map or lookup tables. The first two methods do not include the dynamics of the propulsion plant. Vrijdag et al. [2010] used three lookup tables based on available information. The data included some turbocharger dynamics, and it can predict air excess ratio and engine torque. The advantage of a lookup-table approach is that it is fast; a disadvantage is that there must be reliable data available to implement. Huijgens [2021] used a fuel rack map to demonstrate that the open water HIL setup can be used to study the behaviour of the propulsion plant.

Another approach is to use a filling and emptying mode. This method uses differential equations for mass, composition and energy balances. At crank angle time scale, the flow in and out of the cylinder is calculated. The nominal speed of the engine in this study is 1000 rpm. This corresponds to 0.17 milliseconds time step for one crank angle degree and will result in much simulation time for the complete propulsion in this study. It is also possible to use a fixed crank step size. A disadvantage of this method is that in low engines speed, the model will become numerical unstable. Schulze et al. [2007] used a crank angle based model in a HIL setup to test engine control units for cars. A problem in this study was that the model was unstable due to high time steps at an engine speed of 1700 rpm. Xia et al. [2018] can implement a crank angle based model in a HIL setup. However, to run in real-time, not all parameters could be calculated. Nevertheless, they showed that crank angle-based models could be implemented in a real-time HIL setup.

In a Mean Value First Principle (MVFP), the cylindrical volume is left out and is replaced by an analytical model for the air and exhaust gas flow dynamics. They are making it possible to use a revolution time scale instead of a crank angle time scale. The main advantage is that computational power is decreased by 400, making it possible to simulate real-time. Schulten [2005] and Geertsma [2019] have shown that an MVFP model can give reliable results for the dynamic performance of the propulsion plant.

Huijgens [2021] demonstrated that it is possible to study propulsion plant behaviour with the open water HIL setup. The numerical model he used had no turbocharger dynamics. The present study has implemented the validated MVFP diesel engine model and adaptive pitch control of Geertsma [2019]. A detailed description of the diesel engine model and adaptive pitch control can be found in Appendix A.

2.4. Summary

This chapter elaborates on the proposed approach. First, a full-scale free sailing of an OPV model is used to demonstrate the improvement in the APC strategy. Second, a model of the scaled open water HIL setup is used to prove that it can simulate the dynamic behaviour of a propulsion plant. Also, the fundamentals required to understand the propeller open water HIL setup and the adaptive pitch control strategy are elaborated. Further, the contributions of this thesis are explained, namely, the method for inflow estimation and the Kalman filter.

The adaptive pitch control strategy can provide the requested virtual shaft speed, maintain operation within the cavitation bucket, minimize fuel consumption, maintain engine air excess ratio and prevent over- and underspeed. The control actions of the APC are the pitch and fuelrack settings. These actions are based on the actual pitch and inflow of the propeller and the engine speed and charge pressure.

It is not possible to measure the propeller inflow directly. However, with the measured rotational shaft speed, thrust and propeller pitch, the hydrodynamic pitch angle can be estimated. The measured parameters are used to determine the thrust coefficient. Next, with the open water diagram of a C4-40 propeller, the advance ratio is determined. The last step in the estimation is to transfer the advance ratio into the inflow angle.

The inflow angle is constantly changing in waves. As a result, the APC strategy is continuously adjusting the pitch setting. This study has implemented a Kalman filter to reduce pitch actuations. The inflow estimation is filtered to reduce the disturbance due to waves. The Kalman filter determines if the measured or estimated value is trusted more based on the measurement and process uncertainty.

An objective is to determine whether it is possible to study the effects of APC with the Kalman filter in the HIL setup. In the setup, a CPP is driven by a PMSM. The current that drives the motor is determined with the full-scale diesel engine and gearbox model. The torque of the model is scaled and converted into a current. It is crucial that the model can run in real-time and provide the diesel engine's relevant parameters. The MVFP model validated by Geertsma [2019] meets these requirements and is therefore implemented in the setup.

3

Free Sailing Simulation Results

A ship is always safe at shore but that is not what it's built for

Albert Einstein

The free sailing simulations are used to demonstrate the effect of the added Kalman filter and deadband to reduce pitch actuation. Also, the effect on the measures of performance is discussed. Actuations is an important performance factor in this study. Therefore, it is shortly elaborated how these pitch actuations physically work.

A CPP can change the position of the blades around its longitudinal axis. On the foot of the blade is a yoke that can be moved with hydraulic power that is delivered by a power pack. The hydraulics are fed through the shaft to the CPP via the oil distribution (OD) unit.

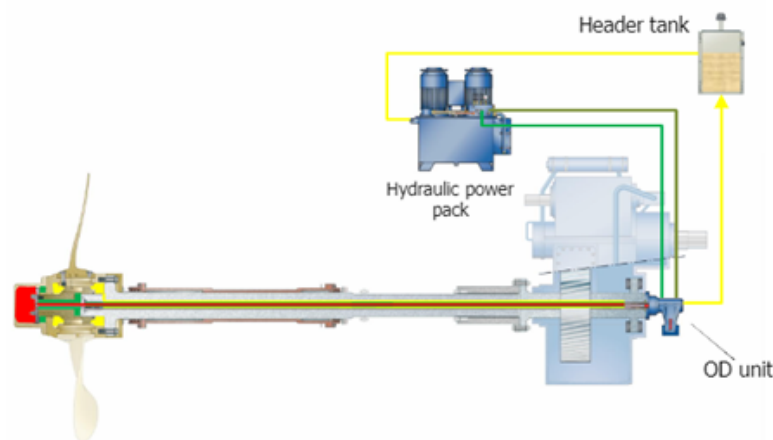


Figure 3.1: Layout CPP unit [19]

A pitch actuation is accounted for if the blade starts to move from a standstill. At the start, this is from zero pitch when it starts moving. However, during sailing, this is when the rotating direction of the blade switches. From standstill to movement requires the highest hydraulic force on the yoke and is, therefore, an actuation. Too many actuations can result in failure of the yoke (Godjevac [2009]). In this chapter, the results are discussed of the modified APC strategy with Kalman filter. The focus is on the pitch actuations and several diesel engine parameters to determine the impact on the measures of performance listed in chapter 2.

3.1. Kalman filter

The Kalman filter in the APC controller affects the speed of the response of the pitch setting. As a result, especially during acceleration, the pitch setting lags. This effect is shown in the following figures with extreme values for r (measurement uncertainty) and q (process uncertainty). In table 3.1, the conditions for the following figures are listed.

Table 3.1: Simulation Parameters of APC with Kalman filter

$H_{1/3}$	2.02 m
ω	0.93 rad/s
Waves	Regular
r	300
q	0.0001
n_{virt}	0 to 120 rpm
Timestep	0.005 s

In figure 3.2, the pitch of the CPP can be seen during acceleration. The blue line is the pitch of the CPP without the Kalman filter. Due to the influence of the regular waves, the pitch is constantly changing. The red line describes the pitch of the CPP with APC with the Kalman filter. The pitch changes are drastically reduced. However, a slight sine movement is visible due to the regular waves, as seen in the right-hand figure. Due to the sine movement, the direction of the pitch actuations is still fluctuating. And as stated before, every change in the direction of rotation is accounted for as an actuation. Implementing the Kalman filter is therefore not sufficient to reduce the number of actuations during constant speed.

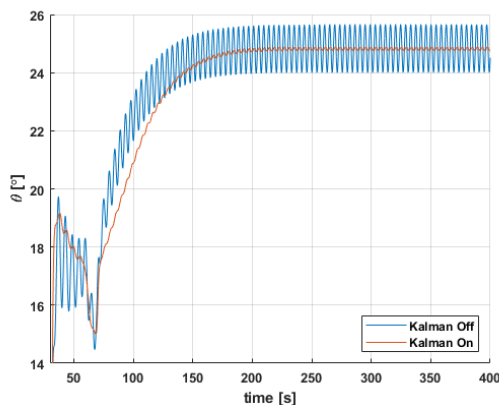


Figure 3.2: Pitch with Kalman filter off and on

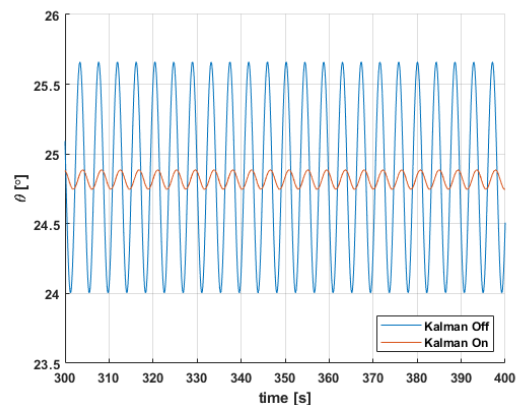


Figure 3.3: Pitch with Kalman filter off and on zoomed in

Another observation is that the pitch changes less rapidly during the acceleration. On the left, in figure 3.2, the effect of this slow pitch actuation can be seen. This is because the control system without the filter is able to change the pitch of the blades more rapidly. In contrast, the Kalman filter causes a delay in pitch actuations. As a result, during the acceleration, it stays behind. Therefore, it takes almost three minutes to achieve the desired angle of attack.

The effect of not achieving the desired effective angle of attack can also be seen in the cavitation bucket in figure 3.5. Without the Kalman filter, the cavitation plot starts at the bottom of the bucket and slowly moves up when the engine speed decreases. However, with Kalman, the movement through the bucket bends to the area where pressure side cavitation can occur. Even though this is a fictive cavitation bucket, it is likely to expect that the propeller starts cavitating more if the Kalman filter is used with these settings. The second Measure Of Performance (MOP) is to stay within the cavitation bucket for the broadest range of operational conditions. An APC with a Kalman filter has a negative influence on this performance. In section 3.1.1 it is quantified how much time the propeller is operating outside the cavitation bucket during acceleration with different Kalman uncertainties.

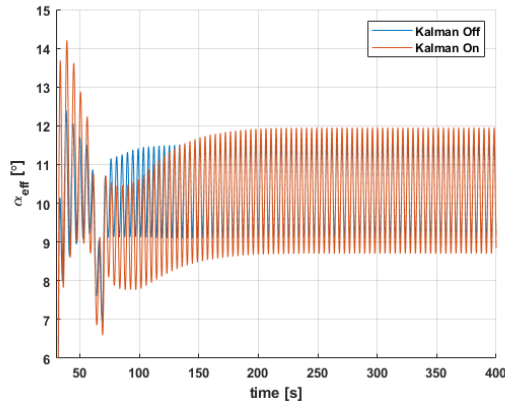


Figure 3.4: Effective angle of attack of the Kalman filter on and off

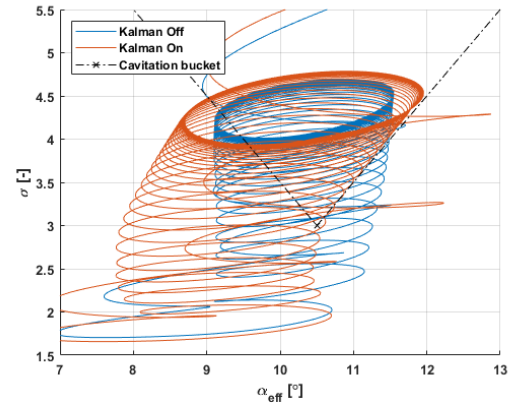


Figure 3.5: Cavitation bucket with Kalman filter on and off

The first MOP is to achieve the requested virtual shaft speed. In figure 3.6 can be seen that this MOP is met for the controller with and without the Kalman filter. The time that both controllers need to reach the requested virtual shaft speed is practically the same. It can therefore be said that the Kalman filter does not influence the first objective. However, note that the fluctuation with Kalman filter is less.

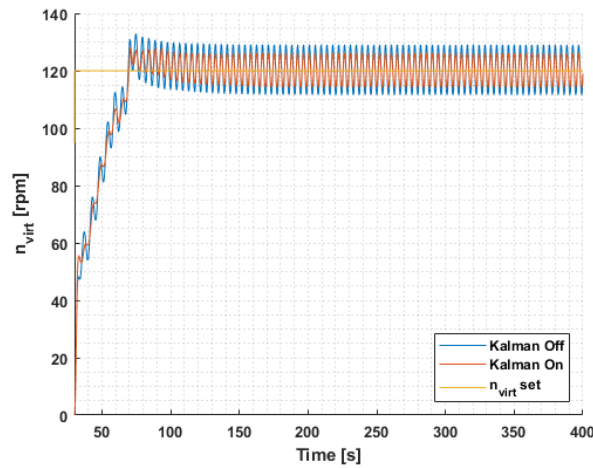


Figure 3.6: Virtual shaft speed with the Kalman filter on and off

In figure 3.2, it was already seen that the pitch with the Kalman filter is lagging. The only way to achieve the virtual shaft speed as soon as a controller without a filter is by increasing the propeller speed and, therefore, the engine speed, as can be concluded from equation 3.1:

$$n_{virt}(t) = \frac{P_{pd}(t) - P_{pd,0}}{P_{pd,nom} - P_{pd,0}} n_p \quad (3.1)$$

In figure 3.7 can be seen that the engine speed with the Kalman filter on is higher as was expected. The higher engine speed also results in a higher air excess ratio, as shown in figure 3.8. Therefore, a higher air excess ratio will result in lower thermal loading. In this case, especially during acceleration, at a constant speed, there is little difference.

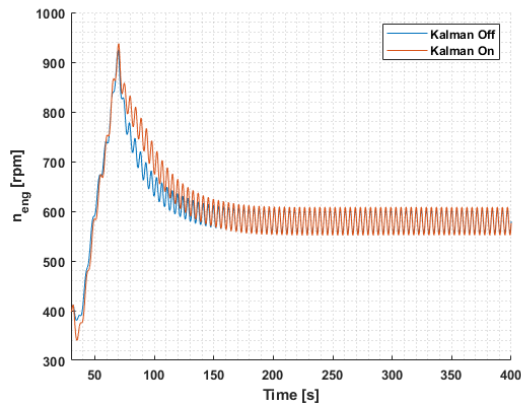


Figure 3.7: Engine speed with the Kalman filter on and off

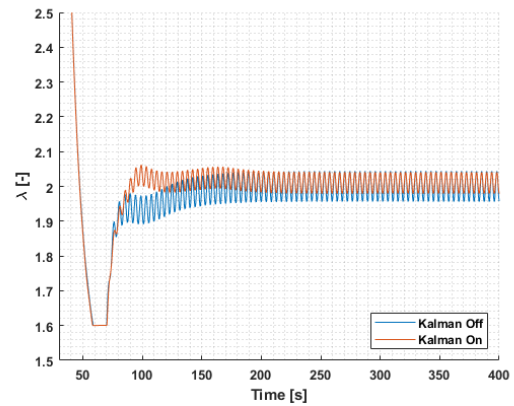


Figure 3.8: Air excess ratio with Kalman filter on and off

In figure 3.8 can be seen that the minimum level of the air excess ratio is not breached. However, there is another negative effect, in figure 3.2, can be seen that at the same time that the air excess ratio is at its minimum, the pitch reduction is activated, resulting in a different angle of attack and cavitation.

Another advantage of a higher air excess ratio is that the exhaust valve temperature is lower during acceleration, decreasing the thermal loading, as shown in figure 3.9. It can be noticed that the maximum temperature and the steady-state temperature are the same.

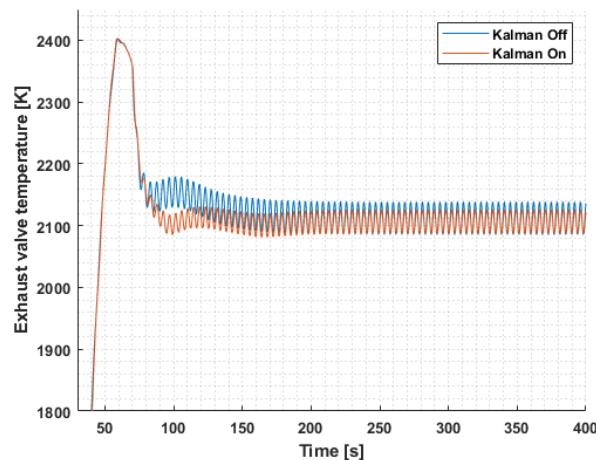


Figure 3.9: Exhaust valve temperature with and without the Kalman filter

Control objective three is to minimize fuel consumption. In figure 3.10, it can be seen that during the acceleration, the system with the Kalman filter has a lower specific fuel consumption. The engine speed is higher, and in the engine envelope, the brake specific fuel consumption is lower in that area.

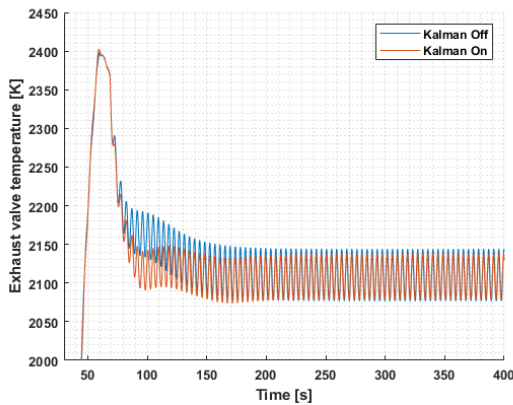


Figure 3.10: Specific fuel consumption with the Kalman filter on and off

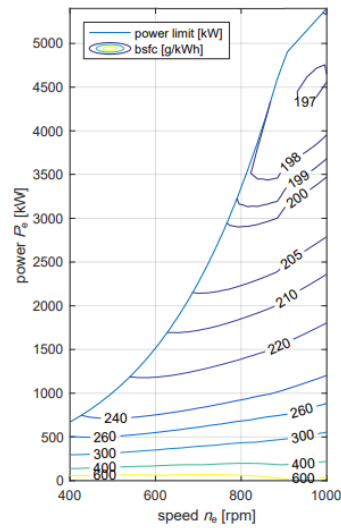


Figure 3.11: Brake specific fuel consumption in engine envelope [Geertsma [2019]]

In figure 3.12 the ship speed is plotted over time. It can be seen that the acceleration with filter is faster than without the Kalman filter. This is due to the higher rotational speed of the propeller as a result of the lagging pitch setting.

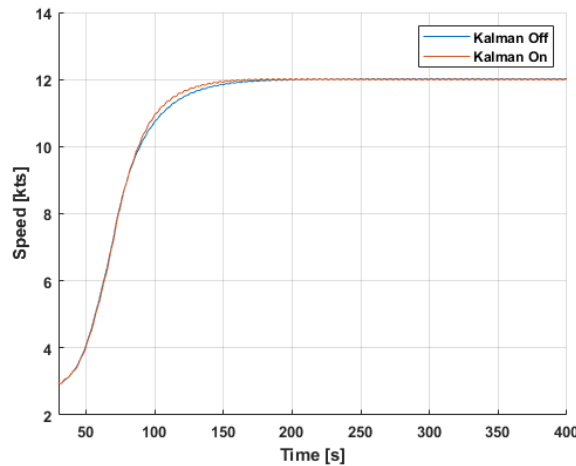


Figure 3.12: Ship speed the Kalman filter on and off

The Kalman filter settings that are used in the previous case are not the best; however, to illustrate the effect of a filter in the APC controller, a slow setting is used. It can be concluded that the Kalman filter negatively influences the cavitation performance of the propeller. However, the Kalman filter has no negative and sometimes better results on the other four MOP's. Accelerating with APC and the Kalman filter is even faster than without the filter. However, the problem with the number of pitch actuations is not solved by implementing a Kalman filter. The size of the actuations is decreased, but the sine movement in the pitch is still present.

3.1.1. Dependency uncertainties with sea state

The Kalman filter has a negative influence on cavitation behaviour. To reduce unwanted cavitation, the filter is tuned. Therefore, different settings for r (measurement uncertainty) and q (process uncertainty) are studied in different sea-states in regular waves. The goal is to find a setting in which the Kalman filter is still fast enough to keep the desired angle of attack to stay within the cavitation bucket, but is still reducing the size of the pitch changes. The sea-state is predefined with a significant wave height and frequency, as shown in table 2.

Table 3.2: Significant wave height and frequency at different sea-states

Sea-state	$H_{1/3}$	ω [rad/s]
0	0	0
4	1.26	1.18
5	2.02	0.93
6	2.97	0.77

The effect of process uncertainty is studied to take a fixed value for the measurement uncertainty (250) and different values for q . The first 300 seconds of acceleration from 0 to 120 rpm are taken into account in the following figures. Figure 3.13, shows that if the process uncertainty gets smaller, the number of actuations is decreasing. However, decreasing the q also results in more seconds out of the bucket during acceleration due to the slower reaction of the Kalman filter. So a trade off must be made between the number of actuations during acceleration, and the time the propeller operates outside the cavitation bucket.

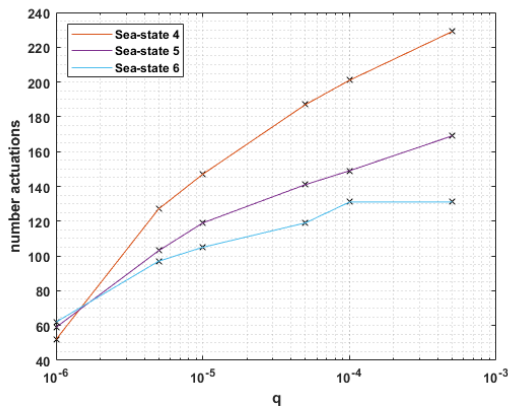


Figure 3.13: Effect of the process uncertainty on the number of actuations

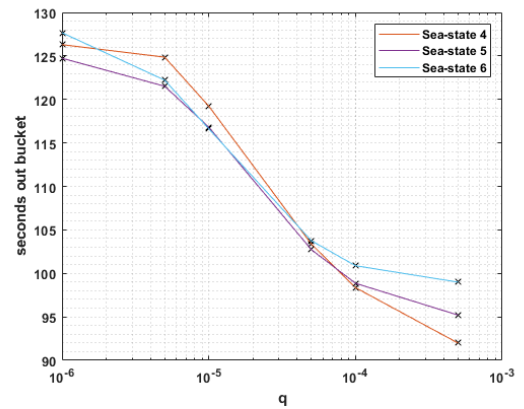


Figure 3.14: Effect of the process uncertainty on the seconds out of the bucket during acceleration

To study the effect of the measurement uncertainty a fixed value of $1e^{-5}$ is used for q . In figure 3.15 and 3.16, the effect of r on the number of actuations during acceleration and time of operation outside the cavitation bucket can be seen. Also, for the measurement uncertainty, a trade-off must be made. A small uncertainty causes less operating time outside the cavitation bucket but many actuations and vice versa.

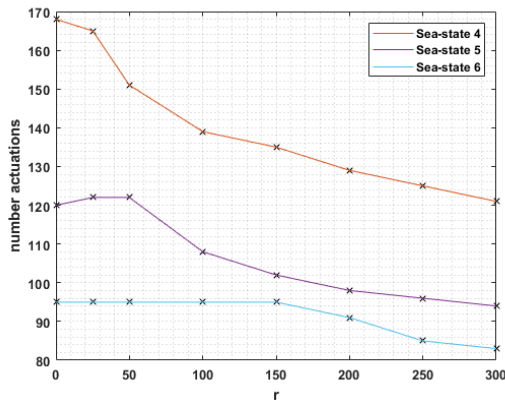


Figure 3.15: Effect of the measurement uncertainty on the number of actuations

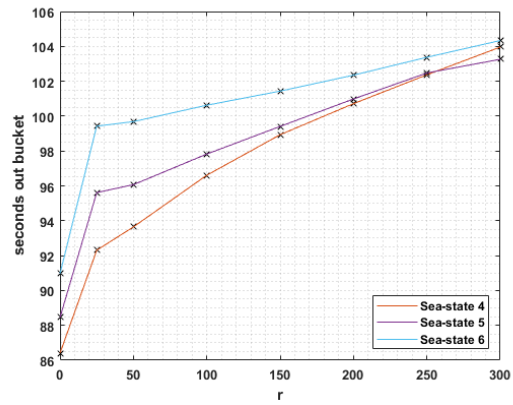


Figure 3.16: Effect of the measurement uncertainty on the seconds out of the bucket during acceleration

It was already noticed that the Kalman filter reduces the size of the pitch actuations. However, there are still actuations, especially at a constant speed. Therefore, the final settings for the Kalman filter are chosen to reduce the pitch size of actuation but hardly affect the speed pitch setting. This way the propeller operates inside the cavitation bucket. The measurement uncertainty is 50, and the process uncertainty is $5e^{-4}$. The following figures illustrate a comparison of the acceleration runs with the Kalman filter on and off with these settings.

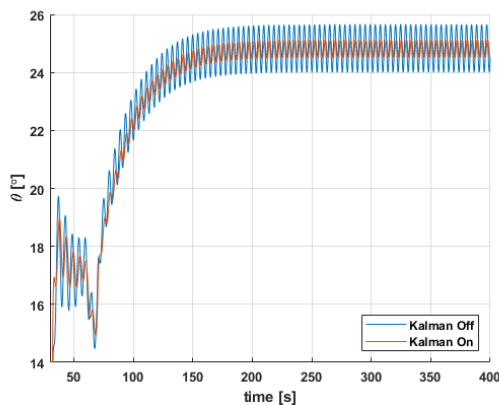


Figure 3.17: Pitch actuations with tuned Kalman filter

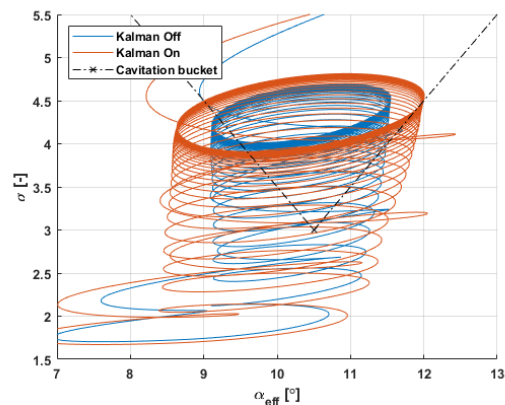


Figure 3.18: Cavitation bucket with tuned Kalman filter

With the earlier mentioned uncertainties, the pitch with Kalman filter hardly lags compared to the APC without the filter. The pitch actuations are reduced from 1.25 degrees to 0.32 degrees, reducing 74 per cent. Nevertheless, it is no reduction in the number of pitch actuations. In figure 3.18, the operating circle is wider with the Kalman filter in the cavitation bucket. Due to the low uncertainties, it doesn't bend to the left, to the pressure side cavitation.

3.2. Deadband

Another solution to reduce pitch actuations during constant speed is introducing a deadband in the adaptive pitch controller. The deadband should be able to reduce the pitch changes to zero degrees. This band is implemented in the Pitch Control block that is shown in figure 2.6. Simulations show that the deadband causes the propeller to operate more left in the cavitation bucket, and pressure side cavitation can occur. This is an undesirable effect of the deadband. To compensate for this effect, a quarter of the degrees of the deadband are added to the desired effective angle of attack.

$$\alpha_{eff,deadband} = \alpha_{eff} + \frac{\theta_{deadband}}{4} \quad (3.2)$$

Adding the deadband to the pitch controller realized a drastic decrease in pitch actuations. However, the influence on the MOP's must first be studied before it can be said that a deadband is a simple but adequate solution.

In the following simulation, a deadband of 2.7 degrees is implemented without the Kalman filter. Figure 3.19 shows that the pitch actuations are decreased due to the deadband. On the other hand, the pitch setting is higher due to the compensation of the deadband that was added in equation 3.2. As a result, the operating area in the cavitation bucket is almost one degree wider. Nevertheless, the operating area moves directly into the cavitation bucket without bending to the pressure side cavitation side.

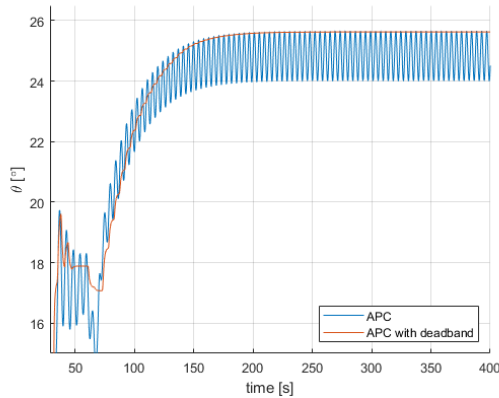


Figure 3.19: Pitch actuations with deadband in APC

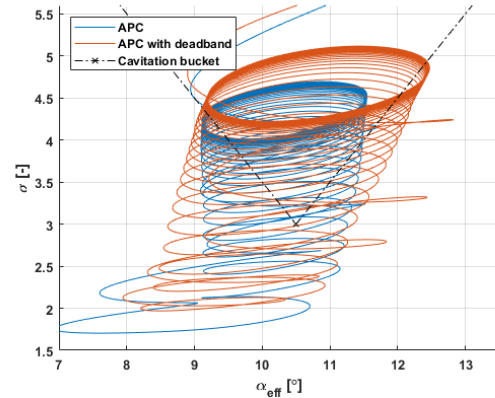


Figure 3.20: Cavitation bucket with deadband

The most significant difference is the lower air excess ratio. This is caused by a lower engine speed and results in a higher thermal loading of the engine. However, these temperatures and engine speeds are still within the operating limits, as shown in figures 3.21, 3.22, and 3.23.

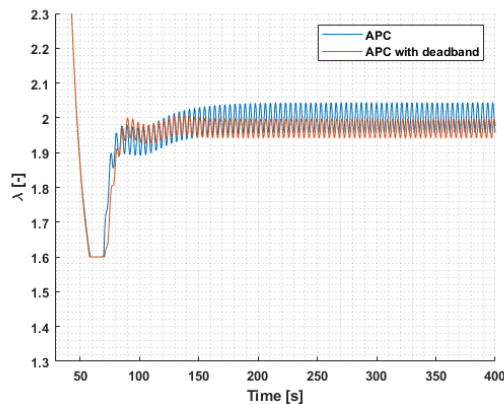


Figure 3.21: Air excess ratio with deadband in APC

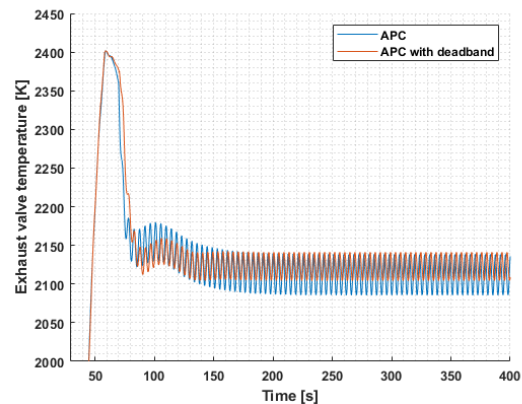


Figure 3.22: Exhaust valve temperature with deadband in APC

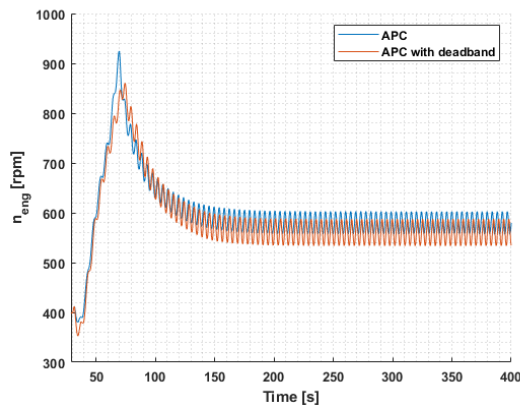


Figure 3.23: Engine speed with deadband in APC

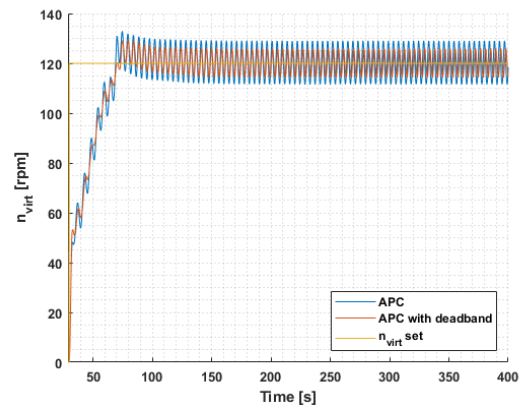


Figure 3.24: Virtual shaft speed with deadband in APC

The objective to achieve the requested virtual shaft speed is also met, as shown in figure 3.24. The final objective is to minimize fuel consumption. The figure below shows that there is hardly any difference between the APC with and without deadband.

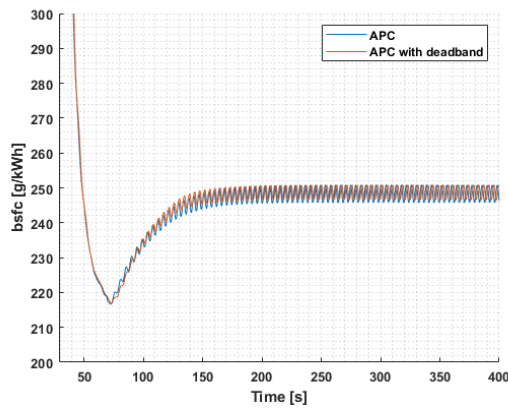


Figure 3.25: Specific fuel consumption with deadband in APC

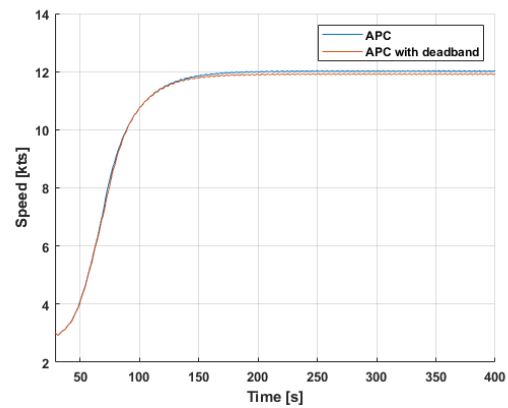


Figure 3.26: Ship speed with deadband in APC

A drawback of the deadband is shown in figure 3.26. Although all the demands for performance measures are met, the end speed is slower with only a deadband. Implementing only the deadband in the APC strategy is therefore not desirable.

3.3. Kalman filter and deadband

APC with Kalman filter causes more operating time outside the cavitation bucket but a higher air excess ratio and lower operating temperatures. Also, the acceleration with Kalman is faster than without the filter. On the other hand, the deadband had less time outside the bucket but resulted in a lower air excess ratio resulting in higher temperatures. However, the acceleration and end speed is lower in comparison without the deadband. Due to that reason, the two methods are combined. The settings for the simulations are listed in table 3.3.

Table 3.3: Simulation parameters Kalman filter with deadband in regular waves

$H_{1/3}$	2.02 m
ω	0.93 rad/s
Waves	Regular
r	100
q	0.0005
Deadband	0.85°
n_{virt}	0 to 120
Timestep	0.005 s

In figure 3.27, the pitch of the CPP is shown with the Kalman filter off and on with a deadband. During the acceleration, the pitch experiences a few actuations. However, after approximately 3 minutes, the pitch stays constant, as seen in the figure on the right. So it can be said that a Kalman filter with a deadband can reduce the pitch actuations at a constant speed. However, the effect on the dynamic behaviour of the propeller and engine is not known at this moment.

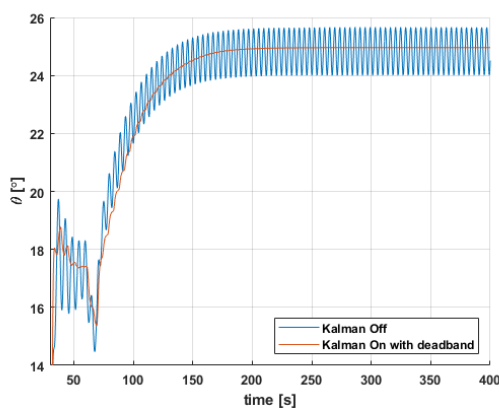


Figure 3.27: Pitch with the Kalman filter and deadband

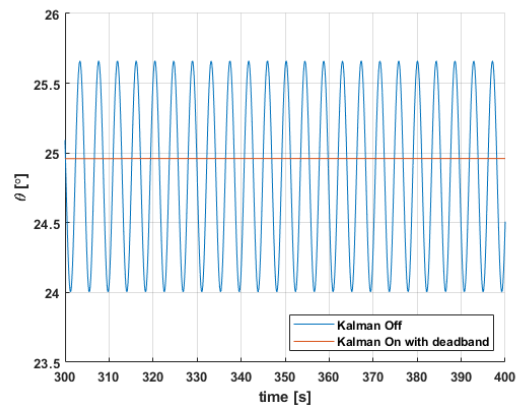


Figure 3.28: Pitch with the Kalman filter and deadband zoomed in

In the cavitation bucket, figure 3.29, there is little difference between Kalman filter on or off. The operating range with Kalman filter on is almost one degree wider. For propellers with a narrow cavitation bucket, this could result in more underwater noise.

The fourth measure of performance is to keep the air excess ratio within predefined limits. In figure 3.30 it can be seen that even with deadband, this demand still holds. However, the air excess ratio with the Kalman filter on is a bit lower during the steady-state situation. Because there is less air the temperature of the exhaust valve is also slightly increasing, as can be seen in figure 3.31. The lower air excess ratio can be explained due to the slightly lower engine speed.

In figure 3.33, can be seen that the second objective is met. The requested virtual shaft speed is reached. In figure 3.34 can be seen that there is hardly any change in the brake specific fuel consumption. So the Kalman filter with deadband does not influence the fuel consumption, the third objective.

In figure 3.35, the ship speed with and without the Kalman filter and deadband is shown. There is no significant difference in the acceleration and end speed. This is an improvement to the previous simulations with only the deadband.

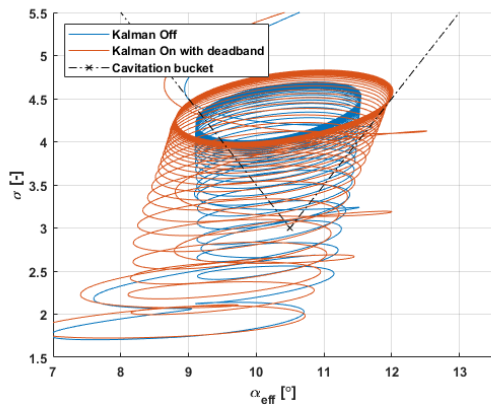


Figure 3.29: Cavitation with the Kalman filter and deadband

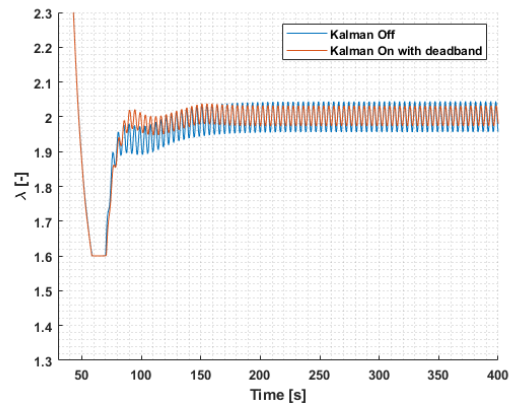


Figure 3.30: Air excess ratio with the Kalman filter and deadband

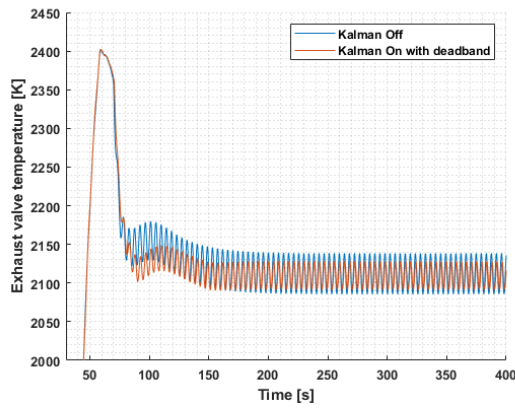


Figure 3.31: Exhaust valve temperature with the Kalman filter and deadband

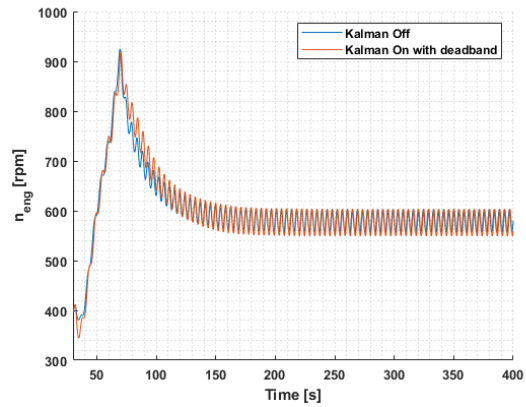


Figure 3.32: Engine speed with the Kalman filter and deadband

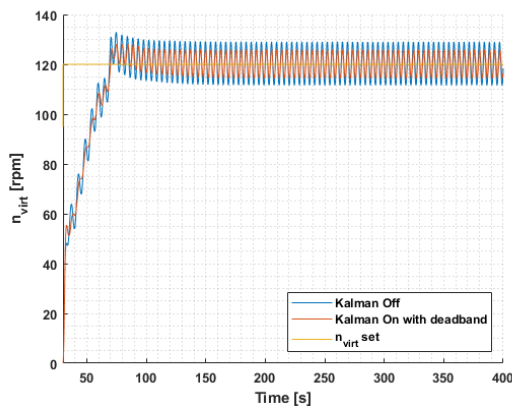


Figure 3.33: Virtual shaft speed with the Kalman filter and deadband

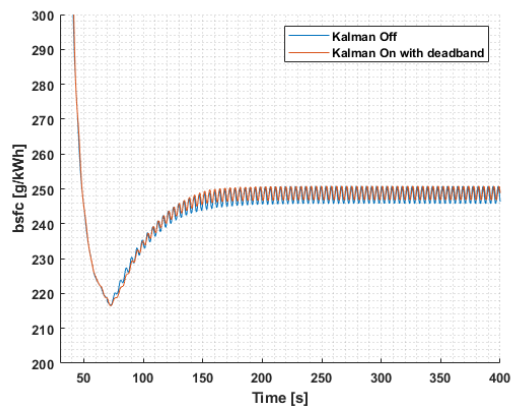


Figure 3.34: Specific fuel consumption with the Kalman filter and deadband

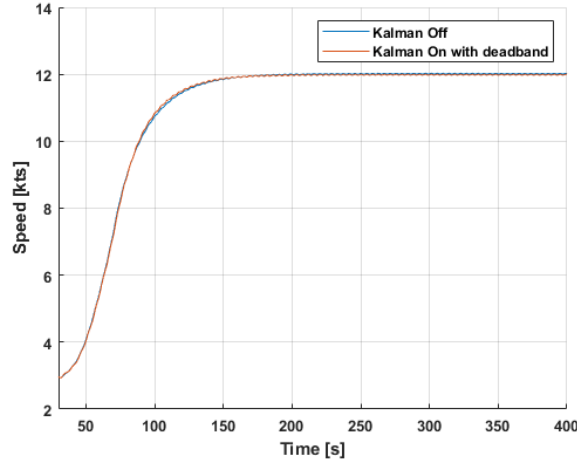


Figure 3.35: Ship speed with the Kalman filter and deadband

The tuned Kalman setting is applied in different sea states. In table 3.4, the number of actuations can be seen at different sea states during acceleration simulations as shown in the previous figures. It can be seen that in sea state four and five, the Kalman filter and deadband can reduce the pitch actuations drastically. However, in sea state six, the effect of the filter significantly diminished.

Table 3.4: Actuations in regular waves at different sea states

Sea state	APC	APC with filter and deadband	Difference [%]
4	264	7	-97
5	190	11	-94
6	150	125	-17

As shown in figure 3.29, due to the Kalman filter and deadband, the propeller operates more time outside the cavitation bucket. The higher the sea state is, the longer the operation is not able to gain its desired effective angle of attack. Especially in sea state six, the extra time is significant. However, it can be argued if a quiet propeller in this sea state is relevant, as the waves and slamming of the ship will also result in much transient noise. Nevertheless, if this filter is applied on navy ships, it would be recommended to switch the filter and deadband if there is a submarine or mine threat.

Table 3.5: Seconds out of bucket in regular waves at different sea states

Sea state	APC [s]	APC with filter and deadband [s]	Difference [%]
4	108.3	123.0	12
5	138.0	167.0	17
6	153.3	212.8	28

In table 3.6, an overview is given of the different control strategies and their impact on performance measures. The differences are minor and, therefore, hard to compare. The main conclusion is that APC without filter or deadband has a good performance on the five original MOP's, however, not on pitch actuations. APC with the Kalman filter and deadband has a good performance on the pitch actuations and reasonable performance in the cavitation bucket. Nevertheless, the cavitation performance is still significantly better than the original combinator curve control strategy.

Table 3.6: Overview of control strategies on measures of performance

	# pitch actuactions	λ	n_{virt}	bsfc	cavitation	Under / overspeed
APC	-	+	+	+	+	+
APC with Kalman	-	+/-	+	+	-	+
APC with deadband	+	-/+	+	+	-/+	+
APC with Kalman and deadband	+/-	+	+	+	+/-	+

3.4. Gain scheduling

In the speed controller of the diesel engine model, gain scheduling is implemented. If the engine speed is under 450 rpm, the fast PI controller is activated constantly. It can also occur that in waves, the engine speed fluctuates around 450 rpm. As a result, the fast PI and slow I controller are switching in a short amount of time. Both effects can be seen in the following figures. In sea state 5, acceleration is made from 0 to 70 rpm and 70 to 90 rpm. During the first acceleration, the engine speed stays under 450 rpm, and the second part the engine speed is fluctuating at 450 rpm. The first objective of APC is to provide the requested virtual shaft speed. In figure 3.36 can be seen that the virtual shaft speed cannot be provided. The simulations are performed with and without the Kalman filter, and the effect can be seen in both situations.

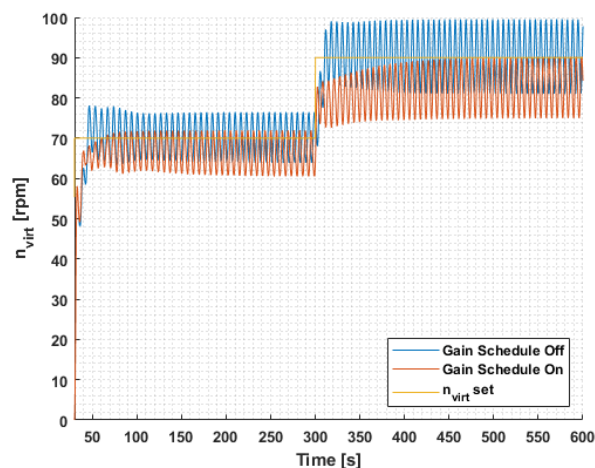


Figure 3.36: Virtual shaft speed with gain schedule on and off

The mean virtual shaft speed is lower due to a lower engine speed. This is a result of the fast PI controller. In figure 3.37 can be seen that this gain scheduling is activated. Note that the gain scheduling is active at the start of the acceleration from virtual shaft speed zero. A fast PI controller at a virtual shaft speed request of zero results in a constant engine speed of 400 rpm.

Due to the lower engine speed, and therefore also the lower rotational speed of the propeller, there is a difference in speed. With a slow I controller, the ship speed is higher, as can be seen in figure 3.39. The break specific fuel consumption is also less with only the slow I controller. A lower engine speed results in a poor performance in fuel consumption.

The fast PI controller tries harder to reach a stable engine speed and will, therefore, react more severe to wave disturbance. This can also be seen in the fuel rack position, as can be seen in figure 3.41. The fuelrack position fluctuates more with the gain schedule on that when it is off. A fluctuating fuelrack also results in a highly fluctuating exhaust valve temperature.

It can be summarised that if the virtual shaft speed is higher than zero, the fast PI controller has a negative influence on the performance of the propulsion plant with APC. The requested virtual shaft speed is not reached, the fuel consumption is higher, and the ships is lower. For this reason when the virtual shaft speed is set above zero the slow integral controller is active.

Studying the effect of gain scheduling is not inside the scope of the research. The conclusion holds for this propulsion plant and its current settings. Other controller settings could result in different results.

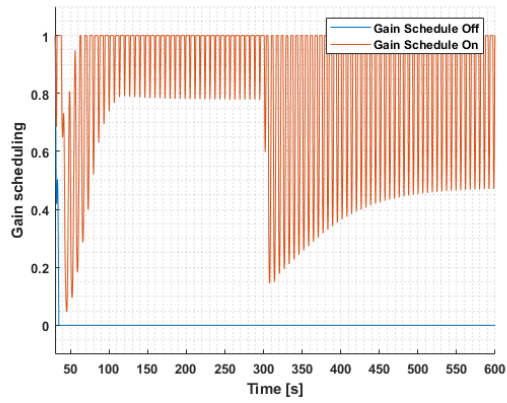


Figure 3.37: Gain scheduling

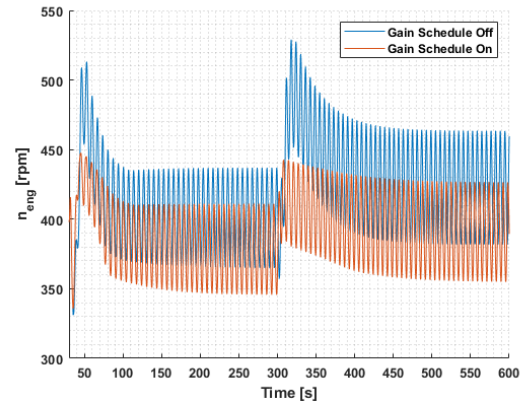


Figure 3.38: Engine speed with gain schedule on and off

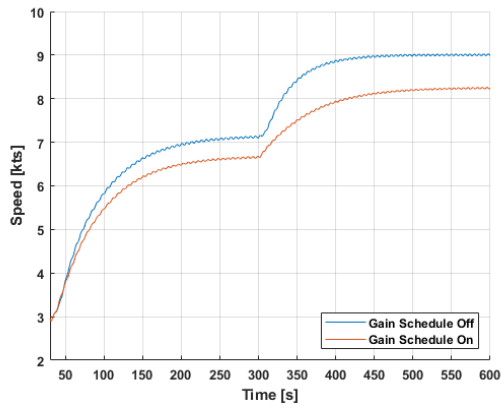


Figure 3.39: Ship speed with gain scheduling on and off

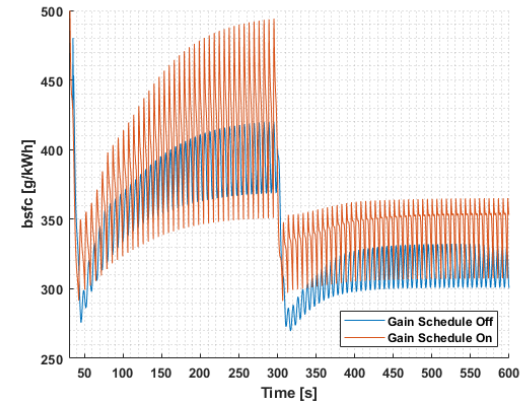


Figure 3.40: Specific fuel consumption with gain schedule on and off

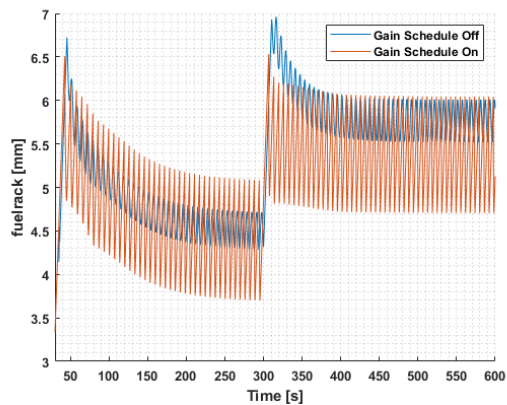


Figure 3.41: Fuelrack with gain scheduling on and off

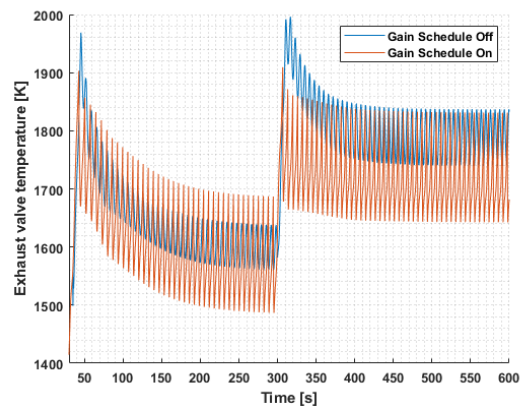


Figure 3.42: Exhaust valve temperature with gain schedule on and off

3.5. Irregular waves

The previous simulations were all performed at sea state 5 with regular waves. Regular waves are predictable and always have the same mean value over any time period. Irregular waves are a superposition of regular waves and can have lower and higher amplitudes and frequencies at the same sea state. The following simulations are required to determine whether the chosen control system with APC, Kalman Filter and deadband perform as predicted with regular waves. In figure 3.43 and 3.44, the wave speed of regular and irregular waves are shown. It can be seen that the regular waves always have the same maximum and minimum speed. However, irregular waves have different frequencies and amplitudes over time, making it harder for the system to determine the correct control actions.

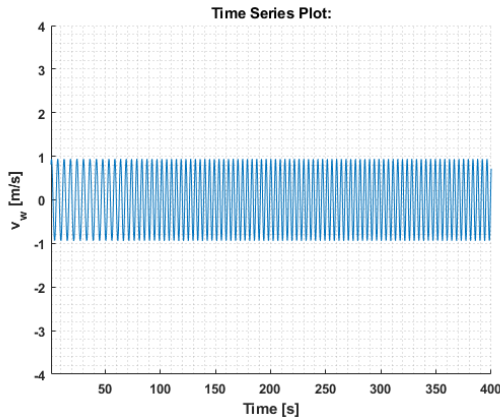


Figure 3.43: Wave speed in regular waves

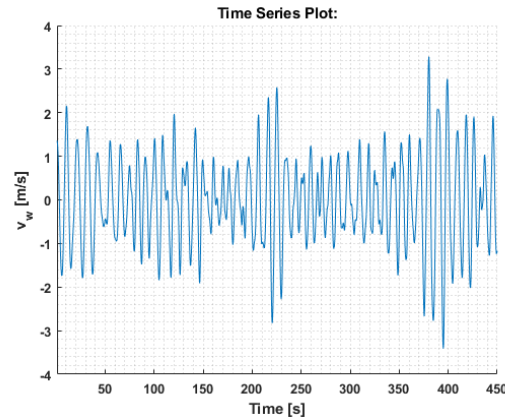


Figure 3.44: Wave speed in irregular waves

The encounter frequency of irregular waves is lower in comparison with regular waves. As a result, the Kalman filter can be slower. Since in irregular waves the ship sometimes encounters higher waves, the deadband is also increased. The wave and Kalman settings are listed in table 3.7.

Table 3.7: Simulation parameters irregular waves

$H_{1/3}$	2.02 m
ω	0.93 rad/s
Waves	Irregular
r	150
q	0.0005
Deadband	1°
n_{virt}	0 to 120
Gain schedule	Off
Timestep	0.005 s

The virtual shaft speed fluctuates more due to the different waves the ship encounters. Nevertheless, the APC controller with and without Kalman filter can provide the requested shaft speed, as shown in figure 3.45. In the pitch figure can be seen that without the Kalman filter there are many actuations. With the slower Kalman filter, many actuations are prevented. However, when heavier waves hit the ship, a few actuations are visible.

With regular waves, the ellipse in the cavitation bucket was marginal larger with the Kalman filter. However, with irregular waves, the ellipse in the bucket is significantly more extensive than in figure 3.47. This is a result of filtering out larger pitch actuations.

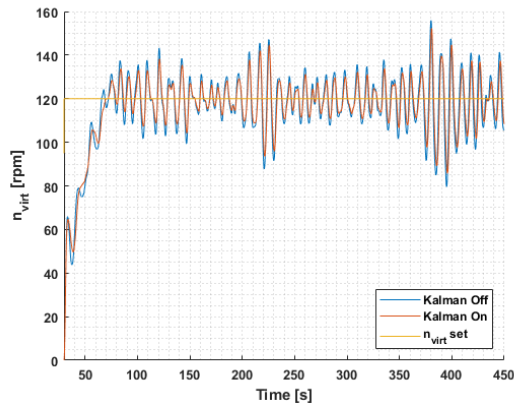


Figure 3.45: virtual shaft speed in irregular waves with the Kalman filter on and off

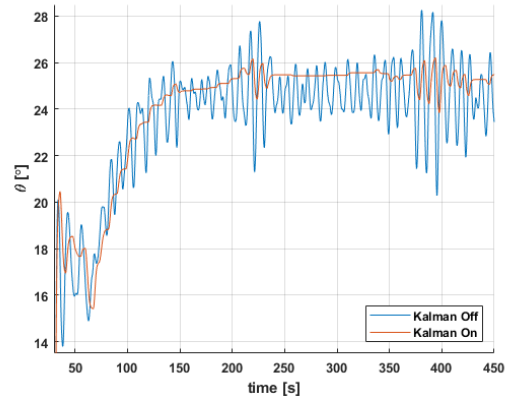


Figure 3.46: Pitch in irregular waves with the Kalman filter on and off

Even though more cavitation occurs with the Kalman filter and deadband, its cavitation behaviour is still significantly better than the standard combinator curve. With this older control strategy, the propeller operates most of the time outside the cavitation bucket in the pressure side cavitation area (Geertsma [2019] page 129). So even though the control strategy with Kalman filter performance less in cavitation behaviour, it is still worthwhile to implement it because it reduces pitch actuations and has a better cavitation performance than the combinator curve.

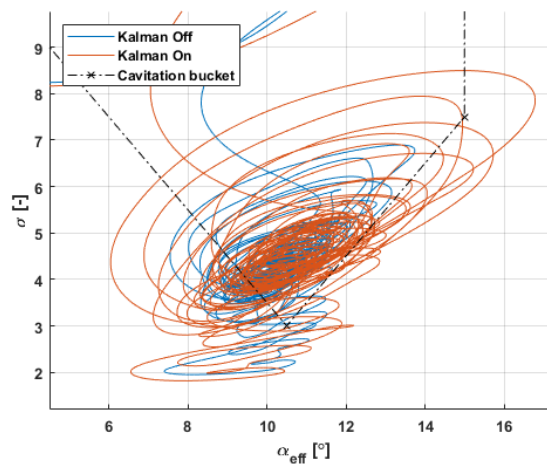


Figure 3.47: Cavitation bucket in irregular waves with Kalman filter on and off

There are no significant differences with or without Kalman filter in irregular waves for the other engine parameters like speed, break specific fuel consumption, air excess ratio, and exhaust valve temperature as can be seen in figure 3.48 to 3.51. This could be expected, as it was also the result of the simulations with regular waves. Therefore the same conclusion can be made. It is possible to reduce pitch actuations with a Kalman filter and deadband. However, the propeller starts cavitating more because of the broader ellipse in the cavitation bucket.

In table 3.8, the performance of the APC with Kalman filter and deadband is shown in the different sea states. The reduction of pitch actuations is lesser in comparison to regular waves. The different wave amplitude and frequencies can explain this. Nevertheless, in sea state four and five, the reduction is still significant.

Also, the operating time outside the cavitation bucket is more significant in irregular waves in all the sea states, as shown in table 3.9. These results acknowledge the same conclusion as that was made with regular waves. Therefore, with a submarine or mine threat, a navy ship should switch the Filter and deadband.

Table 3.8: Number of actuations in irregular waves

Seastate	APC	APC with filter and deadband	Difference [%]
4	108	8	-92.6
5	112	44	-60.7
6	105	87	-17.1

Table 3.9: Seconds out of the cavitation bucket in irregular waves

Seastate	APC [s]	APC with filter and deadband [s]	Difference [%]
4	66.93	84.50	21
5	125.04	167.25	25
6	228.16	303.30	25

The Kalman filter predicts one timestep ahead. Model Predictive Control (MPC) can expand this prediction horizon and can better predict the incoming disturbances due to waves. However, it can be argued if MPC can deal with irregular waves. To reduce cavitation, it would be better to measure the incoming waves and use this information as a control input for the APC with Kalman filter and deadband.

3.6. Summary

The effect of the control strategy is first simulated with full-scale free sailing simulations. The objective is to determine if a Kalman filter can reduce pitch actuations. A pitch actuation is when a propeller blade starts to move from a standstill or when the movement changes direction.

The effects of the Kalman uncertainties are studied. Simulations show that a lower measurement uncertainty reduces the number of actuations. However, the propeller will operate more outside the cavitation bucket. The same holds for a higher process uncertainty. So, there is a trade-off between cavitation and actuations. The Kalman filter is tuned so that it reduces the size of the pitch actuations, but hardly lags in pitch setting compared to the original APC strategy.

To reduce the actuations during constant speed a deadband is added to the pitch control. The combination of the Kalman filter and the deadband resulted in no pitch actuations during constant speed in regular waves. However, there is more pressure side cavitation.

The APC with Kalman filter and deadband is also simulated in irregular waves. It is shown that it reduces the pitch actuations during acceleration and constant speed. However, the filter and deadband cannot filter out the more giant waves, and some actuations can be observed. Nevertheless, a significant pitch actuation is observed at sea state four and five. However, at the cost of 25 per cent more operating time outside the cavitation bucket. Nevertheless, the cavitation behaviour is still significantly better than the traditional combinator curve control strategy.

Finally, simulations show that the fast PI controller for the engine under a speed of 450 had a negative influence on delivering the virtual shaft speed and fuel consumption. Due to that reason, the slow integral speed controller is applied for all virtual shaft speed demands above zero.

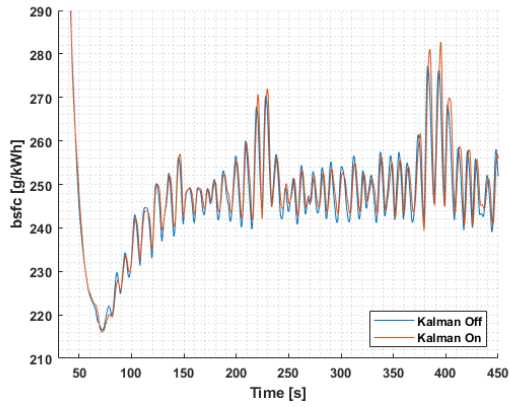


Figure 3.48: specific fuel consumption in irregular waves with the Kalman filter on and off

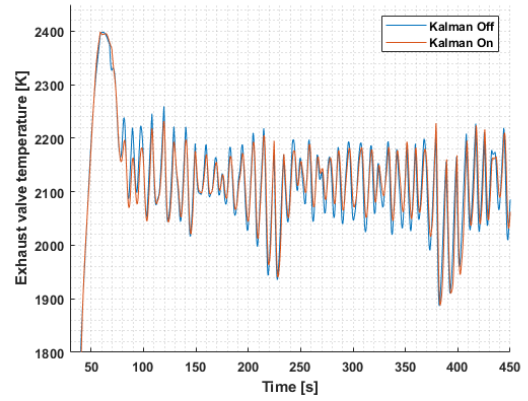


Figure 3.49: Exhaust valve temperature in irregular waves with the Kalman filter on and off

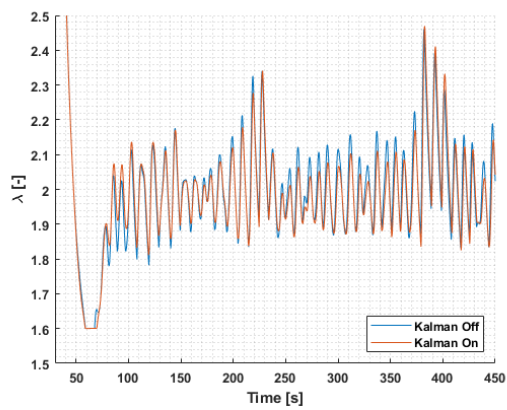


Figure 3.50: Air excess ratio in irregular waves with the Kalman filter on and off

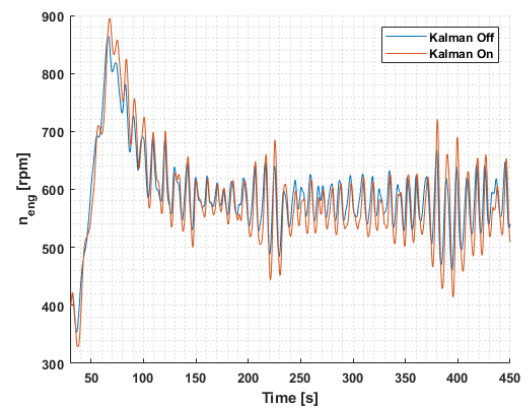


Figure 3.51: Engine speed in irregular waves with the Kalman filter on and off

4

Open water HIL setup simulation results

People who are really serious about software,
should make their own hardware

Alan Kay

A feasibility study is performed in this research to determine whether an open water HIL setup can improve numerical models and control strategies. In a hardware in the loop setup, a numerical model is replaced by a hardware component. In the open water HIL setup, the propeller is the hardware part. Also, the wave model is replaced by waves in the model basin.

Huijgens [2021] studied if the scale effects in the model basin influence the dynamic behaviour of the propulsion plant. Implementing a virtual flywheel and a compensation for the friction torque makes it possible to let the electric motor behave like a diesel engine. The motor is controlled by a MATLAB-Simulink model of the propulsion plant. This model sets the current that drives the motor.

Behind the propeller, a torque and thrust sensor mounted. In this study, the measurements of this sensor are used to determine the inflow of the propeller. Together with the actual rotational speed and pitch, these are essential control parameters for the adaptive pitch controller.

4.1. Towing tank and full-scale simulations

For the comparison of the towing tank and full-scale simulations, the settings of chapter 3 are used. So there is no gain scheduling for a virtual shaft speed greater than zero, and if the Kalman filter is used it is always in combination with a deadband.

The towing tank of the TU Delft has some physical limitations. The tank is 144 meters long and therefore is the length of the runs limited. In this scaled distance, the propulsion plant model must be able to reach the desired point. Also, the acceleration is restricted between 0.3 and 0.9 m/s^2 . This means that if acceleration runs are performed, the acceleration doesn't have Froude similarity with full scale runs. To be able to make a fair comparison, the differences at a constant speed are compared.

Froude scaling is applied in the open water HIL setup simulations. It is assumed that by applying these scaling laws, comparing full and model scale results are valid, even though Reynolds similarity cannot be achieved. Nevertheless, this is also according to the ITTC procedure (ITTC [2015]). More theoretical background of Froude and Reynolds scaling can be found in Appendix A.

The geometric scale factor (λ) is 9.697. This factor is used to scale the other parameters according to table 4.1. In the following figures, the results of full-scale simulations and open water scaled simulations are compared.

Time scaling is applied to the parameters that influence time constants. These are the integral gain of the speed governor, but also the time delays in the model. There are delays for filling the exhaust receiver ($\tau_{p,d}$), for pitch actuation delay (τ_p) and fuel injection delay (τ_X). Also, the torque rate limiter in the PID controller is time scaled.

Table 4.1: Froude scaling

Distance	λ^1
Energy	λ^4
Linear speed	$\lambda^{0.5}$
Mass	λ^3
Moment of inertia	λ^5
Power	$\lambda^{3.5}$
Rotative speed	$\lambda^{-0.5}$
Time	$\lambda^{0.5}$
Torque	λ^4

This study aims to determine whether the HIL setup can be used to improve numerical models. In this research, a Kalman filter and deadband are added to the APC strategy. The Kalman uncertainties are time dependent, and therefore need to be scaled. However, the effect of this scaling is unknown. The uncertainties are scaled according to the following equations.

$$q_{MS} = q_{FS}\lambda^{0.5} \quad (4.1)$$

$$r_{MS} = r_{FS}\lambda^{-0.5} \quad (4.2)$$

These scaling effects are chosen as a result of an empirical study performed with these uncertainties in section 3.1.1. The results showed that if the process uncertainty increases and measurement uncertainty decreases, the Kalman filter becomes faster. Therefore, a faster filter is required to compensate for the time scaling effects.

Before a comparison is made with waves, the difference in a steady-state situation is compared. First, the simulations are done with a virtual shaft speed of 120 rpm. Then, the full scale-free sailing simulation is compared with the open water simulation. For the latter, the end speed of the free sailing simulation is scaled and enforced.

In table 4.2, the results are shown. It can be seen that the virtual shaft speed, pitch and effective pitch angle are the same. However, there are differences in fuel rack and, therefore, in engine speed. This results in differences in the air excess ratio, exhaust valve temperature and brake specific fuel consumption. These differences are a result of the difference between an open water setup and the free sailing simulation.

Table 4.2: Difference free sailing and open water simulation without waves

	Full scale	Model scale	Difference
n_{virt} [rpm]	120	120	0%
Pitch [deg]	24.76	24.76	0%
α_{eff} [deg]	10.22	10.22	0%
Eng speed [rpm]	582.1	580.9	0.2%
Fuelrack [mm]	8.304	8.018	3.7%
Air excess ratio [-]	2.008	1.949	3.0%
Exhaust valve temperature [K]	2108	2140	1.5%
Bsfc [g/kWh]	248.4	245.3	1.3 %

It can be concluded that there are slight differences between the full and model scale steady state simulations. However, in a steady-state condition this is a maximum a difference off 3.7%. In this study, the dynamic behaviour in waves is examined. For this reason the difference in regular waves is studied.

In figure 4.1, the wave speed at full and model scale is illustrated. Due to Froude similarity, the frequency and speed are different, making it harder to make a fair comparison. Therefore, the other results are split in full and model scale results with a different x-axis scale, as shown in Figures 4.2 to 4.10. Due to the time scaling of 3.114 has the x-axis a different scale.

An important measure of performance is the virtual shaft speed. In figure 4.2, the results are shown for the full scale (top) and model scale simulations. It can be seen that there is no difference in the delivered virtual shaft speed during constant speed settings.

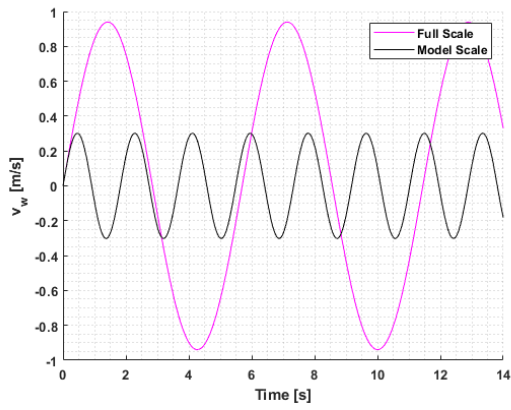


Figure 4.1: Wavespeed at full and model scale with Froude similarity

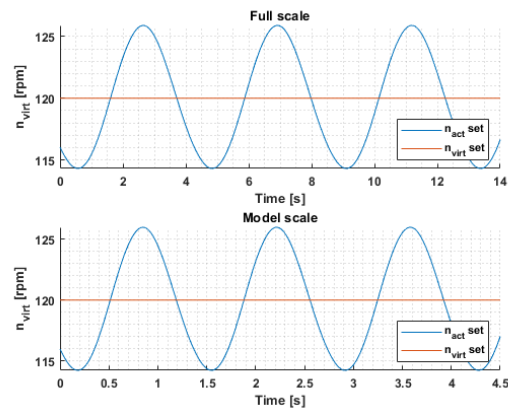


Figure 4.2: Virtual shaft speed

In figure 4.3 and 4.4, the propeller and engine speed can be seen. Note that the propeller speed is different between the model and full-scale simulations. It seems that the difference is a multiplication of the time scaling factor. However, if we look at the engine speed, there are differences at full scale. The engine speed at full-scale simulations is a bit higher than at the model scale. Also, the difference is a bit higher than in steady-state; it is one per cent.

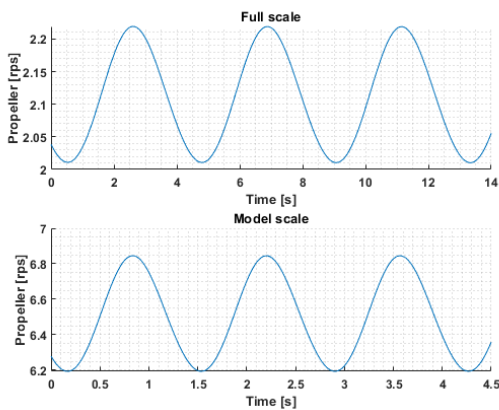


Figure 4.3: Propeller speed

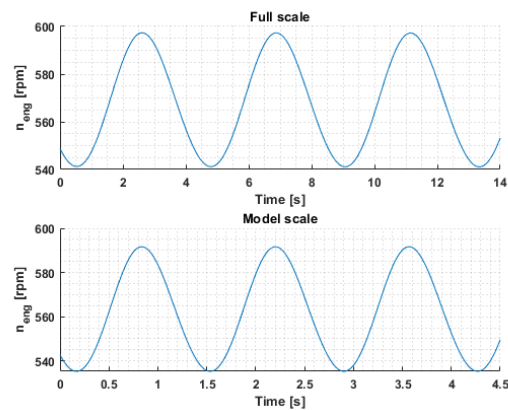


Figure 4.4: Engine speed

The difference in fuel rack is 2.6 per cent. The fuel rack is higher in the model scale simulation due to the lower engine speed and lower brake specific fuel consumption. The difference between full and model scales is 0.8 per cent for brake specific fuel consumption.

As a result of the difference in engine speed, the air excess ratio also varies approximately 2.5 per cent. In figure 4.8 can be seen that a higher air excess ratio results in a lower exhaust temperate. Nevertheless, the results are similar, and the temperature has a difference of roughly 1.2 per cent.

The parameters to determine the cavitation number from model are transferred to full-scale, so a better comparison can be made. The difference in cavitation number in figure 4.9 can be explained by the difference in engine and propeller speed between full and model scale. In figure 4.10, the filtered inflow angle can be seen. Due to the time scaling of the Kalman filter's measurement and process uncertainty, the difference in the estimated inflow is small, 1.8 per cent.

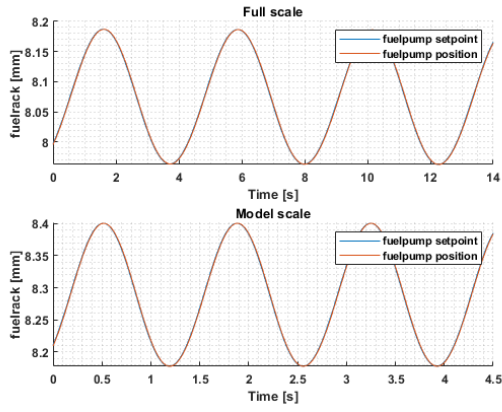


Figure 4.5: Fuelrack

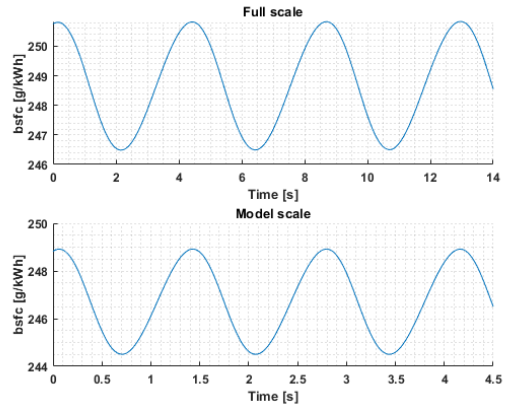


Figure 4.6: Brake specific fuel consumption

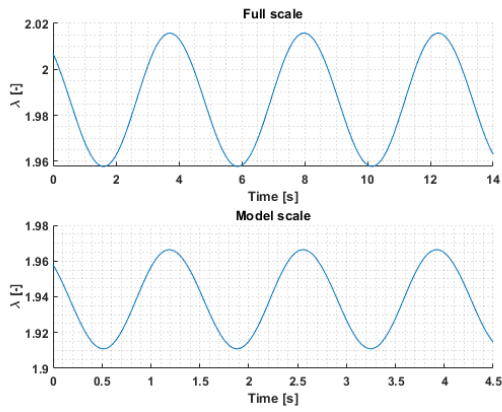


Figure 4.7: Air excess ratio

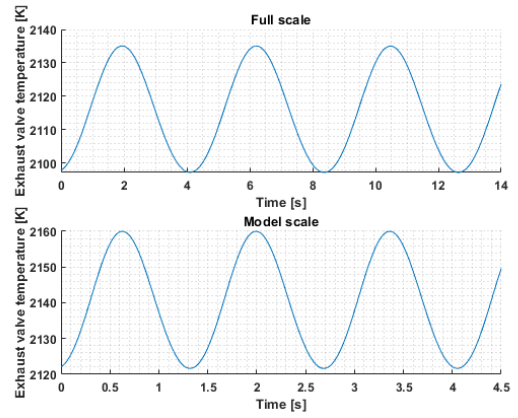


Figure 4.8: Exhaust valve temperature

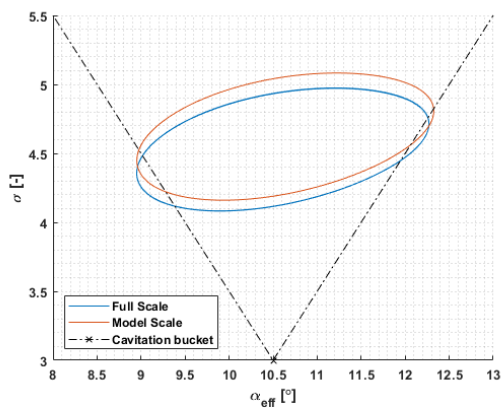


Figure 4.9: Cavitation bucket

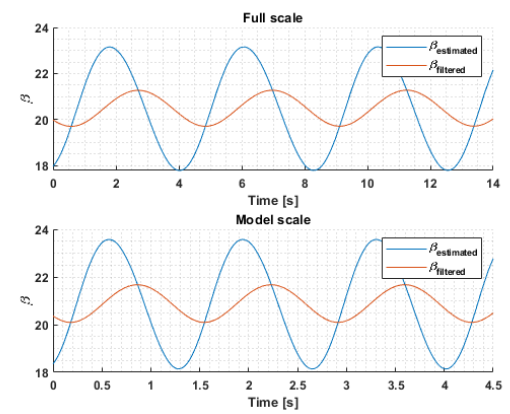


Figure 4.10: Inflow with Kalman filter

There are few differences in the results between full and model scale simulations, as shown in table 4.3. However, these differences are minor, and it can therefore be said that the HIL setup can provide reliable results in dynamic conditions such as waves. Nevertheless, the previously discussed results provide little extra information. Actual HIL experiments can differ due to the hydrodynamic effects, such as the free surface effect. However, minor differences are expected because the full-scale simulations are performed with a validated engine and propeller.

Table 4.3: Difference in waves between full- and model scale simulations

	Δ
n_{virt} [rpm]	0%
Pitch [deg]	1.8%
α_{eff}	1%
Engine speed [rpm]	1.0%
Fuel rack [mm]	2.6%
Air excess ratio [-]	2.5%
Exhaust valve temp [K]	1.2%
bsfc [g/kWh]	0.8%

4.2. Preparation of HIL experiments

For the preparations of the HIL experiments, the limitations of the hardware of the setup is studied. If the components react differently than expected, the dynamic behaviour can be significantly influenced. To be able to perform HIL experiments it is therefore crucial that the hardware is accurate.

4.2.1. Dynamic acceleration comparison

The acceleration of the towing car has no Froude similarity with the acceleration of a free sailing ship. Therefore, the conclusion is already made that it is impossible to perform dynamic acceleration runs with the HIL setup. However, to demonstrate the differences due to dissimilarity, a comparison is made during acceleration in waves. The simulation settings are listed in table 4.4.

Table 4.4: Simulation parameters for acceleration runs

$H_{\frac{1}{3}}$	2.02 m
ω	0.93 rad/s
Waves	Regular
Kalman	Off
Deadband	0°
n_{virt}	0 to 120 rpm
Gain schedule	Off

In figure 4.11, the difference in acceleration can be seen. Note that also here, the x-axis is time scaled. Despite the scaling of the axis, it can be concluded that the towing car in the model scale simulation accelerates too fast with a minimum acceleration speed of 0.3 m/s^2 . This fast acceleration also influences the speed at which the desired virtual shaft speed is reached. Figure 4.12 shows that the virtual shaft speed in model speed is delivered requires half of the time compared to the full-scale free sailing acceleration.

The dissimilarity can also be seen in the dynamic behaviour of the engine. In figure 4.13, the engine speed is depicted. Due to the fast acceleration of the towing car, the engine has no overshoot of its desired engine speed. This same behaviour can be seen in the fuel rack position, air excess ratio and temperatures.

Due to the lower engine speed, the cavitation number is higher in the model scale simulation, as shown in figure 4.14. The full-scale simulation first goes to the bottom of the cavitation bucket and then slowly moves up. Notice that the engine speed is similar at the end of the simulation, and the ellipse in the bucket overlaps.

These simulations confirm that the HIL setup is not suitable to perform dynamic acceleration runs. This is due to the fast acceleration of the towing car. However, at a constant speed, the dynamic behaviour is the same. Therefore, it is confirmed that the HIL setup can be used to study the dynamic behaviour at a constant speed.

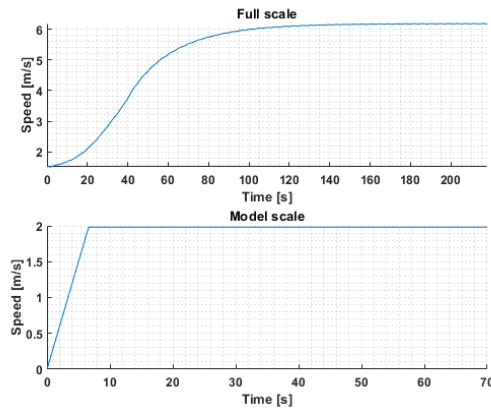


Figure 4.11: Ship speed during acceleration at FS and MS

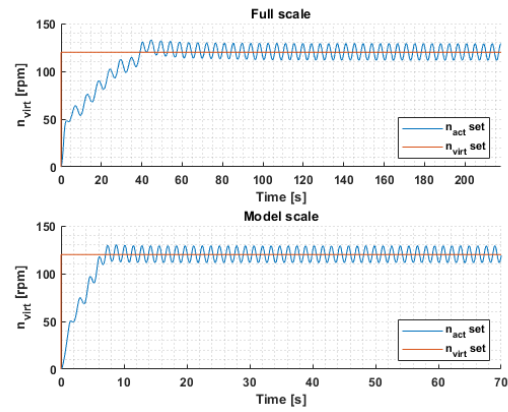


Figure 4.12: Virtual shaft speed during acceleration at FS and MS

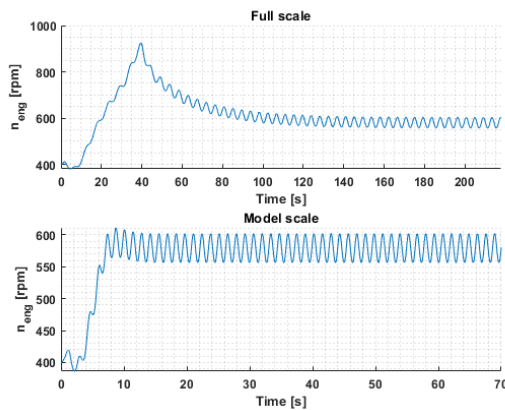


Figure 4.13: Engine speed during acceleration at FS and MS

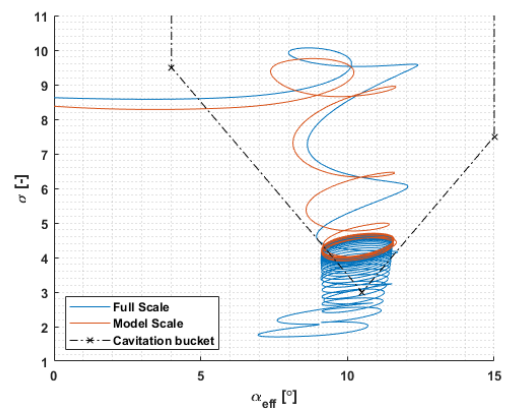


Figure 4.14: Cavitation bucket during acceleration at FS and MS

4.2.2. Hardware CPP

The TU Delft has developed a hardware CPP that can be mounted on the open water HIL setup; it is a scaled C4-40 propeller. A servomotor in the propeller's hub is controlled by the simulation computer and can change the pitch of the blades. The actual pitch setting can be sent back to the simulation computer.

The cables that deliver the power to the motor also carry the control signal for the pitch, using a TCP/IP protocol from and to the computer. Since the current and signal are delivered by the same wire, there is a limitation in the number of control signals. At this moment, the propeller can send and receive a command three times per second. However, several tests have demonstrated that the signal is not always stable.

A sample rate of 0.33 seconds is too slow for low sea states where the wave frequency is higher. In figure 4.15 can be seen that with the open water HIL setup at sea state 4, the APC without Kalman filter cannot deliver a steady virtual shaft speed. The same sinus movement can be seen in the engine speed and PD settings. The reason for the unstable virtual shaft and engine speed is the low sample rate. In figure 4.17, the blue line represents the pitch setting with a high sample rate. The redline shows aliasing due to the low sample rate. The minimal sample rate should be twice the measured frequency; this is called the Nyquist rate.

In the hardware CPP, is also backlash detected. The blades can move five degrees before the servomotor corrects the position. The pitch actuations with the APC strategy in waves fluctuate is approximately 2.3 degrees. Due to the backlash of five degrees, this actuation cannot be detected. Also, the inflow angle is different, resulting in a lower effective angle of attack. Also, the engine speed is higher, causing a lower cavitation number, as can be seen in figure 4.19.

The open water HIL setup can be used to study the dynamic effects of a propulsion plant. However, due to the communication and backlash problems, the results of HIL experiments would not be representative at this moment. Problems with backlash in model scaled CPP systems have also caused difficulties in other studies (Tanizawa et al. [2014] and Kitagawa et al. [2018]).

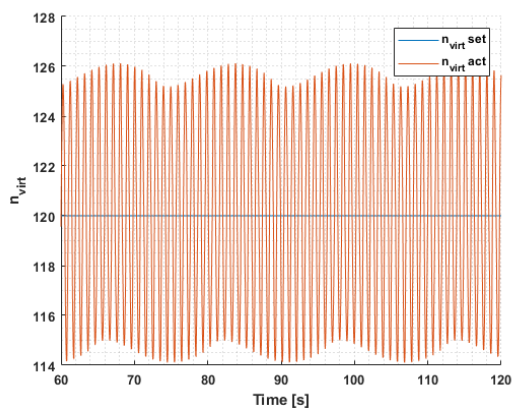


Figure 4.15: Virtual shaft speed due to low sample rate

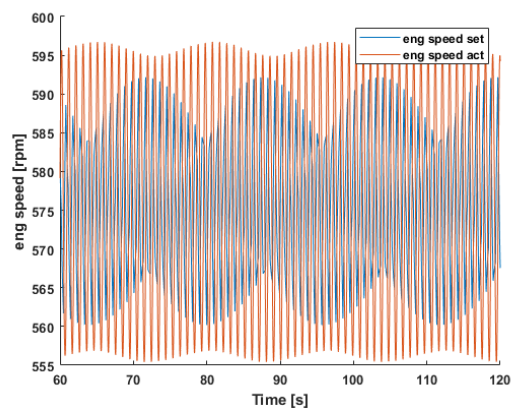


Figure 4.16: Engine speed due to low sample rate

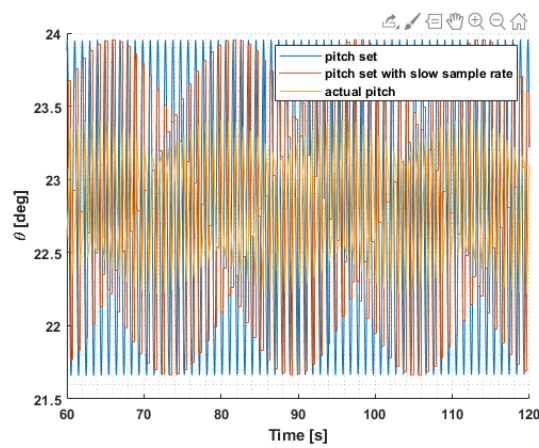


Figure 4.17: Pitch due to low sample rate

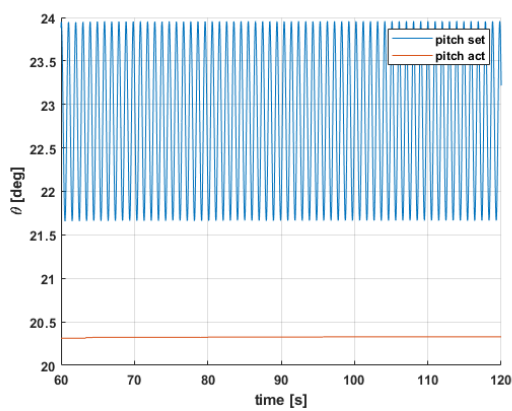


Figure 4.18: Pitch due to backlash in hardware CPP

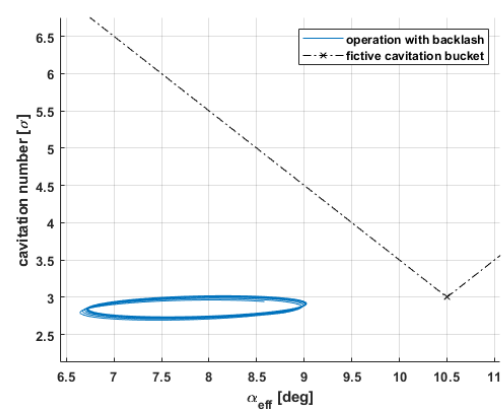


Figure 4.19: Cavitation bucket due to backlash in hardware CPP

4.2.3. Discussion

The technical challenges must be solved before the HIL setup can be used to perform an experiment. So the sample rate needs to increase, the backlash minimised, and the towing car should be modified so it can accelerate with Froude similarity. And even though in regular waves, the open water HIL setup provides little less extra information than a numerical model. It is possible that in extreme conditions, such as propeller ventilation, the setup can provide valuable information. Several studies have been done research on propeller ventilation; however, they all have a significant margin of uncertainty (Kozłowska et al. [2020]). Complex hydrodynamic phenomena are taken into account in the hardware scaled CPP. Though, the results of an open water HIL setup with ventilation should not be trusted without further research. Savio et al. [2013] compared full and model scale ventilation. The comparison is valuable and showed difficulties with scaling effects. The air can be assumed incompressible in model scale, while this is not true in full-scale. It is resulting in differences between the full and model scale result, even with Froude similarity.

The new cavitation tunnel of the TU Delft has a pressure range from the vapour pressure to 2 bar overpressure, making it possible to simulate the cavitation behaviour of the model scaled propeller. Nevertheless, it is hard to simulate waves in the cavitation tunnel. However, by measuring with different advance speeds it is, likely, possible to see how the propulsion plant with its control systems behaves.

An alternative is to use the open water HIL setup in MARIN's Depressurised Wave Basin (DWB) in the Netherlands. This towing tank can decrease the atmospheric pressure, making it possible to determine the propeller's cavitation behaviour [25]. However, a challenge would be to operate the setup by remote control due to the vacuum. Nevertheless, in this basin, the open water HIL setup can provide new information about the dynamic behaviour of a propulsion plant and its controller, especially in situations where cavitation occurs.

Currently, there is a significant difference between the modelled and measured values during a turn, as is concluded by Schulten 2005. Furthermore, Coraddu 2013 reported that there are relative slow wake speed fluctuations in turns. Therefore, expects Geertsma 2019 that APC can maintain a constant angle of attack during these turns. Placing the propeller under an angle makes it possible to simulate oblique inflow and determine with a HIL experiment if this expectation holds. Oblique inflow is also relevant for ships that have a wind-assisted propulsion system. The results of such experiments can give new insights in improving the numerical models and control strategies. However, the applied angle is limited due to the forces that the strut of the setup will experience when it is moving forward.

HIL experiments do not replace full-scale trials. The HIL setup can measure the thrust, which is used to determine the inflow angle. However, in an actual system, the measurement/noise ratio can be different and can result in difficulties to estimate the inflow. Another reason is that it is likely that an actual system has delays that influence the control strategy's performance. An example of such a delay is the time it takes for the hydraulic system to deliver the needed pressure to start a pitch actuation.

4.3. Summary

In the HIL setup, a full-scale diesel engine model drives the scaled hardware CPP. So, as a result, the in- and output of the CPP need to be scaled. But also, the time-dependent phenomena need to be time-scaled. Due to that reason, the integral gain of the speed governor, the time delays of the pitch actuation, exhaust filling and fuel injection and the torque rate limiter are time-scaled. The Kalman filter predicts one timestep ahead. The time step is the same, but the disturbance is more significant in one-time step due to the scaling effects. Due to that reason, the Kalman uncertainties are also scaled.

A comparison is made between the full-scale free sailing simulation and the model scale open water HIL simulation to determine if the Froude scaling laws are applied correctly at a constant speed. In the simulation without any waves, the differences in diesel engine parameters are minor; the most significant difference was 3.7 per cent. Due to the slight difference in simulation results, it is concluded that Froude scaling is applied correctly.

The next step is to compare the results in waves. A similar conclusion can be drawn after assessing the outcomes of the dynamic simulations. The most significant difference is even more minor, 2.6 per cent. Therefore, it can be assumed that the HIL setup can simulate the non-linear behaviour at a constant speed.

It is not worthwhile to perform HIL experiments with the current setup. First, the low sample rate of the pitch's control signal results in aliasing, making the controller unstable. Secondly, the five degrees backlash in the blades of the CPP. Novel control strategies require an accurate pitch setting. Due to the backlash, the impact of the APC strategy cannot be observed. Finally, due to Froude dissimilarity in the acceleration of the

towing car, is it not possible to do dynamic acceleration runs with the HIL setup.

This study aims to determine if HIL experiments can contribute to improving numerical models of propulsion plants. No actual experiment is performed; therefore, it is discussed if HIL can add value in numerical models. Other studies have used HIL setups to study propeller ventilation effects. However, it can be questioned if Froude scaling is correct in this circumstance. This is since it can be assumed that air is incompressible in model scale, but this is not true in full scale. Nevertheless, it is possible to force an oblique flow on the hardware propeller. Oblique HIL experiments can confirm if APC is able to keep the required angle of attack in turns. The results can be used to improve the numerical model and the control strategy.

It is unlikely that HIL experiments entirely replace full-scale trials. This is due to two reasons. First, because in existing propulsion systems, there are delays that can influence the performance of the control strategy. Secondly, another measurement/noise ratio of the sensors could result in a different outcome of the control strategy.

5

Conclusions and recommendations

After climbing a great hill, one only finds that
there are many more hills to climb

Nelson Mandela

The shipping industry is forced to reduce emissions and radiated noise to lower their impact on the environment and limit global warming. A way to achieve this is to use novel control strategies. Often numerical models are used to predict the performance of a modern control strategy for propulsion plants. However, in these models, the hydrodynamic effects are frequently simplified. An alternative is towing tank experiment and full-scale trials. However, these methods also have their limitations. Towing tank experiments have scaling effects, and full-scale trials are complex and expensive to set up. For the latter, it is also harder to compare the results because the environmental conditions are often different. Hardware In the Loop experiments can combine the benefits of numerical models and towing tank experiments. Results could provide new insights and be used for improving control strategies and mathematical models.

The main question is answered with a case study and is split up into three sub-questions. The propulsion plant of an ocean-going patrol vessel is used. This plant consists of a diesel engine with a controllable pitch propeller and is controlled by the novel adaptive pitch control. To achieve the most effective inflow of the propeller, the pitch is continually changing in waves. More actuations result in less time between maintenance and, therefore, a lower operational availability. Also, current pitch actuations systems are not able to keep up with the required pitch setting. Due to these two reasons, it is studied how the pitch actuations can be reduced and the impact on the propulsion plant's dynamic performance.

5.1. Answer to research questions

Adding a tuned Kalman filter with a small deadband in the APC makes it possible to reduce the pitch actuations. However, the propeller can cavitate more due to the more extensive operation area outside the cavitation bucket. In irregular waves, when a ship encounters different waves sizes and frequencies, the reduction of 92 per cent can be achieved in sea state four. However, at a cost of approximately 21 per cent more operating time outside the cavitation bucket. The other measures of performance are hardly affected by the addition in the control strategy.

To determine if the HIL setup can simulate the dynamic behaviour of a propulsion plant, full-scale free sailing and model scale open water HIL simulations are compared. It is crucial that Froude scaling is applied correctly to get similar results. Huijgens [2021] already demonstrated that a diesel engine without non-linearities could be emulated with HIL by applying a virtual flywheel and a friction torque correction.

Furthermore, Huijgens [2021] applied Froude scaling. The input to and output from the hardware components were already scaled accordingly. Also, the integral gain of the speed controller of the fuel injection and the thrust and torque coefficients are correctly scaled. Nevertheless, the difference in this propulsion model is that in this thesis, the model takes into account non-linearities. Therefore, dynamics should also be Froude scaled, such as the time delay for filling the exhaust receiver, pitch actuation, and fuel injection are time scaled. The same scaling is applied in the torque limiter in the APC. Finally, the Kalman measurement

and process uncertainty are also scaled. A Kalman filter is predicting one timestep ahead. The timestep in the models stays the same; however, disturbances due to the waves are more extensive because of the higher frequency due to time scaling. Therefore, scaling of the Kalman uncertainties is required.

With these scaling parameters applied, a comparison is made between the full- and model scale simulations. The results are similar between the two models at a constant speed, with and without waves. The minor differences are a result of the hull that is taken into account in the full-scale simulations, while there is no hull interaction with the open water setup. Nevertheless, it can be concluded that the applied scaling parameters are correct.

With the non-linear propulsion plant scaled correctly, it is possible to determine the answer for the final sub-question. However, no actual HIL experiments are performed due to the physical limitations of the HIL setup. Backlash in the blades, sample rate of the pitch and acceleration limitation of the towing car are making it impossible to do accurate experiments. Nevertheless, we discuss how the HIL setup can contribute to improving numerical models and control strategies.

Full-scale simulations can be used to prove that improvements in the control strategies are effective. If the scaling laws are applied correctly, the open water HIL setup can provide similar results as full-scale numerical models. However, it is expected that no extra information in dynamic behaviour can be obtained in waves at a constant speed. An option is to perform propeller ventilation experiments, determine the propulsion plant's impact, and simulate the controller's reaction. However, air can be assumed incompressible in model scale, while this is not true at full scale. This could result in scaling effects, even when Froude scaling is applied.

Another option is to place the HIL setup under a small angle to simulate a turn and determine the effects of oblique inflow. It is expected that APC can keep the effective angle of attack in turns. This could be assessed in a controlled environment with the HIL setup. Information about the dynamic responses with oblique inflow could be used to expand the numerical model and improve the control strategy.

A desirable outcome would be if HIL experiments could replace or shorten full-scale trials. However, it is not expected that HIL can provide extra information in standard sailing conditions. A full-scale trial to determine the performance of adaptive pitch control is therefore still valuable, especially to determine the influence of delays in an actual system and tuning the controller.

5.2. Additional conclusions

Due to gain scheduling, the fast PI controller was activated if the engine speed dropped below 450 rpm. Full-scale simulations showed that the fast PI controller has a negative influence on all the measures of performance. Therefore, only the slow I controller was used for all engine speeds if the requested virtual shaft speed was above zero. Also, the over- and underspeed P gain is still active. This resulted in a better dynamic performance of the propulsion plant.

Switching off the fast PI for all engine speeds has positive effects in this case study. However, the focus of this thesis was not on improving the speed controller of the diesel engine. Different propulsion plants can have different responses. Therefore, it is advised to study the effects of gain scheduling and APC with different propulsion plants.

5.3. Recommendations

This study demonstrated how pitch actuation can be reduced and how a non-linear propulsion model can be implemented in the HIL setup and prepared HIL experiments. Nevertheless, no actual experiments are performed. The recommendations can be used to improve the setup so it can be used for future research.

5.3.1. Regarding the HIL setup

The sample rate of the pitch of the CPP is three times per second. If the wave frequency becomes too high, aliasing of the pitch setting can occur. This results in an unstable pitch setting, the control strategy compensates this with the engine speed setting. However, the settings become unbalanced. Therefore, to prevent aliasing, the sample rate should be twice as high as the wave frequency to prevent aliasing.

There is also a mechanical issue with the hardware CPP, there is a backlash in the blades. Due to this, the blades can move five degrees freely before the servo motors can correct their position. As a result, the pitch actions with a novel control strategy that controls the propeller inflow can not be observed.

Finally, it is recommended to investigate applying a variable speed drive with accurate control acceleration speed on the towing car. This is to control the acceleration of the towing car accurately. This, because in the current setup, it is not possible to accelerate with Froude similarity.

5.3.2. APC with Kalman filter and deadband

To increase the time between maintenance of the actuations systems of the CPP, it is worthwhile to implement the APC with Kalman filter and deadband. The simulations showed that at sea state four, an actuation reduction of 92 per cent could be achieved in irregular waves. In sea state five, this was almost 61 per cent.

However, the propeller cavitates more due to the filter and deadband. Especially for navy ships, this can be life-threatening if there is a submarine or mine threat. Therefore, we recommend to have the option to switch the filter and deadband off. Because when the filter and deadband are activated, the propeller operates 25 per cent more time outside the cavitation bucket. Nevertheless, the cavitation performance is still significantly better than with a combinator curve controller.

For APC to function correctly, an accurate inflow estimation is crucial. The simulations and HIL experiments can demonstrate the concept of the inflow measurement. However, at full-scale the noise to measurement ratio can be different. Therefore, it is still required to perform a full-scale measurement to demonstrate the accuracy of the inflow estimation.

Another reason to perform a full scale is to determine the performance of APC in an existing propulsion system. There are likely different reasons for delays resulting in different dynamic behaviour. An example of a delay is the pressure build-up in the hydraulic actuation system.

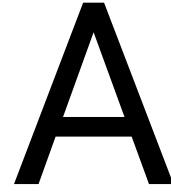
5.3.3. Improving numerical models and control strategies

To do further research with the HIL setup, the sample speed must increase and the backlash minimised. Also, the towing car needs to be modified to accelerate with Froude similarity. It is concluded that at constant speed in waves, the setup provides little extra information. However, further research must be performed in ventilation and oblique inflow to determine if the setup can improve models and control strategies.

Nevertheless, HIL experiments do not replace full-scale trials. These complex trials are still required because it is expected that the noise/measurement ratio of the sensors is different in a full-scale system. This could result in different responses from the control strategy. Furthermore, delays in an existing system will likely influence the performance of the propulsion plant. Full-scale trials are therefore required to tune the control parameters to achieve the required performance.

5.4. Closing summary

This research proposed to add a Kalman filter and deadband to the APC strategy to reduce pitch actuations. A trade-off is that the propeller cavitates 25 per cent more. However, the other control objectives of the dynamic performance of the propulsion plant are hardly influenced. By correctly implementing scale effects, it is possible to study the dynamic behaviour of the plant with the open water HIL setup. Still, in waves, HIL experiments are expected to provide little extra information compared to numerical models. Nevertheless, oblique inflow can be forced in controlled conditions and give new insights to improve numerical models and control strategies, thus investigating the behaviour in turns. These improvements can lead to emission and noise reduction to decrease the environmental impact and prevent detection of naval vessels under threat.



Theoretical background

The theoretical background gives an overview of relevant knowledge for this master thesis. This is done by elaborating the background on scale effects, adaptive pitch control, and the diesel engine model. An extensive description can be found in the dissertation of Huijgens [2021] and Geertsma [2019].

A.1. Scale effects

Relevant scale effects are hydrodynamic and mechanical scale effects. The former results in incorrect forces due to inaccurate scaled flow and water around the propeller. Incorrect scaling of the moment of inertia will result in mechanical scale effects.

Hydrodynamic scale effects

The propeller in the HIL setup is smaller than of real frigate. Due to that reason, scale effects will play an essential role in HIL experiments in a towing tank. The possibility of dealing with these effects is by keeping dimensionless parameters, such as the Froude and Reynolds number, the same for the model and the full-scale propeller.

There are 19 dimensionless parameters relevant in fluid mechanics. Examples are the Mach, Prandtl, and Rayleigh number. However, for this master thesis, the relevant parameters are the Reynolds and Froude number. These parameters are for incompressible flows with a free surface.

The Reynolds number is always significant, especially when the inertia and viscous forces are essential in a flow. However, it is almost impossible to achieve similarity in full scale and the model. The Froude number is critical when gravity forces become relevant and if there is free-surface or waves (Journee and Massie [2001], White [2008]). In table A.1, an overview of these dimensionless parameters is given.

Table A.1: Dimensionless parameters (White [2008], p. 311)

Parameter	Definition	Qualitative ratio of effects	Importance
Reynolds number	$Re = \frac{vL}{\nu}$	$\frac{Inertia}{Viscosity}$	Almost always
Froude number	$Fr = \frac{v^2}{gL}$	$\frac{Inertia}{Gravity}$	Free-surface flow

A scale model will behave the same as a full-scale ship if all the dimensionless parameters are similar. However, in practice, this is not possible during experiments. The following paragraphs explain why this is impossible. Instead of complete similarity, it is common to use specific types of similarity. The most common are geometric, kinematic and dynamic similarity.

In a model with geometric similarity, all lengths are scaled linearly in comparison with the full-scale model. This results in similar flow directions and the same angles for the surroundings. In the upper illustration in figure A.1, spheres with geometric similarity are shown. Below the ellipsoids are dissimilar. Kinematic similarity entails that the model's length and time scale ratio and full scale are the same. This can be achieved by keeping the Froude numbers equal this is achieved.

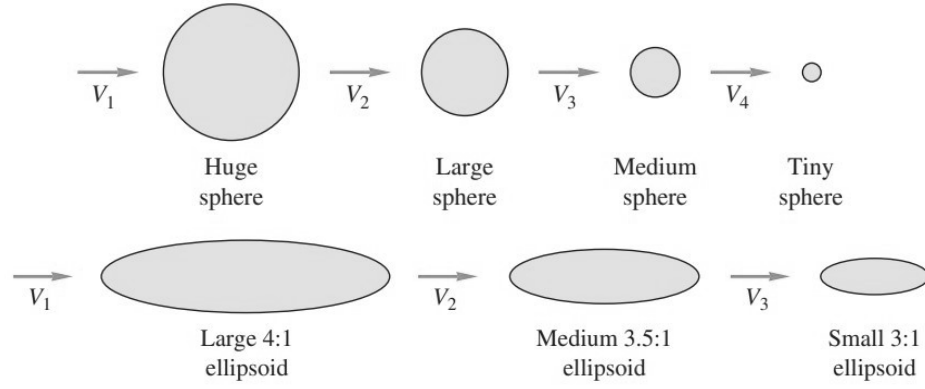


Figure A.1: Similarity (above) and dissimilarity (White [2008], p. 317)

$$Fr_{MS} = \frac{v_{MS}^2}{gL_{MS}} = \frac{v_{FS}^2}{gL_{FS}} = Fr_{FS} \quad (\text{A.1})$$

The following equation holds if the length scale ratio is linear:

$$\lambda = \frac{L_{FS}}{L_{MS}} \quad (\text{A.2})$$

Combining equation A.1 and A.2 will result in the following velocity and time scale equations:

$$\frac{v_{FS}}{v_m} = \sqrt{\frac{L_{FS}}{L_{MS}}} = \sqrt{\lambda} \quad (\text{A.3})$$

$$\frac{t_{FS}}{t_{MS}} = \frac{\frac{L_{FS}}{v_{FS}}}{\frac{L_{MS}}{v_{MS}}} = \frac{L_{MS}}{L_{MS}} \frac{v_{MS}}{v_{FS}} = \sqrt{\lambda} \quad (\text{A.4})$$

By keeping the Reynolds number of the model and full-scale equal, it possible to achieve dynamic similarity. Then the length, time, and force scale are the same.

$$Re_{MS} = \frac{v_{MS}L_{MS}}{\nu_{MS}} = \frac{v_{FS}L_{FS}}{\nu_{FS}} = Re_{FS} \quad (\text{A.5})$$

Combining this with equations A.2 and A.4 will result in the following equation:

$$\frac{v_{fs}}{\nu_m} = \frac{L_{fs}}{L_m} \frac{v_{fs}}{\nu_m} = \lambda \sqrt{\lambda} \quad (\text{A.6})$$

λ for the HIL setup is 9.697, so $\lambda\sqrt{\lambda} = 30.20$. The viscosity of water is $1.10 \cdot 10^{-6} \text{ m}^2/\text{s}$. To achieve the same Reynolds number a fluid must be used with a viscosity of $3.64 \cdot 10^{-8} \text{ m}^2/\text{s}$. Such a fluid does not exist. A liquid that comes relatively close this viscosity is mercury with $1.17 \cdot 10^{-7} \text{ m}^2/\text{s}$. However, this fluid expensive and unhealthy.

The Reynolds number of an open water propeller is determined with the equation A.7:

$$Re_{0.7} = \frac{c_{0.7} \sqrt{v_a^2 + (0.7\pi nD)^2}}{\nu} \quad (\text{A.7})$$

Where $c_{0.7}$ is the chord length at 0.7R.

It is possible to extrapolate the model Reynolds data to full-scale Reynolds data. However, extrapolation will result in results with large uncertainties. Nevertheless, it is common practise to correct the towing tank's viscous friction according to the ITTC Open Water Test procedure (ITTC [2014a]). However, Huijgens [2021] showed that the similarity in the Reynolds number hardly influences the dynamic effects.

As stated above the scaling factor for length, linear speed and time are derived. Similar derivations are made for energy, mass, moment of inertia and other relevant parameters. Without derivation, these scaling factors from model to full scale are given in table A.2 (Huijgens [2021]).

Table A.2: Scaling factors

	λ -power
Distance	1
Energy	4
Linear speed	0.5
Mass	3
Moment of inertia	5
Power	3.5
Rotative speed	-0.5
Time	0.5
Torque	4

As mentioned earlier, it is practically impossible to scale viscosity correctly. Imprecise scaling can result in static and dynamic effects. A static result is that the non-dimensional thrust coefficient can have an offset or rotation in the open water diagram, as shown in figure A.2.

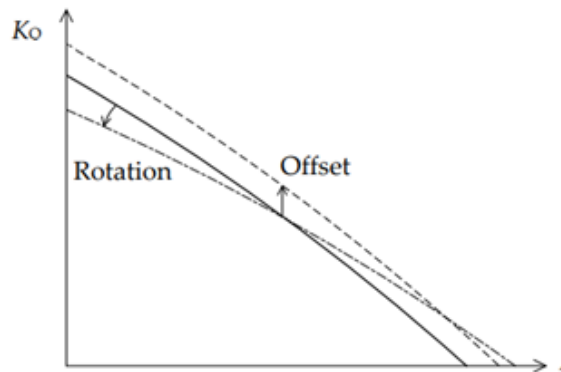


Figure A.2: Open water diagram with static effect (Huijgens [2021])

Kuiper [1992] developed a model to determine the offset of the torque and thrust coefficients for a Wageningen B series propeller. The International Towing Tank Conference adopts the same model for Open Water Test (ITTC [2014a]). The following equations are used in the model:

$$K_T = \frac{T}{\rho n_p^2 D_p^4} \quad (\text{A.8})$$

$$K_Q = \frac{Q}{\rho n_p^2 D_p^5} \quad (\text{A.9})$$

Where K_T and K_Q are the dimensionless thrust and torque coefficient. T the thrust, Q the torque, ρ the density of fluid, n_p and D_p the revolutions and the diameter of the propeller.

There is a discussion on whether this model is accurate enough. These equations assume a linear correlation between change in friction drag and torque and thrust coefficients. This is not always true, especially for modern propeller design. Brown et al. [2014] concluded that the traditional ITTC procedure was not valid for a tip loaded propeller. Kuiper [1992] already pointed out that the statistical basis for this assumption is small, and this should be kept in mind by assessing accuracy.

Another argument against this model is that it does not distinguish between a propeller with or without a camber. And finally, the extrapolated results for full-scale propeller are dependent on the Reynolds number in which the model test is performed (Helma et al. [2018]). Huijgens [2021] demonstrated that using the model from Kuiper [1992] will result in a 5% lower static torque effect. However, the dynamic effects are so small they could be neglected.

The new methods to determine the thrust and torque coefficients by Brown et al. [2014] and Helma et al. [2018] show promising results. However, they all conclude that more research must be done to improve their models. The ITTC uses the model from Kuiper [1992], and at the moment this is common practice. This is the reason why equation A.8 and A.9 are used in this master thesis research.

Dynamic effects can result in different vortex shedding around the propeller. This can occur due to interactions between propeller and appendages and has been the focus of many studies. They all concluded that the impact of dynamics is also relatively small. It can be concluded that keeping Froude similarity and having a discrepancy in the Reynolds number will lead to comparable results with full-scale measurements.

Mechanical scale effects

Mechanical scale effects are a result of incorrect scaling of the moment of inertia. As a result, the dynamic behaviour of the shaft distorted (Huijgens [2021]). This can lead to a difference in angular acceleration, as can be seen in equation A.10.

$$\frac{d\omega}{dt} = \frac{M_d - M_l}{I_{tot}} \quad (\text{A.10})$$

Where $\frac{d\omega}{dt}$ is the angular acceleration, $M_d - M_l$ the drive minus the load torque and I_{tot} the total moment of inertia of the propulsion system. Assuming that the drive and load torque are correctly scaled, a difference in the total moment of inertia will result in inaccurate shaft dynamics.

The total moment of inertia can be divided into the inertia of the propulsion motor (I_d), the propeller (I_p) and the added mass (I_{H_2O}) as can be seen in equation A.11.

$$I_{tot} = I_d + I_p + I_{H_2O} \quad (\text{A.11})$$

The used material and its shape determine the inertia of the motor and the propeller. The added mass inertia depends on the advance speed, angular velocity, propeller pitch, and the number of blades and is a complex hydrodynamic phenomenon.

If a body is moving at a constant speed through unbounded fluid, it experiences no force. However, if that body is accelerating, it experiences forces. This force is the added mass or added moment of inertia (Lewandowski [2004], p. 36).

There are two empirical approaches to determine the added moment of inertia of a propeller's entrained water. The first method is with a propeller in rotating condition, and the second method is in locked condition. Wereldsma [1965]) did his experiments in rotating condition with different propellers. Burrill and Robson [1962] have done many experiments to determine the added mass in locked condition and came up with an empirical expression. Huijgens [2021] used this expression to determine the added mass and moment of inertia. The values that are chosen are constants. However, this is not correct if advance speed, angular velocity, propeller pitch is not constant.

MacPherson et al. [2007] showed the errors in the earlier mentioned empirical approaches and gave a numerical improvement. For a 6-bladed propeller, this new method overestimates. Nevertheless, it takes into account the P/D ratio. For a CPP, this ratio is not constant, and as a consequence, the added mass and moment of inertia can change if the pitch adapts. The expression for a 4-bladed propeller is shown in the following expression.

$$I_{H_2O} = \left(0.00394 \frac{A_e}{A_O} \frac{P}{D} - 0.00087 \right) \rho D^5 \quad (\text{A.12})$$

Where $\frac{A_e}{A_O}$ is the expanded area ratio and $\frac{P}{D}$ the blade pitch ratio. Both parameters are dimensionless.

However, it is expected that the effect of the added moment of inertia is relatively small, and the proposed method will give enough accuracy. Nevertheless, it is worthwhile to do separate research into accurate estimations of added mass, as is also suggested by Huijgens [2021]. The moment of inertia can be corrected by adding material, such as a flywheel, or by removing material. However, this is not possible in the HIL setup without influencing the underwater shape. Huijgens [2021] used a "virtual flywheel" by adding an inertia correction (I_c) to equation A.13.

$$I_{tot} = I_d + I_{prop} + I_{H_2O} + I_c \quad (\text{A.13})$$

This correction is the difference between the ideal mechanical inertia ($I_{mech,id}$) and the mechanical inertia of the HIL setup ($I_{mech,HIL}$). The later must be determined during HIL experiments.

The load torque can be split into the friction torque and the propeller load torque as shown in equation A.14.

$$M_l = M_{fr} + M_{prop,hydro} \quad (A.14)$$

The friction and propeller load torque are determined with the following equations.

$$M_{prop,hydro} = \rho n_p^2 D^5 K_Q \quad (A.15)$$

$$M_{fr} = k_t i_{fr} \quad (A.16)$$

Where k_t is the motor torque constant and i_{fr} the current friction. Huijgens [2021] measured the current friction by enforcing a slow, sinusoidal variation of the shaft speed around an equilibrium. By measuring current at different angular velocities, a fit is made with polynomial regression. These measurements were performed outside the towing tank for inertia identification and underwater for the HIL experiments. The difference between dry and wet measurements can be explained by the additional friction of the water on the shaft.

The motor torque constant k_t is given by the manufacturer. However, it might not be accurate. To determine this constant Huijgens [2021] derived the following equation:

$$k_t = \frac{M_{prop}}{i_m - i_{fr}} \quad (A.17)$$

Where M_{prop} is the measured propeller torque, i_m the measured motor current and i_{fr} the friction current.

The motor torque constant determined by Huijgens [2021] was 3.8% higher than the manufacturer's value. This could be because one, a combination or all of the following reasons:

1. Manufacturers specifications are incorrect.
2. Current is not correctly measured.
3. The estimated friction current is too high.
4. The measured torque is too high.

It is unclear which of these reasons are the cause of the deviation of the manufacturer's value.

A.2. Adaptive Pitch Control Strategy

The interaction between the diesel engine and the CPP will be controlled by adaptive pitch control. The inputs for this control is the effective angle of attack and the engine speed. With these two parameters are used to influence the Measures of Performance (MOP's) as proposed by Geertsma [2019]:

1. Provide requested virtual shaft speed.
2. Maintain operation within cavitation bucket for the broadest possible operating conditions.
3. Minimise fuel consumption across the ship speed profile and for all operation conditions.
4. Maintain engineer air excess ratio within predefined limits.
5. Prevent engine over- and under-speed.

Virtual shaft speed

Adaptive Pitch Control uses the estimated effective angle of attack and the engine speed to control to optimise the fuel consumption, engine thermal loading and cavitation noise while providing the requested virtual shaft speed Geertsma [2019]. The virtual shaft speed is often used on navy frigates because it has almost a linear relationship with the ship speed. This virtual speed can be determined with the following equation:

$$n_{virt}(t) = \frac{P_{pd}(t) - P_{pd,0}}{P_{pd,nom} - P_{pd,0}} n_p \quad (\text{A.18})$$

Where P_{pd} is the actual pitch ratio, $P_{pd,0}$ the pitch ratio at zero thrust, $P_{pd,nom}$ the nominal pitch ratio and n_p the actual shaft speed.

The virtual shaft speed is an input for the speed setpoint. It is possible to change the actual pitch $P_{pd}(t)$ as can be seen in equation A.19:

$$n_{e,set}(t) = \frac{P_{pd,nom} - P_{pd,0}}{P_{pd}(t) - P_{pd,0}} n_{virt,set}(t) \quad (\text{A.19})$$

Cavitation Bucket

The effective angle of attack is the second input for the control system. This angle is estimated with the thrust and torque sensor that is located in the shaft of the HIL setup behind the propeller. Together with the known rotational speed of the shaft, it is possible to determine the effective angle of attack (α_{eff}) (Vrijdag [2009]).

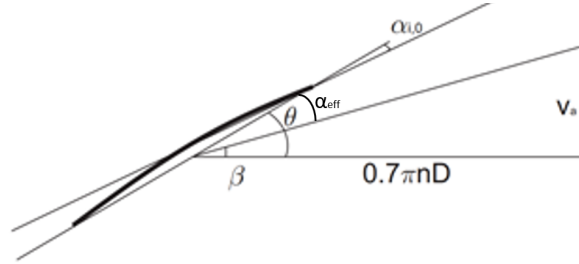


Figure A.3: Velocity triangle (Vrijdag [2009])

In figure A.3, the inflow angles are sketched. These are dependent on advance speed, rotational speed, wakefield, propeller geometry and the loading dependent induced velocities. From this figure, the effective angle of attack can be derived.

$$\alpha_{eff} = \theta - \beta - \alpha_i \quad (\text{A.20})$$

$$\alpha_{eff} = \text{atan}\left(\frac{P_{0.7R}}{0.7\pi D}\right) - \text{atan}\left(\frac{c_1 V_a}{0.7\pi n D}\right) - \alpha_i \quad (\text{A.21})$$

The effective angle of attack is the pitch (θ) minus the flow angle (β) and the correction for the shock-free entry angle (α_i). c_1 is the correction factor, also known as the Vrijdag coefficient, which can be used for tuning. By choosing the correct c_1 it is possible to calibrate the α_{eff} in such a way that the cavitation buckets overlaps for different pitch settings (Vrijdag [2009] pp. 116 - 120).

To prevent cavitation, the effective angle of attack must stay within the cavitation bucket. Cavitation occurs when water changes from liquid to gas, due to low pressures in a flow. On the y-axis of the bucket is the dimensionless cavitation number:

$$\sigma_n = \frac{p_o - p_v + \rho g z}{0.5 \rho n^2 D^2} \quad (\text{A.22})$$

Where p_o is the atmospheric pressure, p_v is the vapour pressure of the (sea)water, ρ is the density of the (sea)water, g the gravitational acceleration, z the water height above the propeller shaft, n rotational shaft speed and D the propeller diameter.

Traditionally on the x-axis, the torque or thrust coefficient was shown. However, if the angle of attack would change than would change the location of the bucket also. This would be inconvenient for a propulsion

system with a CPP. For this reason, the effective angle of attack is used on the horizontal axis. As a result, the bucket will not shift due to pitch changes. Figure A.4 illustrates a sketch of the cavitation bucket. Cavitation may occur inside the bucket due to dynamics of waves and ship motions (Schulten [2005]).

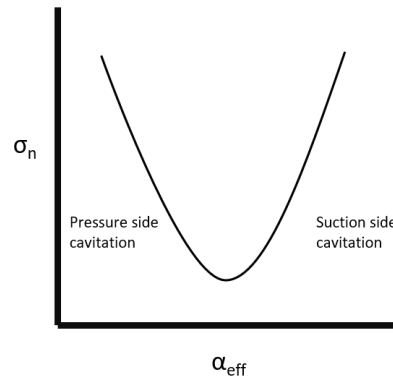


Figure A.4: Cavitation bucket

Fuel consumption

The third control objective is to minimise fuel consumption. The operating points of the diesel engine, gear-box, shaft and propeller determine the fuel consumption. In figure A.5 the specific fuel consumption of an engine is shown. It is illustrated that the fuel consumption is not constant for the same delivered power. The control system will try to get the engine's operation point in the lowest specific fuel consumption at the required power.

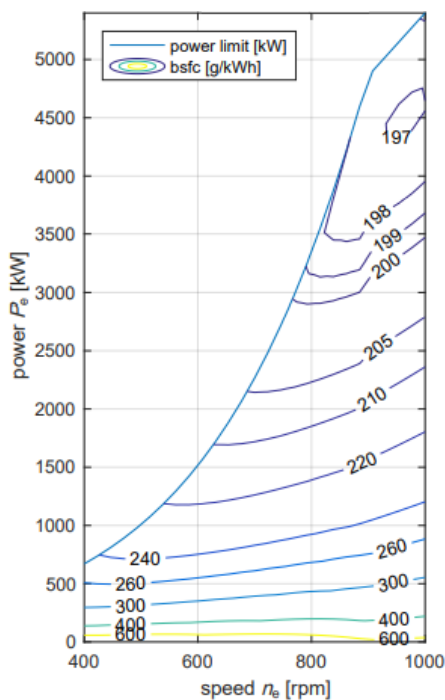


Figure A.5: Specific fuel consumption (Geertsma [2019])

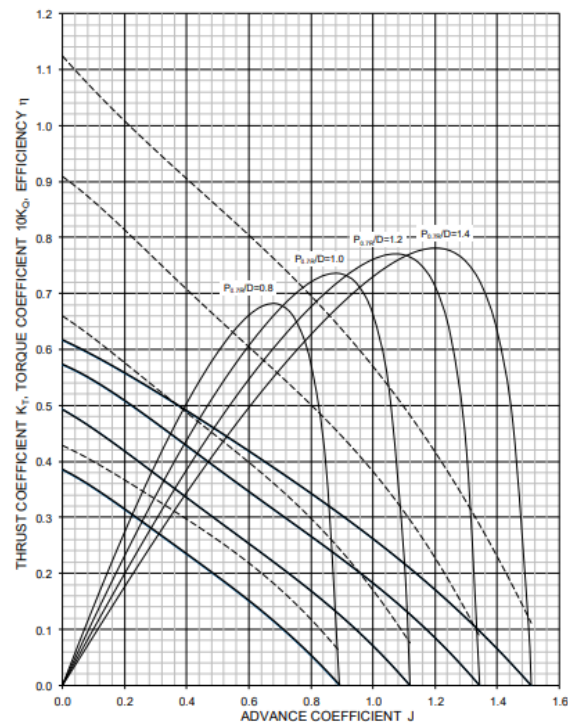


Figure A.6: Open Water Diagram (Dang et al. [2013])

The losses in the gearbox and shaft are relatively small and are not considered for the control strategy. However, the operating point of the propeller has a significant influence. In figure A.6 the open water characteristics are illustrated of a controllable pitch propeller. The maximum efficiency is not the same for different pitches. Also, the advance ratio coefficient (J) influences the efficiency. The advance velocity v_a , the pro-

propeller speed n_p and the propeller diameter (D) determine the advance ratio coefficient as can be seen in the following equation:

$$J = \frac{v_a}{n_p D} \quad (\text{A.23})$$

Keeping the propeller torque coefficient constant will result in low fuel consumption. However, torque control will result in a fluctuating engine speed. This will result in an changing effective angle of attack and harms the virtual shaft speed and cavitation.

If the Froude number is low, the assumption is that the resistance curve is cubed and a constant effective angle of attack will also result in a constant torque coefficient Geertsma [2019]. The Froude number of the HIL setup is low. For this reason, a setpoint value of the effective angle of attack will result in low fuel consumption.

Engine thermal loading

By burning too much fuel in a short amount of time without enough cooling capacity, an engine can be thermally overloaded and increase emissions. This can result in less time between necessary overhaul. If all the air is burned in the cylinder, then there is no cooling capacity left. It is therefore relevant to keep some air in the combustion chamber after combustion for cooling. The amount of air left for cooling is called the engine air excess ratio (λ).

$$\lambda = \frac{m_{ca}}{m_a} \quad (\text{A.24})$$

Where m_{ca} is the mass of the combustion air and (m_a) is the total amount of air in the process (Stapersma [2010a]).

To prevent thermal overloading, it is essential to keep the engine air excess ratio above a minimum value. There are two ways to achieve this goal. First, by limiting the fuel pump position based on the charge pressure. Secondly by reducing the angle of attack set point.

Geertsma [2019] has demonstrated that torque control can eliminate these fluctuations due to turbocharger lag. However, as mentioned in the earlier section, torque control will fluctuate engine speed and negatively influence the angle of attack. Instead of torque control, it is possible to use slow integrating speed control. This type of control has good performance in waves and shows similar dynamic behaviour as torque control.

During acceleration, the engine air excess will be lower than the theoretical value because of the turbocharger inertia. Waves can have the same effect. Limiting the fuel rack position based on the charge pressure will prevent thermal overloading.

$$X_{lim,\lambda}(t) = \frac{p_1(t)V_1}{R_a T_1 \sigma_f m_{f,nom} \lambda_{min}} \quad (\text{A.25})$$

Where $X_{lim,\lambda}$ is the fuel injection limitation, p_1 is the charge pressure, V_1 cylinder volume at the start of compression, R_a the gas constant, T_1 the charge temperature, σ_f the stoichiometric air-fuel ratio of fuel, $m_{f,nom}$ mass of fuel and λ_{min} the minimum air excess ratio.

Over- and underspeed

Slow integrating speed control can result in over or underspeed of the diesel engine. Geertsma [2019] has suggested introducing fuel limitations:

$$X_{lim,os}(t) = \frac{n_{e,max} - n_e(t)}{n_{e,nom}} P_{os} \quad (\text{A.26})$$

$$X_{min}(t) = \frac{n_{e,min} - n_e(t)}{n_{e,nom}} P_{us} \quad (\text{A.27})$$

Where $X_{lim,os}$ is the fuel limitation to prevent overspeed and X_{min} to prevent underspeed. $n_{e,max}$ is the maximum engine speed, $n_{e,min}$ minimum engine speed, P_{os} is the overspeed limitation gain and P_{us} underspeed gain. When applying a minimum engine speed, the pitch should also be limited when using adaptive pitch control to prevent high engine torque.

When applying a maximum engine speed, the pitch should also be limited when using adaptive pitch control to prevent high engine torque.

$$P_{pd,max}^*(t) = \frac{n_{virt,set}(t) i_g b}{n_{e,min}} \quad (A.28)$$

$$P_{pd,set}(t) = P_{pd,0} + \max(P_{pd,max}^*(t), P_{pd,set}^*(t))(P_{pd,nom} - P_{pd,0}) \quad (A.29)$$

A.3. Diesel Engine

The objective of this thesis is to determine the dynamic behaviour between propeller and engine. An Mean Value First Principle (MVFP) can represent the dynamic performance of the diesel engine. The model that will be used in this thesis is improved and used by Geertsma [2019]. Six sub-models interact with each other to represent the dynamic performance of the diesel engine. These are the fuel pump, air swallow, heat release, Seiliger cycle, exhaust receiver and turbocharger, and mechanical conversion. In figure A.7, a representation is illustrated.

The diesel engine is simulated by a MVFP model. The cylindrical volume is left out and is replaced by an analytical model for the air and exhaust gas flow dynamics, making it possible to use a revolution time scale instead of crank angle time scale. This has the advantage that the computation time decreases with a factor 400 (Schulten [2005]).

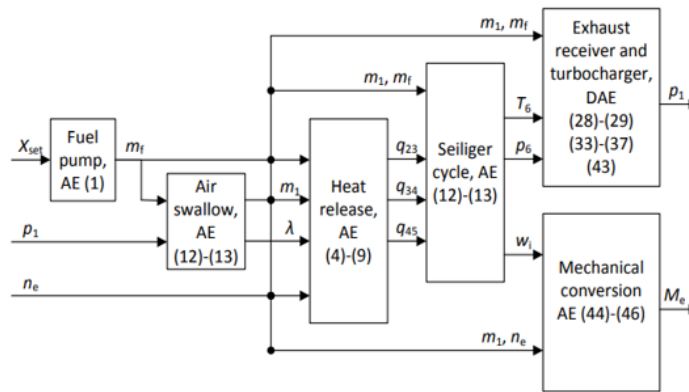


Figure A.7: Representation of the diesel engine model (Geertsma [2019] p 69)

Fuel pump

Geertsma [2019] proposed that amount of fuel injected per cylinder per cycle m_f is represented by the fuel pump and is shown in the following equation:

$$\frac{dm_f(t)}{dt} = \frac{m_{f,nom} X_{set}(t) - m_f(t)}{\tau_X} \quad (A.30)$$

Where $m_{f,nom}$ is the nominal amount of fuel injected per cylinder per engine cycle in kg, $X_{set}(t)$ fuel pump injection setpoint in % of nominal fuel injection and τ_X is the injection time delay. The time delay is the time that it takes for half a stroke:

$$\tau_X = \frac{1}{4n_{e,nom}} \quad (A.31)$$

Where $n_{e,nom}$ is the nominal engine speed in Hz.

The nominal fuel injection, $m_{f,nom}$, is determined with the following equation:

$$m_{f,nom} = \frac{b_{bsfc,nom} P_{e,nom} k_e}{i_e n_{e,nom}} \quad (A.32)$$

Where $m_{bsfc,nom}$ is the nominal brake specific fuel consumption, $P_{e,nom}$ is the nominal engine power, k_e the number of revolutions per cycle and i_e the number of cylinders of the engine.

Air Swallow

An engine's air swallow capacity is the mass flow through the engine and the volume flow at several stages Stapersma [2010a]. The air left after combustion is the air excess ratio (λ). This is an essential parameter for thermal loading (Sapra [2020]). The air excess ratio is expressed as follows:

$$\lambda(t) = \frac{m_1(t)}{m_f(t)\sigma_f} \quad (\text{A.33})$$

Where m_1 is the trapped mass at the start of compression and σ_f is the stoichiometric air fuel ratio.

Seiliger Cycle and Heat Release

A method to calculate the cycle performance is to use the Seiliger model. This can be used to design an engine. The theory in this section is a summary from Stapersma [2010a]. A few assumptions are made in this model:

- The gas is perfect ($pv = mRt$)
- Specific heats are constant ($c_v, c_p = \text{constant}$)
- The fluid is everywhere the same, but not the air
- No mass addition (closed volume approach)
- All processes are internally reversible
- Compression and expansion are polytropic

The Seiliger cycle consists of six thermodynamic stages.

- 1-2 polytropic compression
- 2-3 iso-volumetric combustion (constant volume)
- 3-4 isobaric combustion and expansion (constant pressure)
- 4-5 isothermal combustion and expansion (constant temperature)
- 5-6 polytropic expansion
- 6-1 iso-volumetric heat rejection (constant volume)

These stages are shown in a PV and TS diagram in figure A.8 and A.9 .

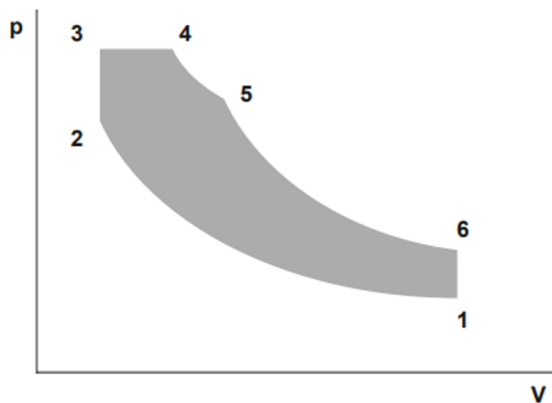


Figure A.8: Seiliger process in PV diagram [35 p. 106-107]

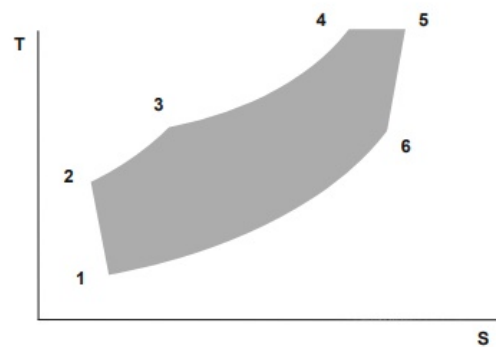


Figure A.9: Seiliger process in TS diagram [35 p. 106-107]

The Seiliger model can be used to determine the work and the heat at all stage. In table A.3 the equations are given, where V_i , p_i , T_i are the volume, pressure and temperature in state i . w_{ij} and q_{ij} are the specific work and heat from state i to j . a , b , and c are Seiliger parameters as defined by Stapersma [2010a]. The total work can be determined with the following equation:

$$w_{tot} = w_{12} + w_{34} + w_{45} + w_{56} \quad (\text{A.34})$$

Table A.3: Seiliger cycle equations

Seiliger stage	Volume ratio	Pressure ratio	Temperature ratio	Specific Work	Heat
1-2 compression	$\frac{V_1}{V_2} = r_c$	$\frac{p_2}{p_1} = r_c^{n_c}$	$\frac{T_2}{T_1} = r_c^{n_c-1}$	$w_{12} = \frac{R_a(T_2-T_1)}{n_e-1}$	-
2-3 Iso-volumetric combustion	$\frac{V_3}{V_2} = 1$	$\frac{p_3}{p_2} = a$	$\frac{T_3}{T_2} = a$	-	$q_{23} = c_{va}(T_3 - T_2)$
3-4 Isobaric combustion	$\frac{V_4}{V_3} = b$	$\frac{p_4}{p_3} = 1$	$\frac{T_4}{T_3} = b$	$w_{34} = R_a(T_4 - T_3)$	$q_{34} = c_{pa}(T_4 - T_3)$
4-5 Isothermal combustion	$\frac{V_5}{V_4} = c$	$\frac{p_4}{p_5} = c$	$\frac{T_5}{T_4} = 1$	$w_{45} = R_a T_4 \ln c$	$q_{45} = R_a T_4 \ln c$
5-6 Expansion	$\frac{V_6}{V_5} = r_e$	$\frac{p_5}{p_6} = r_e^{n_e}$	$\frac{T_5}{T_6} = r_e^{n_e-1}$	$w_{56} = \frac{R_a(T_6-T_5)}{n_e-1}$	-
6-1 Heat rejection	$\frac{V_6}{V_1} = \frac{r_e c b}{r_c}$	$\frac{p_6}{p_1} = \frac{r_c^{n_c} a}{r_e^{n_e} c}$	$\frac{T_6}{T_1} = \frac{r_c^{n_c-1} a b}{r_e^{n_e-1}}$	-	$q_{61} = -c_v(T_6 - T_1)$

The total heat release is expressed in equation A.35:

$$q_{tot} = q_{23} + q_{34} + q_{45} \quad (\text{A.35})$$

Table A.3 parameters are not the heat release model's inputs, as shown in figure A.7. The nominal fuel injection ($m_{f,nom}$), trapped mass at the start of the compression (m_1), pseudo air excess ratio (λ) and the engine speed (n_e) are the inputs.

Schulten [2005] and Geertsma [2019] use the following equations to determine the specific work:

$$q_{23}(t) = X_{cv}(t) \frac{m_f \eta_q(t) \eta_{comb} h^L}{m_1(t)} \quad (\text{A.36})$$

$$q_{34}(t) = (1 - X_{cv}(t) - X_{ct}(t)) \frac{m_f \eta_q(t) \eta_{comb} h^L}{m_1(t)} \quad (\text{A.37})$$

$$q_{45}(t) = X_{ct}(t) \frac{m_f \eta_q(t) \eta_{comb} h^L}{m_1(t)} \quad (\text{A.38})$$

Where X_{cv} and X_{ct} is the portion of heat released at constant volume and constant temperature. η_q is the heat release efficiency, η_{comb} the combustion efficiency and h^L the lower heating value.

Exhaust receiver and turbocharger

The exhaust receiver and turbocharger are based on Zinner blowdown, Büchi flow and power balance, the elliptic law and a variable slip ratio. The Zinner blowdown is the process of after the exhaust valve opens, gas expelling during the exhaust stroke and scavenging after the inlet opens. With the Zinner method, the gases' temperature after blowdown can be determined as can be seen in equation A.39.

$$T_{bld}(t) = \left(\frac{1}{n_{bld}} + \frac{(n_{bld} - 1) p_{d,s}(t)}{n_{bld} p_6(t)} \right) T_6(t) \quad (\text{A.39})$$

Where T_{bld} is the Zinner blowdown temperature, n_{bld} the polytropic expansion coefficient and $p_{d,s}$ the equilibrium pressure in the exhaust receiver.

Mechanical conversion

The output, the engine torque, is the indicated torque (M_i) minus the torque losses (M_{loss}) as can be seen in the following expression:

$$M_e(t) = M_i(t) - M_{loss}(t) \quad (\text{A.40})$$

$$M_i(t) = \frac{w_i(t)m_1(t)i_e}{k_e 2\pi} \quad (\text{A.41})$$

$$M_{loss}(t) = M_{loss,nom} \left(1 + M_{loss,grad} \frac{n_{e,nom} - n_e(t)}{n_{e,nom}} \right) \quad (\text{A.42})$$

$M_{loss,nom}$ is the nominal torque loss, $M_{loss,grad}$ is the torque loss gradient, w_i the specific work, m_1 the trapped mass, i_e is the number of cylinders and k_e is the number of revolutions per cycle.

Shaft line

The shaft line is described with the equation of motion that takes the gearbox, shaft line and propeller:

$$\frac{dn_p(t)}{dt} = \frac{M_{gb}(t) - M_{sl}t(t) - M_p(t)}{2\pi J_{tot}} \quad (\text{A.43})$$

Where n_p is the propeller speed in rps, and M_{gb} , M_{sl} , M_p are respectively the gearbox, shaft line and propeller torque.

A.4. Propeller model

In the propeller model, the advance speed is determined with the following equation:

$$v_a(t) = v_s(t)(1 - w) + v_w(t) \quad (\text{A.44})$$

With the rotational speed, the hydrodynamic pitch angle is determined:

$$\beta(t) = \text{atan} \left(\frac{v_a(t)}{0.7\pi n_p(t)D} \right) \quad (\text{A.45})$$

In the model by Geertsma [2019], this pitch angle is used as an input for the adaptive pitch controller. However, it is not possible to measure the hydrodynamic pitch angle. This one of the reasons to also determine the thrust and torque. Chapter 2 elaborates on how the thrust measurement is used to determine the hydrodynamic pitch angle. The other reason to determine the two parameters in the model is that thrust is used to propel the hull and the torque as feedback to the propulsion plant.

$$v_h(t) = \sqrt{v_a(t)^2 + (0.7\pi n_p(t)D)^2} \quad (\text{A.46})$$

$$T_p(t) = C_T(t) \frac{1}{2} \rho v_h(t)^2 \frac{\pi}{4} D^2 \quad (\text{A.47})$$

$$Q_p(t) = C_Q(t) \frac{1}{2} \rho v_h(t)^2 \frac{\pi}{4} D^3 \quad (\text{A.48})$$

With the torque known, the rotative efficiency of the propeller is taken into account to determine the actual propeller torque:

$$M_p(t) = \frac{Q_p(t)}{\text{eta}_R} \quad (\text{A.49})$$

The pitch is also changed in the propeller model. A first-order linear model is used that takes the time delay into account:

$$\frac{dP_{pd}(t)}{dt} = \frac{P_{pd, set}(t) - P_{pd}(t)}{\tau_p} \quad (\text{A.50})$$

Scale effects

For the thrust and torque coefficients, it is relevant to take the scaling effects into account according to ITTC [2017]. The first step is to transform $C_T(t)$ to $K_T(t)$ and $C_Q(t)$ to $K_Q(t)$:

$$C_T(t) = \frac{\pi}{8} \frac{v_h(t)^2}{n_p(t)^2 D^2} K_T(t) \quad (\text{A.51})$$

$$C_Q(t) = \frac{\pi}{8} \frac{v_h(t)^2}{n_p(t)^2 D^2} K_Q(t) \quad (\text{A.52})$$

The difference in the thrust and torque coefficients is determined with the following equations:

$$K_{T,FS}(t) = K_{T,MS} - \Delta K_T \quad (\text{A.53})$$

$$K_{Q,FS}(t) = K_{Q,MS} - \Delta K_Q \quad (\text{A.54})$$

Where

$$\Delta K_T = -\Delta C_D 0.28 \frac{P}{D} \frac{cZ}{D} \quad (\text{A.55})$$

$$\Delta K_Q = -\Delta C_D 0.248 \frac{P}{D} \frac{cZ}{D} \quad (\text{A.56})$$

Where ΔC_D is the drag difference that is determined with the following equations:

$$\Delta C_D = C_{D,MS} - C_{D,FS} \quad (\text{A.57})$$

Where

$$C_{D,MS} = 2 \left(1 + 2 \frac{t}{c} \right) \left[\frac{0.44}{Re^{\frac{1}{6}}} - \frac{5}{Re^{\frac{2}{3}}} \right] \quad (\text{A.58})$$

$$C_{D,FS} = 2 \left(1 + 2 \frac{t}{c} \right) \left[1.89 + 1.62 \log \frac{c}{k_p} \right]^{-2.5} \quad (\text{A.59})$$

A.5. Matching

The model Geertsma [2019] uses is a MAN12V28 diesel engine that drives a C5-60 propeller. In this thesis, a C4-40 propeller is used. This because the data of the C4-40 propeller can be published and the hardware CPP is also a C4-40 propeller. This makes it possible to compare the simulation with the experiment results. However, it is impossible to simply change the propeller parameters and do the simulations or experiments. Changes are that the propulsion plant components do not match, resulting in an inadequate performing system.

The matching procedure is described in Klein Woud and Stapersma [2003] page 405 – 411. The first step is to determine the optimal pitch ratio of the propeller. This is done with the K_T as a function of the advance ratio:

$$K_T = \frac{R}{(1-t)\rho n^2 D^4} \quad (\text{A.60})$$

$$J = \frac{(1-w)v_s D}{n} \quad (\text{A.61})$$

$$\frac{K_T}{J^2} = \frac{R}{(1-t)(1-w)^2 \rho v_s^2 D^2} \quad (\text{A.62})$$

$$K_T = 0.4087 J^2 \quad (\text{A.63})$$

This relation is the fat line plotted in the open water diagram of the C4-40 in figure A.10. The intersections with the K_T and K_Q lines are shown in table A.4.

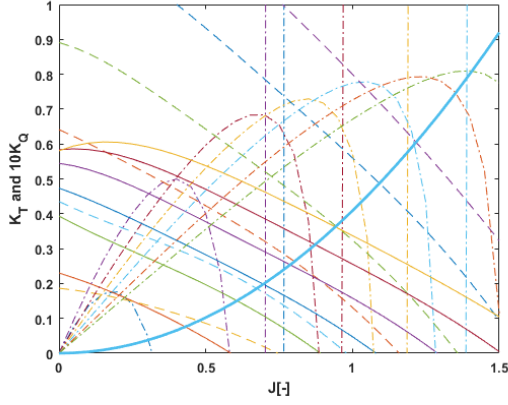


Figure A.10: C4-40 open water diagram with K_T as a function of J plotted.

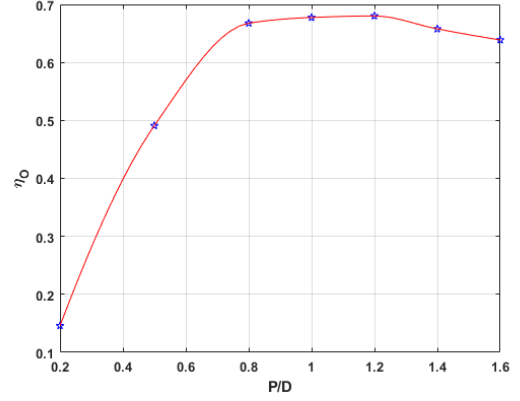


Figure A.11: Optimal P/D ratio

Table A.4: Intersections K_T as a function of J in open water diagram

PD	0.2	0.5	0.8	1.0	1.2	1.4	1.6
J	0.245	0.430	0.606	0.696	0.788	0.873	0.941
K_t	0.025	0.076	0.150	0.198	0.254	0.311	0.362
K_q	0.007	0.011	0.022	0.032	0.047	0.066	0.085
η₀	0.146	0.491	0.668	0.678	0.680	0.658	0.639

From the table and figure A.11 can be seen that the optimum PD ratio is 1.2 due to the highest efficiency. This can also be concluded from figure A.11. With the known optimal PD ratio, it is possible to determine the optimal shaft speed and, therefore, also the gearbox ratio.

$$n_{opt} = \frac{v_s(1-w)}{J_{opt}D} \quad (\text{A.64})$$

$$= 3.715[\text{rps}] \quad (\text{A.65})$$

$$i_{opt} = \frac{n_{eng,nom}}{n_{opt}} \quad (\text{A.66})$$

$$= 4.4859[-] \quad (\text{A.67})$$

The optimum PD ratio is implemented as the nominal pitch, and gearbox ratio is applied in the gearbox model. This results in an adequate working propulsion plant.

A.6. Irregular wave model

Waves are one of the most prominent disturbances for a propulsion plant. The wave model used by Geertsma [2019] is the basis for the model. It takes added resistance on the hull and the average speed into the propeller. The oblique inflow and pitching of the ship are neglected. For this thesis, irregular waves are implemented. This is done by using a linear superposition of regular wave components.

For this thesis, irregular waves are implemented. This is done by using a linear superposition of regular wave components:

$$v_w(t) = \sum_{n=1}^N [S(\omega_n)d\omega]\omega_{wv,n}e^{k_{w,n}z} \cos(\alpha_{wk,n}(t) + \epsilon_n) \quad (\text{A.68})$$

$$\frac{d\alpha_{wk,n}(t)}{dt} = k_{w,n}v_s(t) + \omega_{wv,n} \quad (\text{A.69})$$

$$k_{w,n} = \frac{\omega_{m,n}^2}{g} \quad (\text{A.70})$$

Where v_w is the relative wake speed in m/s , ω_{wv} is the wave frequency. k_w is the wave number in $1/m$, z the centerline of the propeller in m , α_{wk} the angle of the vertical wave movement, ϵ is the random phase angle (rad). The wave amplitude is not constant for irregular waves. This since these waves are a combination of n frequencies. In the model, the frequencies between 0 and 2 rad/s are taken into account. S the surface elevation spectrum. In this thesis the Jonswap spectrum is used according the following equation:

$$S(\omega) = \bar{a} g^2 \omega^{-5} e^{\beta_j (\frac{\omega}{\omega_p})^{-4}} \gamma^a \quad (\text{A.71})$$

Where γ is the peakedness parameter (3.3), ω_p the peak frequency, β_j a shape factor (1.25) and a and \bar{a} modified Phillips constants. A detailed description of the wave model can be found in Vazirizade [2019] page 23 - 29.

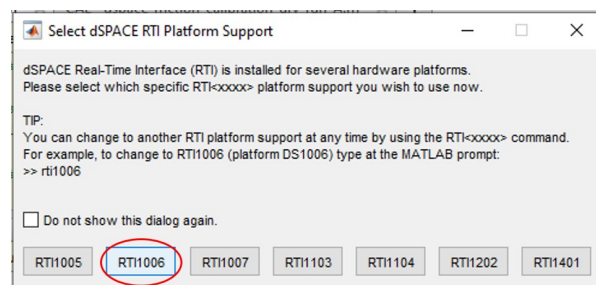
B

Manual HIL setup

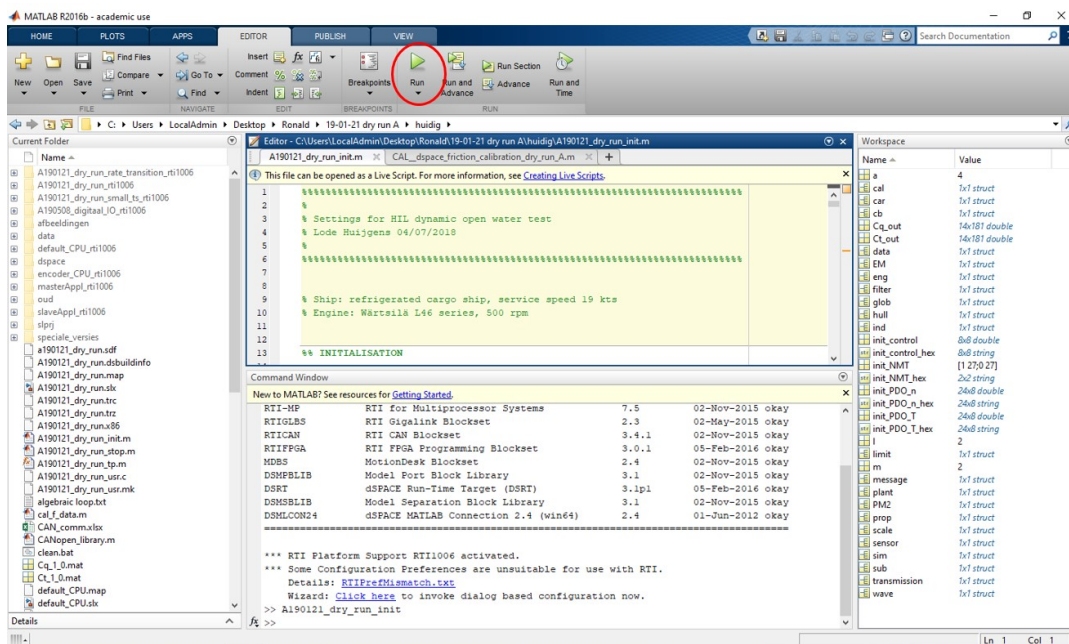
This document is a manual for the open water HIL setup at the TU Delft. The theoretical background is described in the dissertation of Huijgens [2021].

Start-up HIL setup

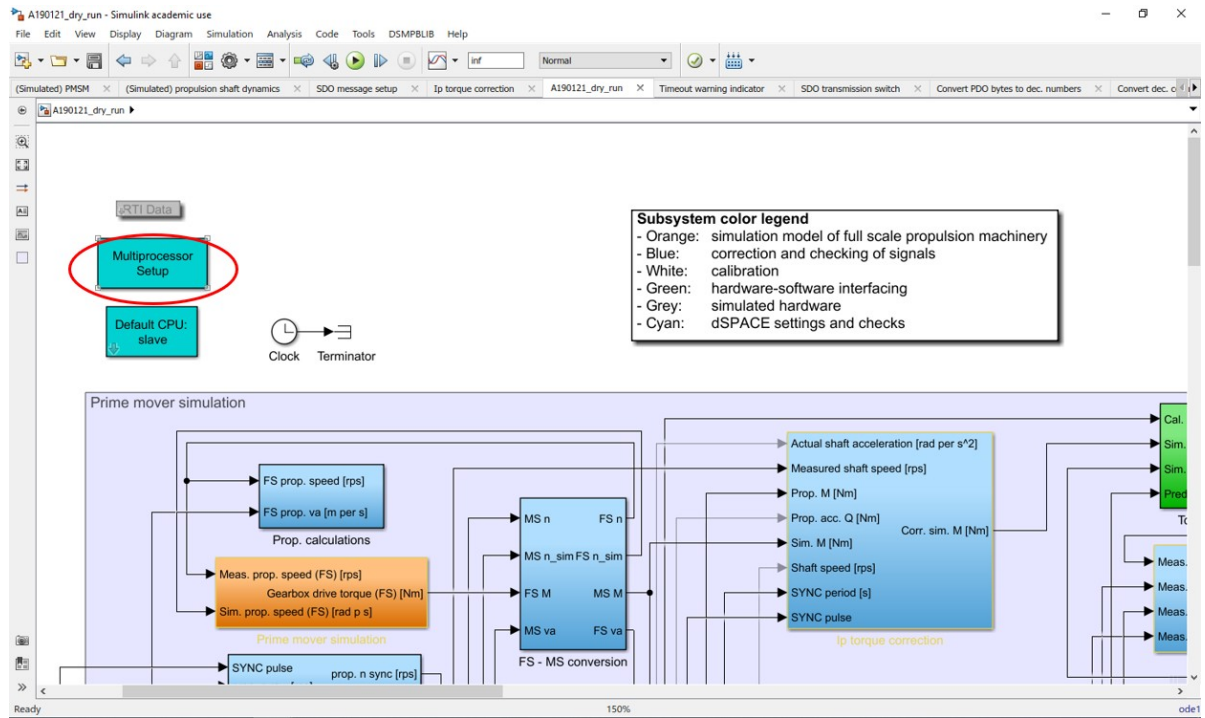
The first step is to start up MATLAB R2016b. RTI1006 can be selected as can be seen in the following figure:



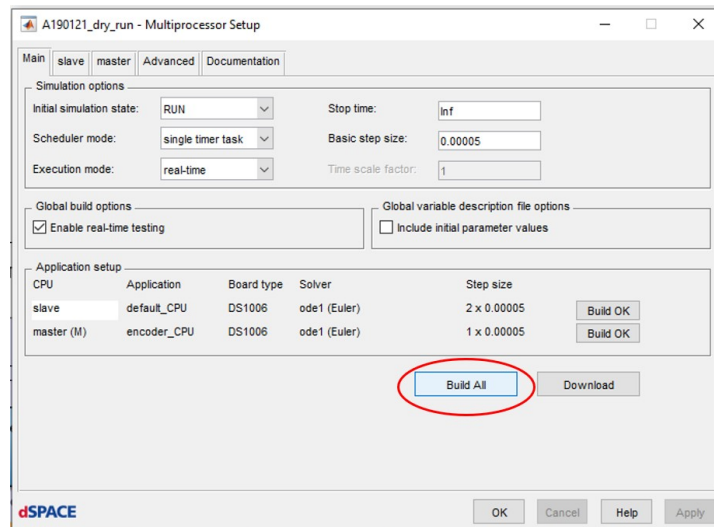
The next step is to run the driver file. The latest version of the original model is: *A190121_dry_run_init.m*. The model with non-linear diesel engine is: *driver.m*



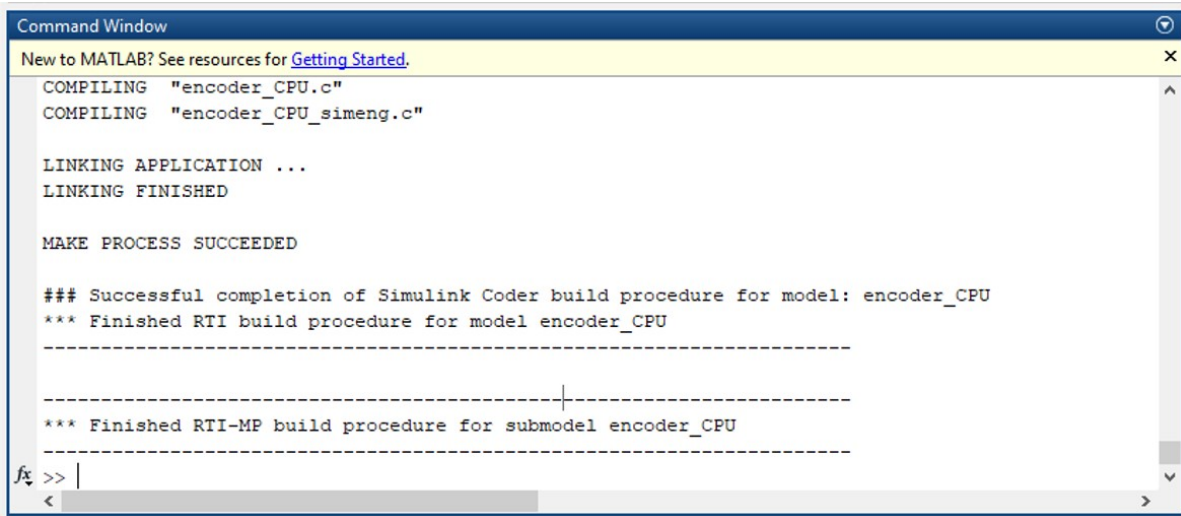
Step two is to start up $A190121_{dry_run}$ in Simulink and open Multiprocessor Setup.



After opening Multiprocessor Setup click on “Build All”.



MATLAB is building the model. When it is finished the following text should be visible in the Command Window of MATLAB:



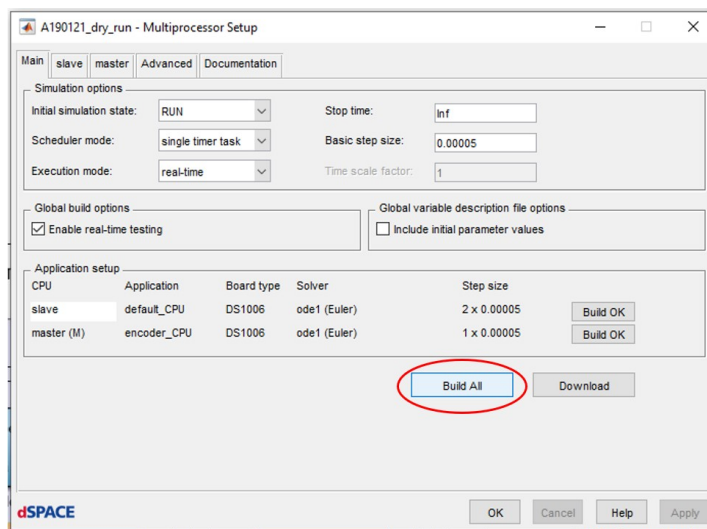
```
Command Window
New to MATLAB? See resources for Getting Started.
COMPILING "encoder_CPU.c"
COMPILING "encoder_CPU_simeng.c"

LINKING APPLICATION ...
LINKING FINISHED

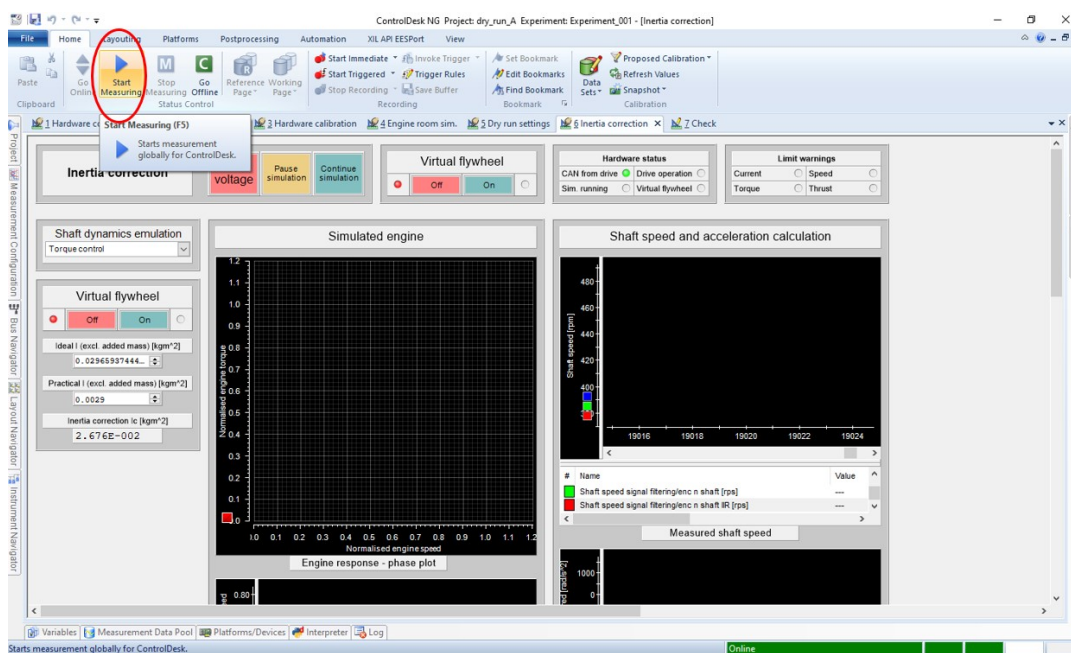
MAKE PROCESS SUCCEEDED

### Successful completion of Simulink Coder build procedure for model: encoder_CPU
*** Finished RTI build procedure for model encoder_CPU
-----
-----
*** Finished RTI-MP build procedure for submodel encoder_CPU
-----
fx >> |
<
```

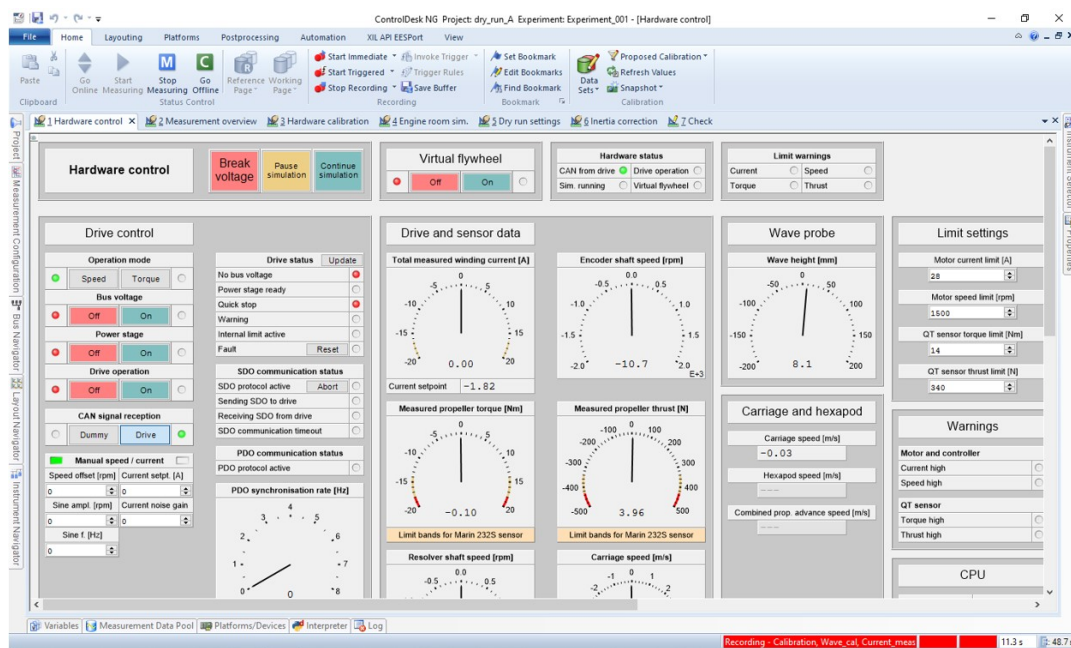
When the Building process is completed press "Ok"



If you want to perform measurements click on “Start Measurements”.



The following screen shot will be visible:



Friction correction

Chapter 5 of the dissertation of Lode Huijgens describes the theoretical background of the friction correction. This correction is performed under water without the propeller attached on the gondola. Also, no stream line fairings are mounted. The next steps describe the practical steps that must be followed. The first step is to check the following settings in tab Hardware Control:

- Operation mode: Speed
- Bus Voltage: On
- Power Stage: On
- Drive Operation: On

The screenshot displays the ControlDesk NG software interface for a hardware control experiment. The 'Hardware control' tab is active, and the 'Drive control' section is highlighted with a red circle. The settings in this section are as follows:

- Operation mode:** Speed (selected)
- Bus voltage:** On (selected)
- Power stage:** On (selected)
- Drive operation:** On (selected)
- CAN signal reception:** Drive (selected)
- Manual speed / current:** Unchecked
- Speed offset [rpm]:** 0
- Current setpt. [A]:** 0
- Sine ampl. [rpm]:** 0
- Current noise gain:** 0
- Sine f [Hz]:** 0

Other visible sections include:

- Virtual flywheel:** Off
- Hardware status:** CAN from drive (On), Drive operation (On), Sim. running (On), Virtual flywheel (Off)
- Limit warnings:** Current (Off), Speed (Off), Torque (Off), Thrust (Off)
- Drive and sensor data:** Total measured winding current [A] (0.23), Encoder shaft speed [rpm] (0.0), Measured propeller torque [Nm] (-0.10), Measured propeller thrust [N] (3.87), Resolver shaft speed [rpm] (0.0), Carriage speed [m/s] (-0.03)
- Wave probe:** Wave height [mm] (8.1)
- Limit settings:** Motor current limit [A] (28), Motor speed limit [rpm] (1500), QT sensor torque limit [Nm] (14), QT sensor thrust limit [N] (340)
- Carriage and hexapod:** Carriage speed [m/s] (-0.03), Hexapod speed [m/s] (---), Combined prop. advance speed [m/s] (---)
- Warnings:** Motor and controller (Current high, Speed high), QT sensor (Torque high, Thrust high), CPU

The second step is to open the “Hardware Calibration” tab. In the speed settings a sinusoidal variation of the shaft speed can be given as input. If the rotational speed is low (approximately between -50 and 50 rpm) the measurements are not accurate.

In this example the following “Speed setting” is used

- Osc offset [rpm]: 250
- Osc amp [rpm]: 200
- Osc f [Hz]: 0.005

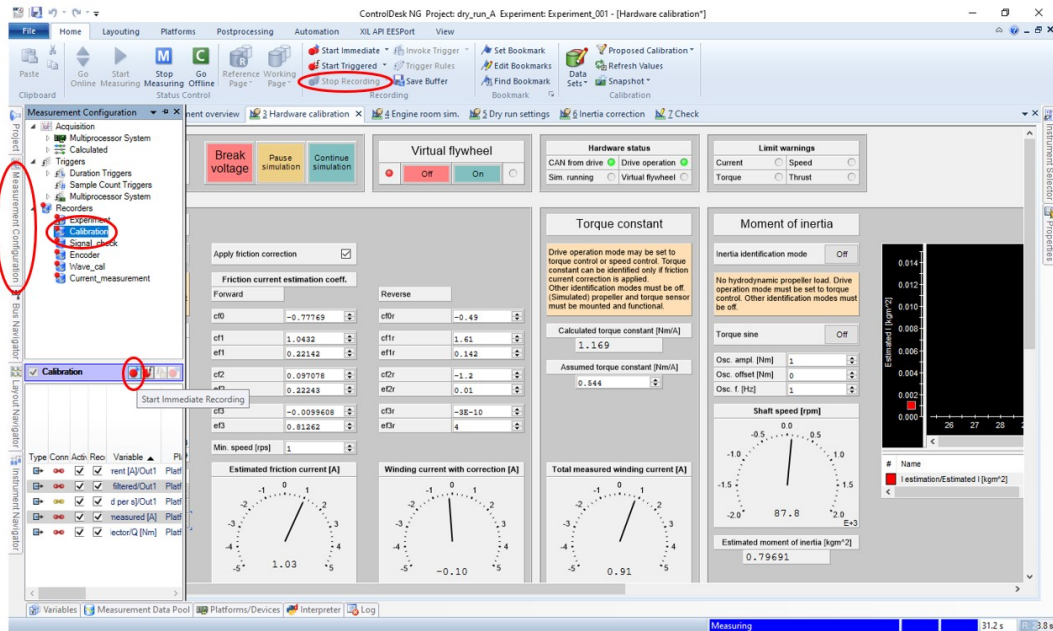
This setting will result in a sinusoidal variation between 50 and 450 rpm (250 ± 200) in 200 seconds ($1/0.005$).

The screenshot shows the ControlDesk NG software interface for a hardware calibration experiment. The main window is titled "ControlDesk NG Project: dry_run_A Experiment: Experiment_001 - [Hardware calibration]". The interface is divided into several sections:

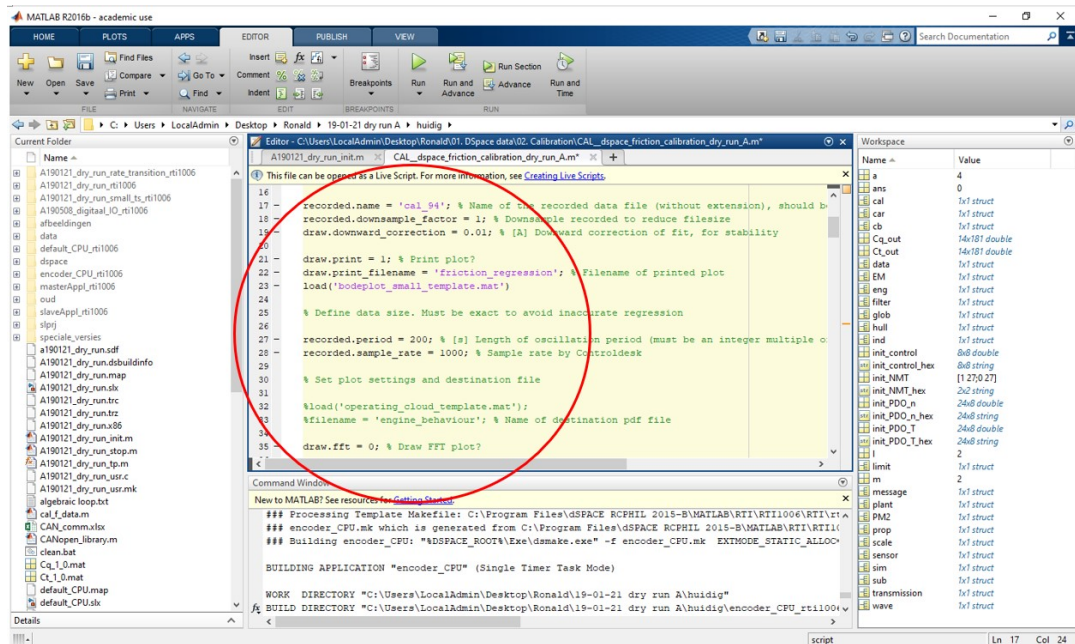
- Hardware calibration:** This section is highlighted with a red circle. It contains a "Speed setting" sub-section with three input fields: "Osc. offset [rpm]" set to 250, "Osc. amp [rpm]" set to 200, and "Osc. f [Hz]" set to 0.005. Above these fields are buttons for "Start Measuring (F5)", "Pause simulation", and "Continue simulation".
- Virtual flywheel:** A section with "Off" and "On" buttons.
- Hardware status:** A section with "CAN from drive", "Drive operation", "Sim. running", and "Virtual flywheel" indicators.
- Limit warnings:** A section with "Current", "Speed", "Torque", and "Thrust" indicators.
- Shaft friction:** A section with "Friction identification mode" set to "Off" and "Apply friction correction" checked. It includes a "Friction current estimation coeff." table with values for forward and reverse directions (cf0 to cf3, cfr0 to cfr3) and a "Shaft speed [rpm]" gauge showing 179.2 rpm.
- Torque constant:** A section with "Drive operation mode" instructions and a "Calculated torque constant [Nm/A]" gauge showing 0.004.
- Moment of inertia:** A section with "Inertia identification mode" set to "Off" and a "Shaft speed [rpm]" gauge showing 179.2 rpm. It also includes an "Estimated moment of inertia [kgm²]" gauge showing 0.23006.

The bottom status bar shows "Measuring" and a time of 11.9 s.

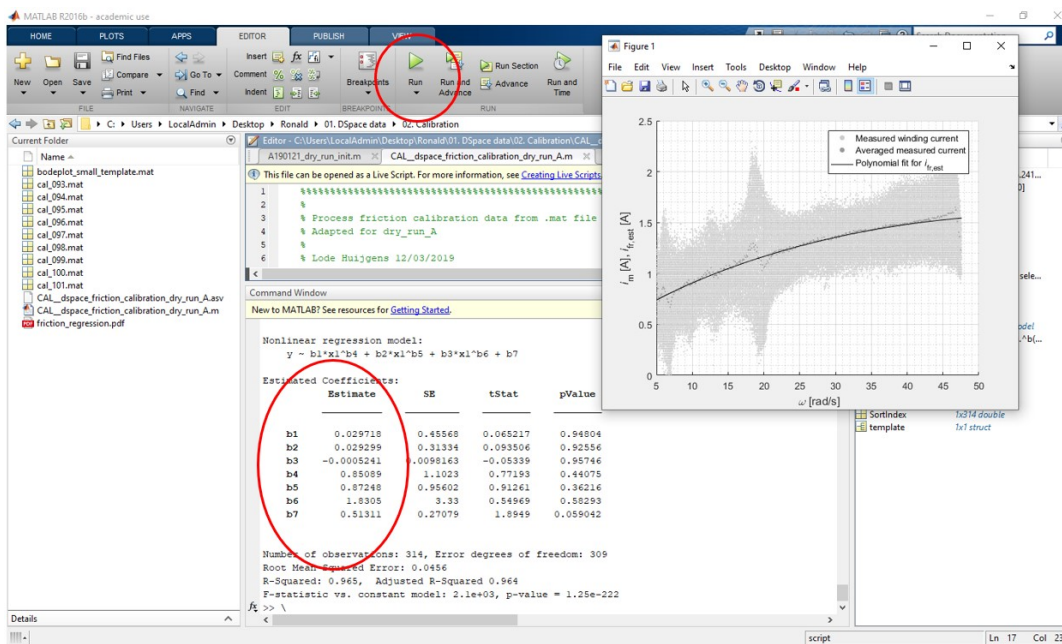
Open “Measurement Configuration”. “Start Immediate Recording” of the “Calibration”. Because the oscillating frequency is 0.005 Hz in this example the minimum measurement time must be 200 seconds (1/0.005). After 200 seconds the recording can be stopped.



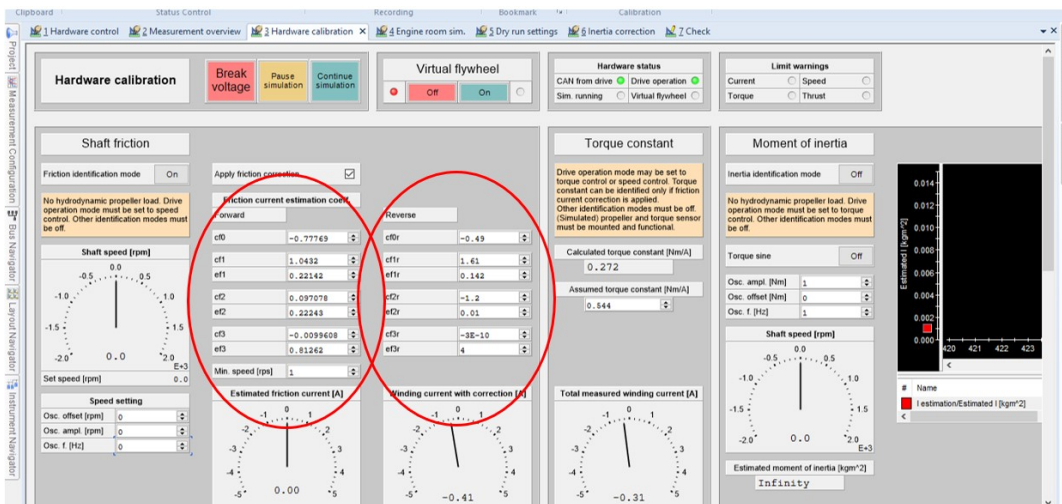
Open “CAL_dspace_friction_calibration_dry_run_run_A.m”.
 Check the following settings: recorded.name.period and sample_rate
 Recorded.name is the name of the .mat file of the measurement. Recorded.period is 200 seconds (1/0.005 is this example). Sample_rate is set in dSPACE.



If the settings are set correctly the m-file can be run. The coefficients of the polynomial will be given.



Fill in these coefficients in dSPACE.



Repeat this measurement with following speed settings for the “Reverse coefficients”

- Osc offset [rpm]: -250
- Osc amp [rpm]: -200
- Osc f [Hz]: 0.005

Moment of inertia measurement

The moment of inertia must be corrected. To measure this correction factor the propeller must be mounted on the gondola. This measurement must be performed outside the water. To determine the moment of inertia, select Operation mode: Torque

The screenshot shows the ControlDesk NG software interface for a hardware control experiment. The main window is titled "ControlDesk NG Project: dry_run_A Experiment: Experiment_001 - [Hardware control]". The interface is divided into several sections:

- Hardware control:** Includes buttons for "Break voltage", "Pause simulation", and "Continue simulation".
- Virtual flywheel:** Has "Off" and "On" buttons.
- Hardware status:** Shows "CAN from drive" and "Drive operation" status.
- Limit warnings:** Includes checkboxes for "Current", "Speed", "Torque", and "Thrust".
- Drive control:** The "Operation mode" dropdown is highlighted with a red circle, showing "Speed" and "Torque" options. Other controls include "Bus voltage", "Power stage", "Drive operation", and "CAN signal reception".
- Drive and sensor data:** Contains several gauges: "Total measured winding current [A]", "Encoder shaft speed [rpm]", "Measured propeller torque [Nm]", "Measured propeller thrust [N]", "Resolver shaft speed [rpm]", and "Carriage speed [m/s]".
- Wave probe:** Shows "Wave height [mm]" with a gauge.
- Limit settings:** Includes sliders for "Motor current limit [A]", "Motor speed limit [rpm]", "QT sensor torque limit [Nm]", and "QT sensor thrust limit [N]".
- Carriage and hexapod:** Shows "Carriage speed [m/s]" and "Hexapod speed [m/s]".
- Warnings:** Lists "Motor and controller" warnings like "Current high", "Speed high", "Torque high", and "Thrust high".
- CPU:** Shows "CPU" status.

The bottom status bar indicates "Recording - Calibration, Wave_cal, Current_meas" and "11.3 s 48.7 s".

Go to tab: Hardware calibration. Make the following settings:

- Inertia identification mode: On
- Torque sine: On
- Osc.ampl [Nm]: 1
- Osc. Offset [Nm]: 0
- Osc.f [Hz]: 1

ControlDesk NG Project: dry_run_A Experiment: Experiment_001 - [Hardware calibration]

Hardware status: CAN from drive Drive operation Sim running Virtual flywheel

Limit warnings: Current Speed Torque Thrust

Torque constant: Drive operation mode may be set to torque control or speed control. Torque constant can be identified only if friction current correction is applied. Other identification modes must be off (Simulated) propeller and torque sensor must be mounted and functional.

Calculated torque constant [Nm/A]: -0.238
Assumed torque constant [Nm/A]: 0.544

Moment of inertia: Inertia identification mode: On
Torque sine: On
Osc. ampl [Nm]: 1
Osc. offset [Nm]: 0
Osc. f [Hz]: 1
Estimated moment of inertia [kgm²]: 0.00983

Wave probe: Wave height [mm]: 8.1
Calibration factors: h [mm] = A + B*(U/V)
A: 9.4
B: 21.52

Write down the lowest value of the “Estimated moment of inertia”.

Go to tab: Inertia Correction. Fill in the “Estimated moment of inertia” at Practical

ControlDesk NG Project: dry_run_A Experiment: Experiment_001 - [Inertia correction]

Inertia correction: Break voltage Pause simulation Continue simulation

Virtual flywheel: Off On

Hardware status: CAN from drive Drive operation Sim running Virtual flywheel

Limit warnings: Current Speed Torque Thrust

Virtual flywheel: Ideal | (excl. added mass) [kgm²]: 0.33965937444
Practical | (excl. added mass) [kgm²]: 0.0029
Inertia correction ic [kgm²]: 2.676E-002

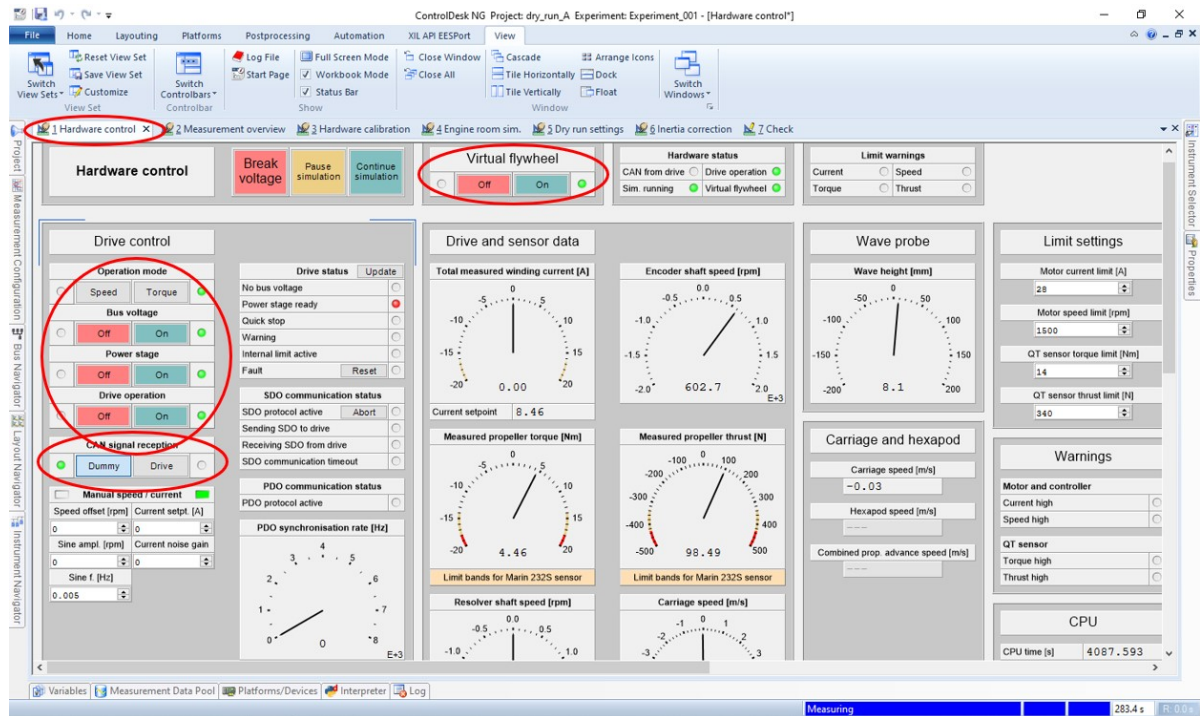
Simulated engine: Measured torque [Nm] vs. Normalised engine speed

Shaft speed and acceleration calculation: Shaft speed [rpm] vs. Time [ms]

Offline modus

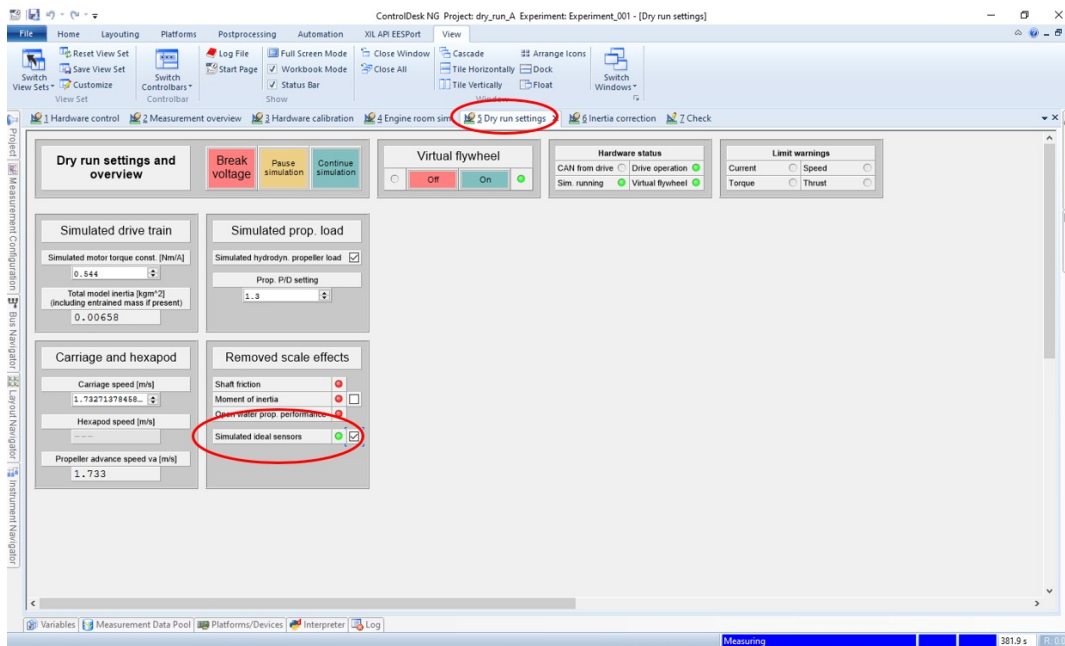
It is possible to run the simulation without the hardware of the open water setup, this is called offline modus. The dSPACE must be connected to the simulator computer and the steps that are described in chapter 2 must be performed. The following settings must be made:

- Go to tab: Hardware control
- CAN signal reception: Dummy
- All operation mode: On
- Virtual Flywheel: On

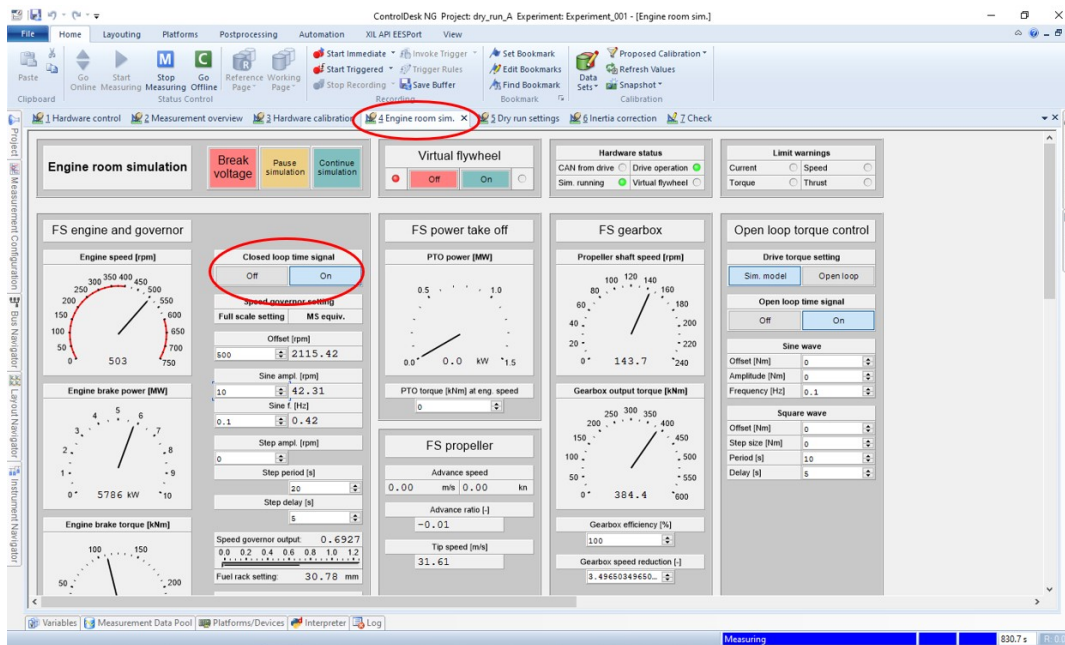


Virtual Flywheel can only be selected if the bus voltage, power stage and drive operation are On. Click on On, this is a condition that must be met.

- Go to tab: Dry run settings
- Select Simulated ideal sensors



- Go to tab: Engine room sim
- Closed loop time signal: On



After these steps are executed the simulation will run in offline modus.

Measurements

The following steps must be performed to do a measurement in the towing tank. (It is possible that these steps are not correct and must be updated during real measurements)

- Select Torque in tab: Hardware Control
- Select the correct settings in tab: Engine room sim
- Select Start Measurement
- Select Pause simulation
- Start to drive the towing carriage for approximately 3 seconds.
- Select Continue simulation
- Start recordings

The screenshot displays the ControlDesk NG software interface for an engine room simulation. The interface is divided into several panels. The top panel shows the 'Automation' menu with 'Start Immediate' and 'Start Trigger' circled in red. Below this, the 'Engine room simulation' tab is active, showing 'Break voltage', 'Pause simulation', and 'Continue simulation' buttons, with 'Pause simulation' and 'Continue simulation' also circled in red. The main area contains several sub-panels: 'FS engine and governor' with a speed gauge and 'Closed loop time signal' controls; 'FS power take off' with a PTO power gauge; 'FS gearbox' with a propeller shaft speed gauge; 'Open loop torque control' with drive torque and sine wave settings; 'FS propeller' with advance speed and tip speed gauges; and 'Engine brake power [MW]' and 'Engine brake torque [kNm]' gauges. The bottom status bar shows 'Measuring' and a time of 830.7 s.

C

Paper

Dynamic behaviour of a propulsion plant and its controller with Hardware In the Loop

R.J. Roberti, R.D. Geertsma, J.W. Reurings,

Highlights

- Novel adaptive pitch control strategy with Kalman filter and deadband
- Dynamic behaviour of a diesel engine with controllable pitch propeller in an open water Hardware In the Loop setup
- Pitch actuation reduction in irregular waves

Abstract

The shipping industry is forced to reduce its emissions and underwater radiated noise in order to decrease the impact on the environment and limit global warming. Moreover, a low acoustic signature can be lifesaving for a navy ship, especially during submarine on mine threats. To be able to operate as flexible as possible under these threats, a flexible propulsion plant is required. A diesel engine with a controllable pitch propeller (CPP) is contributing to this. A method to reduce the emissions and noise of such a plant is to improve the control strategy. Often this is tested with numerical models. However, frequently they contain many simplifications of reality, for example, the neglect of several hydrodynamic effects. Hardware In the Loop (HIL) takes these effects into account by replacing a software part of the model with a hardware component. In this research, the CPP is the scaled hardware part. A feasibility study is performed to determine whether a propeller open water HIL setup can be used to simulate the dynamic behaviour of the propulsion plant. Therefore, a comparison is made between full and model scale numerical simulation of a diesel engine with a CPP controlled by adaptive pitch control (APC). To reduce the pitch actuations with the APC strategy a Kalman filter with deadband is implemented. Full-scale simulations with irregular waves demonstrated that the pitch actuations could be reduced during acceleration and at a constant speed. The validated full-scale model is Froude scaled and implemented in a model of the open water HIL setup. The results of the full and model scale simulations are very similar. Thus, the HIL setup can be used to simulate the dynamic behaviour of a propulsion plant. However, the hardware limitations such as the backlash in the CPP blades, the low sample rate of the actual pitch and the Froude dissimilarity of the acceleration of the towing tank need to be resolved to ensure the scaled simulations are representative for the actual, full scale, vessel. Due to these limitations, it is not possible to use the setup at this moment to perform experiments and improve novel control strategies. If these physical limitations of the current HIL setup are overcome, the effect of the propeller and the pitch control strategy during turns can be investigated by performing experiments with oblique inflow.

1. Introduction

Legislation forces the shipping industry to reduce their emissions and radiated noise to lower their im-

act on the environment and limit global warming (IMO [2020]). A method to improve this for existing ships is to enhance the efficiency with the con-

trol strategies of the propulsion plant. Novel strategies improve the propeller's inflow, resulting in more efficiency, less fuel consumption and less cavitation (Ueno et al. [2013], Geertsma [2019]). A traditional way of determining whether new control strategies have better performance is with numerical models. However, often these models do not represent all the effects that can occur in the real world.

An example is hydrodynamic effects. These are taken into account in towing tank experiments, however, with scaling effects. With a propeller open water Hardware In the Loop (HIL) setup, the benefits of numerical models and towing tank experiments are combined (Huijgens [2021]). This study implements a validated propulsion plant model into the propeller open water HIL setup to determine whether it is possible to simulate the dynamic behaviour of the plant. The results between full-scale simulations and model scale HIL simulations are compared with a case study, the propulsion plant of an Ocean-going Patrol Vessel (OPV) of the Dutch Navy. This is a diesel engine that drives a CPP controlled by the novel adaptive pitch control strategy.

APC controls the water inflow into the propeller by changing the rotational speed and pitch. A downside of inflow control is that the pitch changes continuously in waves to achieve the most effective angle of attack. Modern actuation systems of CPP's are not able to keep up with the speed of the changes. Moreover, high-frequency pitch actuation can lead to increased wear of the propeller hub. Thus, class regulations require an overhaul of a CPP system designed for regular use after 10^7 pitch actuations (DNV). Reducing the actuations would result in more time between overhauls. Therefore, this study implements a Kalman filter with a deadband to reduce the actuations. The simulations are performed in regular and irregular waves.

1.1 Literature review

A method to determine the dynamic behaviour of a diesel engine with a CPP is with numerical models. This can be relatively simple with a transfer function; however, these models often do not consider dynamics (Vrijdag [2009], Huijgens [2021]). On the other hand, a Mean Value First Principle (MVFP) model does take these into account and is, therefore, suitable to determine the dynamic behaviour of a propulsion plant (Schulten [2005], Geertsma [2019]).

A downside of numerical models is that hydrodynamic effects, such as ventilation and free surface effects, are often simplified (White [2008], Niklas and Pruszek [2019], Kozłowska et al. [2020]). However, in a towing tank, these effects can be taken into account with scaling effects (Journee and Massie [2001]). It is assumed that keeping the Froude number the same

for the model and full-scale ship, it is possible to increase the results of the model to full-scale, i.e. the forces can directly be scaled between the model and the full-scale ship. Nevertheless, building a scaled diesel engine with the same dynamic behaviour as a full-scale diesel is impossible.

Full-scale trials do not have scale effects; however, they are time-consuming and complex to organize. Also, it is hard to compare results due to changing environmental conditions (van Terwisga et al. [2004], Vrijdag [2009]). However, the main advantage of full-scale trials is that all the simulation uncertainties are eliminated, and the effect of a novel control strategy can be determined with more certainty.

HIL can combine the hydrodynamics in the towing tank and engine behaviour of a numerical model. In a HIL setup, a software model is replaced by a hardware component. In this study, a hardware CPP is used. Huijgens [2021] demonstrated that it is possible to study propulsion plant behaviour with the open water HIL setup and linear propulsion model. Therefore, the present study has implemented a validated non-linear MVFP diesel engine model with turbocharger dynamics and adaptive pitch control strategy.

The foundation of APC has been researched by Vrijdag [2009]. He concluded that effective angle of attack control reduces cavitation. A thrust sensor on the shaft is used to determine the effective angle of attack. However, the focus of this study was not on the behaviour of the diesel engine. Therefore, Geertsma [2019] filled this gap by studying the dynamic behaviour of the engine. Also, an improvement in the control system was implemented by adding slow integrating speed control. Moreover, he assumed that the angle of attack was known, where Vrijdag [2009] demonstrated how this could be established with a thrust sensor. Thus, an improvement would be to measure the thrust to determine the angle of attack and study whether the APC with slow integrating speed control gets the same results. However, a full-scale trial such as Vrijdag [2009] is costly and complex to set up. Hence, Hardware-In-the-Loop could be a solution to combine the previous two studies.

1.2 Aim and contribution

The contribution of this work is threefold: First, a Kalman filter is implemented in the APC strategy to reduce the pitch actuations in waves. In regular and irregular waves, the dynamic performance of the propulsion plant is studied. Secondly, we investigate the applicability of HIL experiments to determine whether it is possible to simulate the non-linear behaviour of a propulsion plant. Finally, we discuss whether HIL experiments provide more information than traditional numerical models and towing tank

experiments. This extra information can be used to improve numerical models.

2. Methodology

Two models are used to improve and evaluate the novel adaptive pitch control strategy during dynamic conditions, such as acceleration and in waves. The first model is a validated full-scale free sailing model of an OPV with APC strategy. This model is used to demonstrate the effects of the Kalman filter and deadband on the dynamic performance of the propulsion plant and is illustrated in figure C.1.

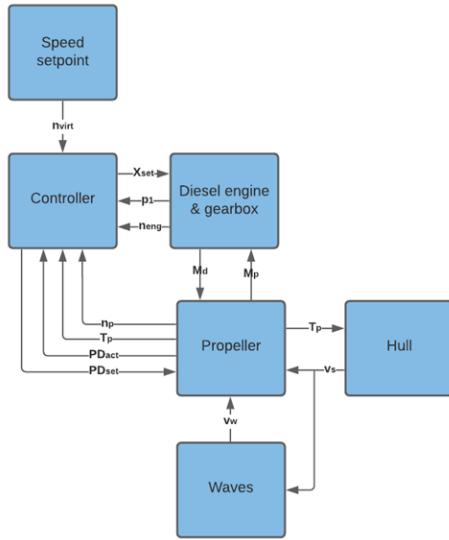


Figure C.1: Full-scale model

The second model represents the propeller open water HIL setup to demonstrate whether it can simulate the dynamic behaviour of a propulsion plant with scaling effects. However, there are more differences besides the scaling effects. First, it is an open water setup, so no hull interaction is present. Secondly, the speed is enforced by the towing car, as can be seen in figure C.2.

A comparison is made between the two models to determine whether the HIL setup can simulate the non-linear dynamic behaviour of a propulsion plant. Similarity between the models is required to demonstrate that it can be used to study dynamic behaviour. The next step is to prepare the actual HIL experiments in the towing tank.

For the preparation of the experiments, the runs are first simulated with the second model. The physical limitations of the setup, such as backlash, the sample rate of the pitch and acceleration speed, gave some interesting insights, and it is concluded that it is not worthwhile to perform experiments at this moment. Nevertheless, it is possible to give recommendations on how to improve the setup and how it can be used to improve numerical models and control

strategies for future research.

3. Full-scale simulations

The full-scale simulations of an OPV are used to demonstrate the effect of improvements of adaptive pitch control. A Kalman filter and deadband are implemented to reduce pitch actuations in regular and irregular waves. The simulations are performed at different sea states.

3.1 Adaptive Pitch Control

The adaptive pitch control strategy sets the pitch and fuel rack; however, these are not fixed. Instead, based on the speed and charge pressure of the engine and the actual pitch and inflow of the propeller, the control actions are determined. Geertsma [2019] assessed the dynamic behaviour of the propulsion plant with predefined Measures of Performance (MOP), these are:

- Provide requested virtual shaft speed.
- Maintain operation within cavitation bucket for the broadest possible operating conditions.
- Minimise fuel consumption across the ship speed profile and for all operating conditions.
- Maintain engine air excess ratio within predefined limits.
- Prevent engine over and under-speed.

This study implements a Kalman filter and a deadband in the APC strategy. This has an influence on the number of pitch actuations and ship speed. Therefore, are these two parameters also taken into account in evaluating the dynamic performance of the control strategy.

The virtual shaft speed is often used on navy frigates because it has almost a linear relationship with the ship speed. In contrast to a combinator curve control strategy, APC requires no fixed rotational speed and pitch of the propeller. As a result, a lower engine speed and higher pitch can result in the same virtual shaft speed has a higher engine speed with a small pitch.

The cavitation bucket represents the operating area of the propeller in which the risk of cavitation is limited in the two-dimensional plane of cavitation number and angle of attack. Vrijdag [2009] demonstrated that if the propeller is operating inside the bucket during acceleration, no cavitation occurs. On the y-axis, the cavitation number is represented:

$$\sigma_n = \frac{p_0 - p_v}{0.5\rho n^2 D^2} \quad (C.1)$$

This is a non-dimensional pressure at mean shaft immersion; the rotational speed of the propeller mainly

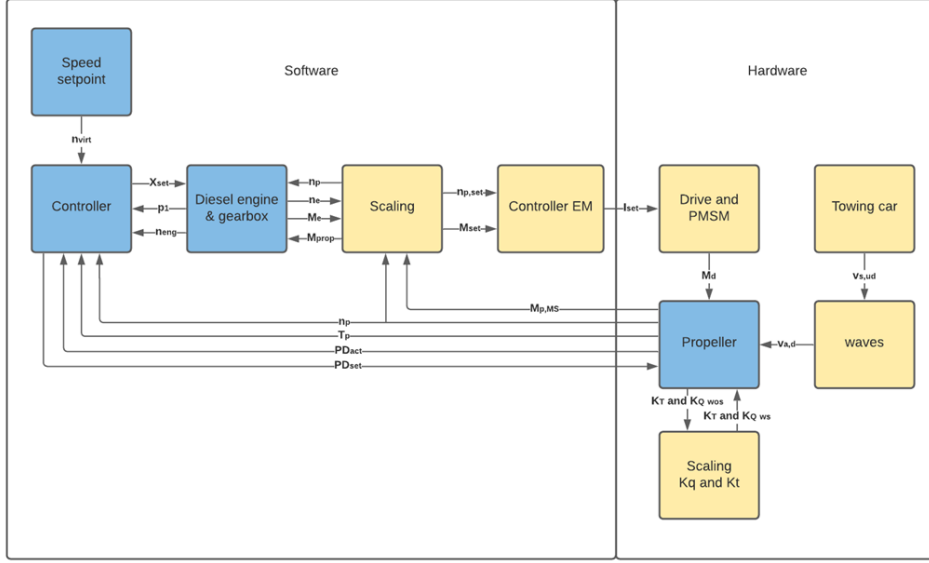


Figure C.2: Open water HIL model

influences this variable. Where p_0 is the atmospheric pressure, p_v is the vapour pressure of the (sea)water, ρ is the density of the (sea)water, n rotational shaft speed and D is the propeller diameter. On the x-axis, the effective angle of attack is given, this is the angle in which the water flows onto the propeller.

3.2 Inflow estimation

It is impossible to measure the inflow of the propeller directly. However, it is possible to determine the inflow with an open water diagram (Pivano et al. [2007], Vrijdag [2009]). The inflow is estimated based on the measured thrust, actual pitch and rotational speed of the propeller. With these parameters, the thrust coefficient is determined with the following equation:

$$K_T = \frac{T}{\rho n_p^2 D_p^4} \quad (C.2)$$

The advance ratio is estimated with the open water diagram with the thrust coefficient and actual pitch known. The first quadrant is implemented in the model so that the inflow can be estimated only in normal forward operation. The hydrodynamic pitch angle is determined with equation C.3. It is required to determine the effective angle off attack with equation C.4. By setting the PD ratio, it is possible to change the angle of attack as can be concluded from equation C.5.

$$\beta = \text{atan}\left(\frac{J}{0.7\pi}\right) \quad (C.3)$$

$$\alpha_{eff} = \theta - \beta - \alpha_i \quad (C.4)$$

$$\alpha_{eff} = \text{atan}\left(\frac{P_{0.7R}}{0.7\pi D}\right) - \text{atan}(c_1 \tan\beta) - \alpha_i \quad (C.5)$$

Where $\frac{P_{0.7R}}{D}$ is the pitch ratio at 0.7 chord length, c_1 is the Vrijdag coefficient that can be used for calibrating the α_{eff} (Vrijdag [2009] pp 116 -120). β is the hydrodynamic pitch angle, also called the inflow angle. α_i the shock free entry angle onto the leading edge of the propeller.

3.3 Kalman Filter

In waves, the measured thrust will constantly fluctuate; as a result, the inflow estimation and required pitch are also changing. Therefore, a Kalman filter is implemented that filters the inflow estimation. It can filter out noise that is Gaussian distributed. It is assumed that regular and irregular waves follow this distribution (Journee and Massie [2001]).

A Kalman filter can estimate the state of a process (\hat{x}_k) with a Kalman gain that performs the filtering (g_k). This is a weight factor that determines whether the one time step older prediction (\hat{x}_{k-1}) or the actual measurement (z_k) is trusted more.

$$\hat{x}_k = \hat{x}_{k-1} + g_k(z_k - \hat{x}_{k-1}) \quad (C.6)$$

A Kalman gain close to one will result in a state close to the measurement, close to zero to the prediction. In this study, the Kalman gain is used to filter out the disturbances due to waves. To achieve this, the Kalman gain needs to be close to zero. The Kalman gain is based on the estimate, measurement and process uncertainties:

$$g_k = p_k(p_k + r)^{-1} \quad (C.7)$$

$$p_k = p_{k-1} + q \quad (C.8)$$

Where p_k is the estimate uncertainty, r the measurement uncertainty and q the process uncertainty.

Tuning these uncertainties is crucial for the dynamic behaviour of the Kalman filter in the APC strategy.

An empirical study of the effects of the uncertainties show that the Kalman filter results in more time outside the cavitation bucket. However, it also reduces actuations. A higher measurement uncertainty results in fewer actuations, however, more operating time outside the bucket. For the process uncertainty, it is vice versa. So a lower process uncertainty results in fewer actuations but more operating time outside the bucket. This relationship is used to determine the correct scaling factors for the Kalman filter and is elaborated in section 4.2.

3.4 Free sailing simulation results

The Kalman filter delays the pitch actuation. As a result, the controller can become slow and needs more time to achieve the desired effective angle of attack. A consequence would be that the propeller is operating more time outside the cavitation bucket. Therefore, it is crucial to tune the Kalman filter so that the pitch does not lag. In the blue line in figure C.3, the pitch actuation without the Kalman filter can be seen. The red line is with the tuned Kalman filter. Notice there is hardly any time delay during the acceleration, the line with Kalman filters follows the line without filter. It can also be seen that the pitch actuations are smaller with the Kalmer filter than APC without the Kalman filter. However, they are still actuations. Therefore, only a Kalman filter is not a solution to reduce the pitch actuations.

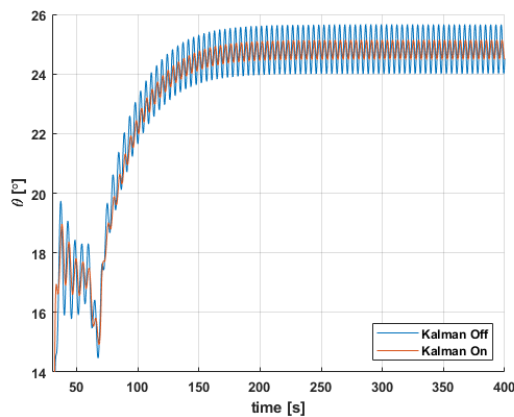


Figure C.3: Pitch actuations with tuned Kalman filter

Not only the pitch actuations are influenced by the Kalman filter. Due to a slower reaction of the pitch setting, the APC strategy sets the engine speed higher to achieve the requested virtual shaft speed. As a result, also the acceleration increases, as can be seen in figure C.4. A positive side effect of adding the Kalman filter to the APC strategy.

A downside of the Kalman filter is illustrated in figure C.5. Even though the Kalman filter is tuned,

it can not be prevented that the propeller is operating more time outside the cavitation bucket. This because the Kalman filter results in a wider operating ellipse. But due to the correct tuning, the operating ellipse moves in a straight line back into the cavitation bucket, and the extra time limited.

Simulations show that the original measures of performance are hardly influenced by the Kalman filter. So the virtual shaft speed is provided, fuel consumption and air excess ratio hardly change. Also, over- and under speed is prevented.

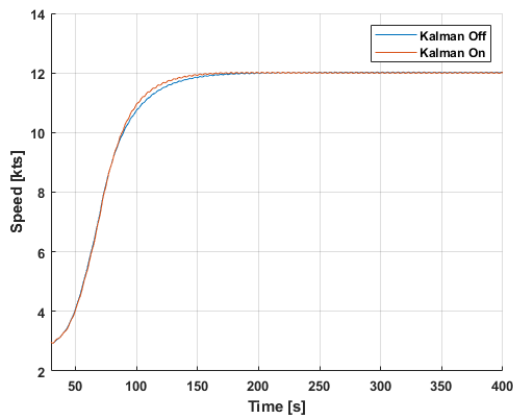


Figure C.4: Ship speed the Kalman filter on and off

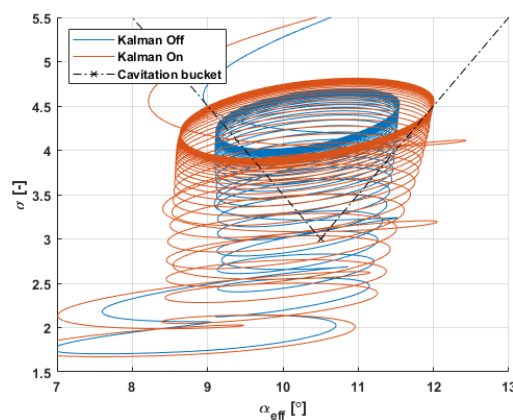


Figure C.5: Cavitation bucket with tuned Kalman filter

3.4.1 Deadband

With the Kalman filter, the size of the pitch changes are decreased. However, the number of actuations at constant speed is the same. For that reason, it is studied if a deadband in the APC controller can reduce the pitch actuation cycles. Simulations show that implementing a deadband moves the operating ellipse to the left flank of the cavitation bucket where pressure side cavitation can occur. Therefore, the desired angle of attack is increased, as can be seen in

equation C.9:

$$\alpha_{eff,deadband} = \alpha_{eff} + \frac{\theta_{deadband}}{4} \quad (C.9)$$

Where $\theta_{deadband}$ is the required deadband in degrees. In figure C.6, it can be seen that the pitch actuations during acceleration is decreased. If the required pitch is reached, the actuations even stop. So, a simple solution with a deadband can solve the actuation problem. However, it is also relevant to study the other parameters, such as cavitation and speed.

Figure C.7 shows the deadband also results in more operating time outside the cavitation bucket. But the operating ellipse is higher in the bucket due to a lower engine speed. The engine speed set lower by the control strategy because the pitch is higher with than without the deadband. This way the requested virtual shaft speed is provided.

A lower engine speed also results in a lower air excess ratio and therefore higher operating temperatures. Nevertheless, these are still within the predefined limits. The other measures of performance are not effected, the virtual shaft speed is provided and the fuel consumption is hardly changed.

The APC with deadband can reduce the pitch actuations at the cost of some suction side cavitation. However, in figure C.8, it can be seen that the end speed is slower due to the deadband. Implementing the deadband is, therefore, not the desired solution.

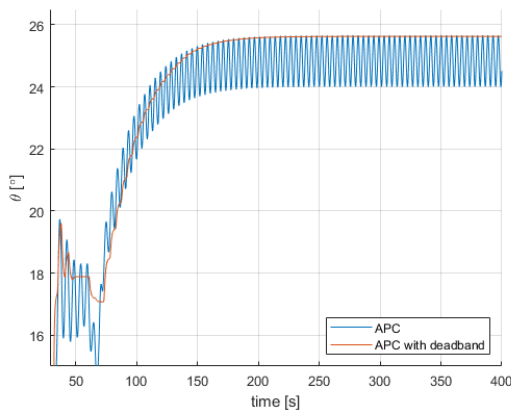


Figure C.6: Pitch actuations with deadband in APC

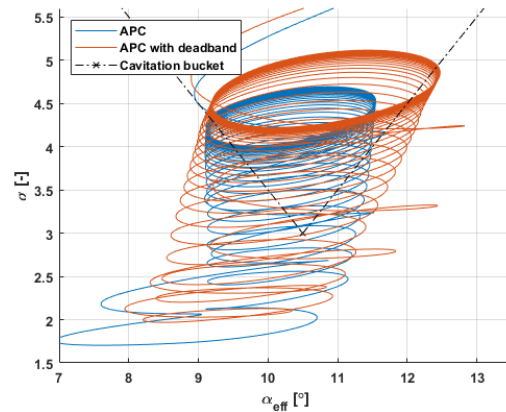


Figure C.7: Cavitation bucket with deadband

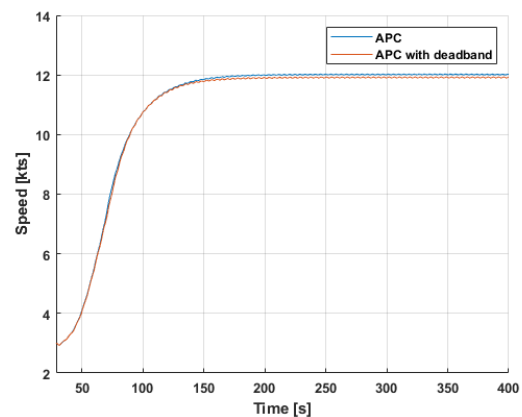


Figure C.8: Ship speed with deadband in APC

3.4.2 Kalman filter and deadband

The Kalman filter increases the speed and reduces the size of the pitch actuations. However, the number of actuations is not reduced. On the other hand, a deadband decreased the speed but was able to reduce the pitch actuations. Therefore, the combination of both methods, the Kalman filter and deadband, are implemented in the APC strategy.

Figure C.9 shows that a properly tuned Kalman filter hardly creates a lag of the pitch setting. The deadband ensures that when the desired pitch setting is achieved that no pitch actuations are performed. However, in the cavitation bucket can be seen that there is more pressure side cavitation and the operating ellipse is wider.

The speed with the Kalman filter was higher and with the deadband lower. Combining the two results in the same speed as the original APC strategy in regular waves, as depicted in figure C.11. The remaining measures of performance for providing virtual shaft speed, fuel consumption, air excess ratio and over- and underspeed are not effected by the combination the Kalman filter and the deadband.

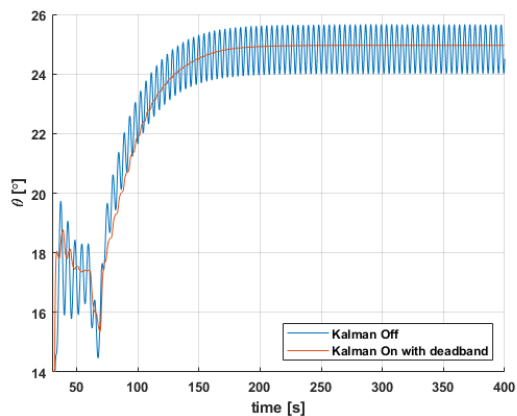


Figure C.9: Pitch with the Kalman filter and deadband

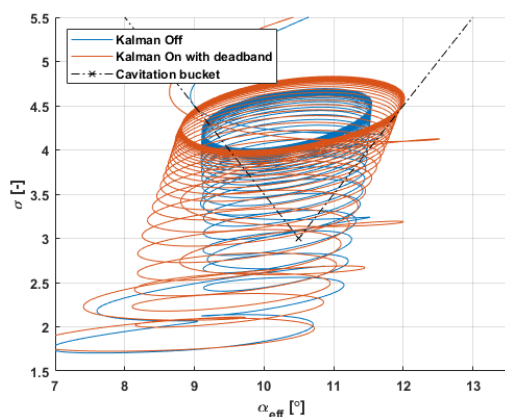


Figure C.10: Cavitation with the Kalman filter and deadband

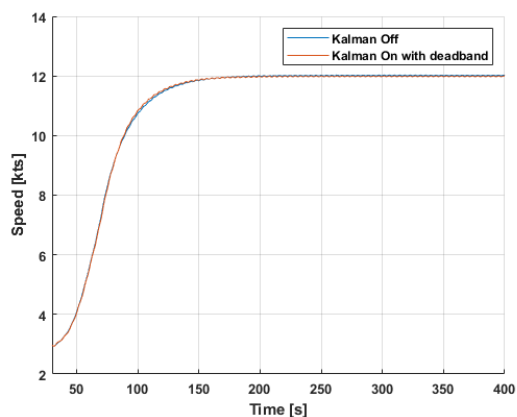


Figure C.11: Ship speed with the Kalman filter and deadband

3.4.3 Irregular waves

The previous simulation results are all performed in regular waves. However, a more realistic wave is a superposition of regular waves, resulting in an irregular wave. In figure C.12, the wave speed at the propeller centre is given in these waves. It can be seen that the ship encounters different wave frequencies and amplitudes.

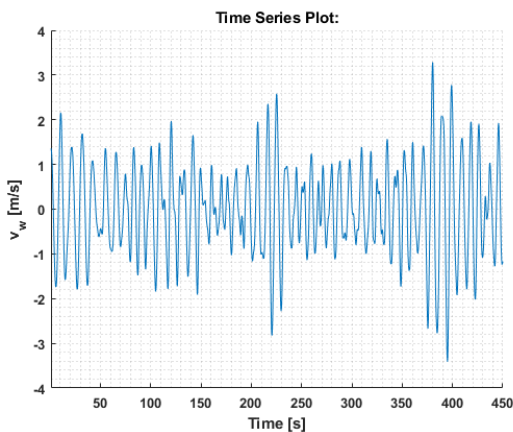


Figure C.12: Wave speed in irregular waves

The acceleration simulation is performed from 0 to 120 virtual shaft speed in sea state five with irregular waves. In figure C.13, the actual pitch is depicted. Note that there are more pitch actuations at a constant speed. These are a result of the higher waves that the ship encounters at these moments.

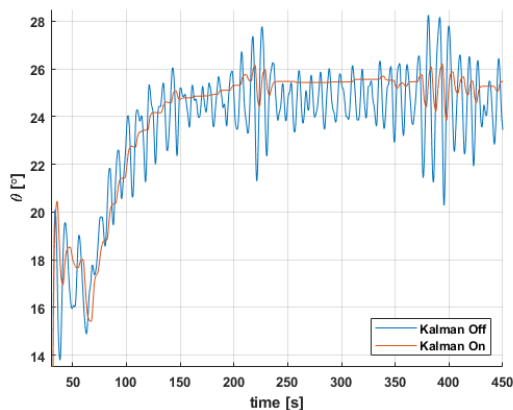


Figure C.13: Pitch in irregular waves with the Kalman filter on and off

The performance of the Kalman filter is sea state depended. Different sea states result in different waves amplitudes and frequencies. In table C.1, the effect on the number of actuations is shown with three sea states. It is concluded that in sea state four and five, the filter with deadband has a significant effect. However, in sea state six the number of actuations hardly decreases.

Table C.1: Number of actuations in irregular waves

Sea state	APC	APC with filter and deadband	Difference [%]
4	108	8	-92.6
5	112	44	-60.7
6	105	87	-17.1

As mentioned before, the Kalman filter and deadband results in more operating time outside the cavitation bucket. In table C.2, the percentage of extra time outside the bucket is listed. It can be seen that the increase is between 20 and 25 per cent for all the sea states.

Table C.2: Seconds out of the cavitation bucket in irregular waves

Sea state	APC [s]	APC with filter and deadband [s]	Difference [%]
4	66.93	84.50	20.8
5	125.04	167.25	25.2
6	228.16	303.30	24.8

It can be concluded that the Kalman filter and deadband can also reduce pitch actuations in irregular waves. However, the control strategy cannot consistently achieve the most effective inflow angle due to the more giant waves encountered in irregular waves. Due to that reason, the propeller starts to cavitate more. Even though the Kalman filter and deadband results in more cavitation, its cavitation behaviour is still significantly better than the standard combinator curve. With this older control strategy, the propeller operates most of the time outside the cavitation bucket.

A limitation of the Kalman filter is that it predicts only one timestep ahead. Model Predictive Control (MPC) can expand this prediction horizon and better predict the incoming disturbances due to waves. However, it can be argued whether MPC can deal with irregular waves. To reduce cavitation, it would be better to measure the incoming waves and use this information as a control input for the APC with Kalman filter and deadband.

4. Open water HIL setup simulation

In the scaled numerical simulation, the open water HIL setup is modelled. It is crucial to apply Froude scaling correctly to compare the full-scale free sailing and propeller open water model simulations. It is assumed that if Froude scaling is applied, forces can directly be scaled between the model and full-scale simulations.

4.1 HIL setup

The TU Delft has a propeller open water HIL setup that can drive a model C4-40 propeller. The setup has the following elements:

- Interface computer
- Simulator
- Motor controller
- Electric Motor

- Thrust and torque sensor
- Controllable pitch propeller
- Towing carriage

The interface computer is used to monitor and control the simulator. A copy of the Simulink model is duplicated on the simulator and runs in real-time. Therefore, it is crucial that the model is able to run in real-time. The MVFP is able to do this and provide the relevant parameters that are required to study the dynamic behaviour of the propulsion plant. The torque that the plant delivers is scaled, and the simulator converts the required torque into a current setpoint. The motor controller ensures that this current goes to the electric motor that drives the shaft. Behind the propeller, a torque and thrust sensor was placed. The thrust measurement is used for the inflow estimation. A servo motor in the hub changes the pitch of the propeller. To control the pitch, a TCP/IP signal is sent to the servo motor over the power cable. A downside to this way of communication is that the number of bites that can be sent per second is limited. Due to this reason the sample rate of the pitch is too low. The effects of this low sample rate is discussed in section 5.

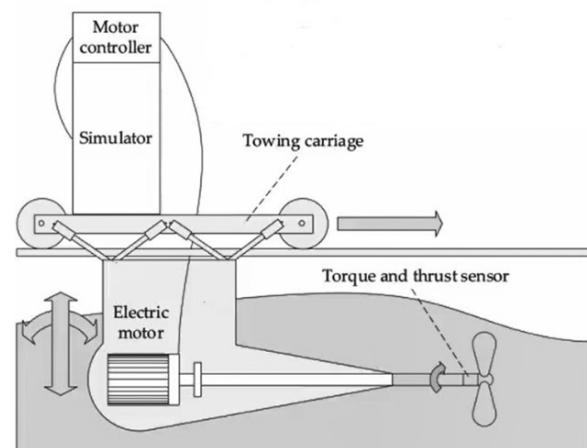


Figure C.14: Open water HIL setup (Huijgens [2021])

4.2 Open water HIL setup simulation results

The following parameters are Froude scaled in the model: Integral gain of the speed governor, time delays for the exhaust receiver, pitch actuation and fuel injection, torque rate limiter, thrust and torque coefficients, and finally, the uncertainty parameters of the Kalman filter. A comparison is made between the full and model scale simulations with constant speed in regular waves to assess if the scaling is applied correctly. The differences in outcomes were minor, 2.6 per cent. Thus, scaling is applied correctly.

The next step is to determine similarity in waves. The waves at full scale and model scale differ in size and frequency due to Froude scaling, as shown in figure C.15. However, if scaling is applied correctly, the dynamic behaviour should be similar in both simulations.

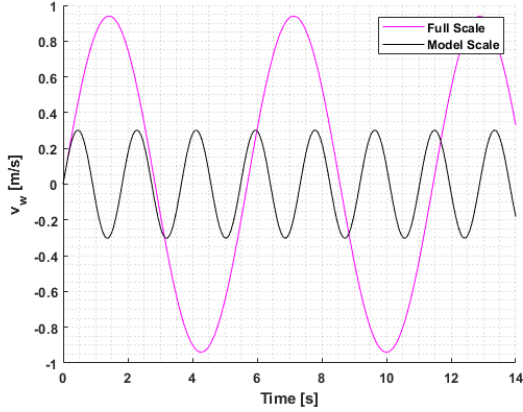


Figure C.15: Wavespeed at full and model scale with Froude similarity

A dynamic response is the virtual shaft speed. In figure C.16, the requested and delivered virtual shaft speed is depicted. Note that the time scale is different in the model scale figures. This is done to be able to compare the results. Froude time scaling is $\lambda^{0.5}$, wherein this model the geometric scale factor (λ) is 9.697 according to equation C.10:

$$\lambda = \frac{D_{FS}}{D_{MS}} \quad (C.10)$$

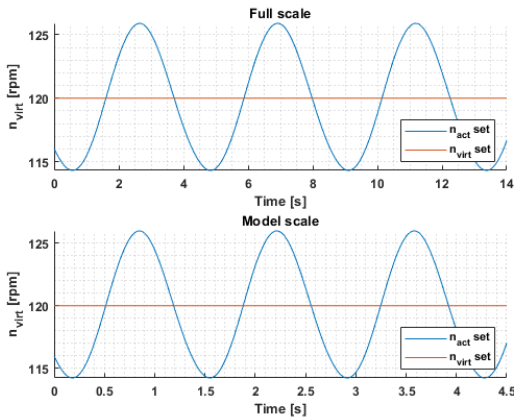


Figure C.16: Virtual shaft speed

In figure C.17, the propeller speed is illustrated. Note that the model scale propeller is rotating faster. Nevertheless, in figure C.18, it can be seen that the engine speed is very similar in waves due to the correctly applied scaling. However, there is a small difference in engine speed. This can be explained by the

difference between a free sailing and open water simulation. In the former, the ship's speed is fluctuation due to waves. In the latter, the towing car realises a constant speed through the water.

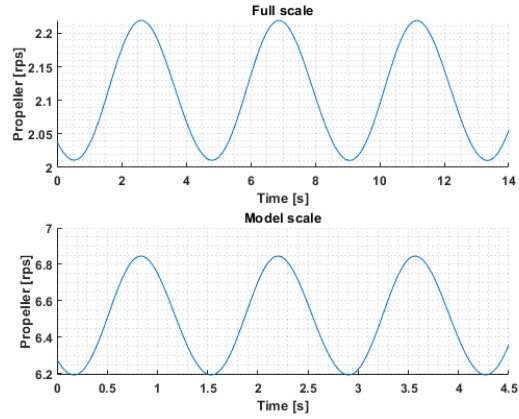


Figure C.17: Propeller speed

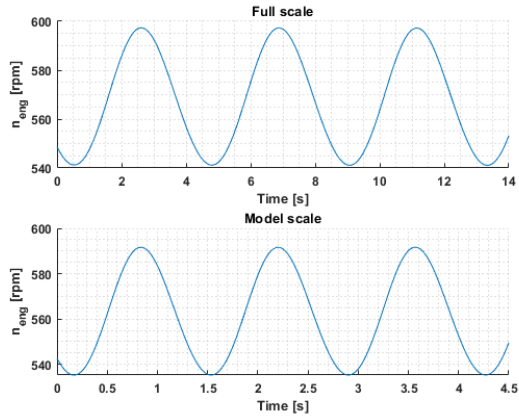


Figure C.18: Engine speed

The focus is mainly on the cavitation bucket and the filtered inflow estimation to determine the effect of reducing pitch actuations in the APC strategy. Therefore, a comparison is made between these two results. In figure C.19, the cavitation bucket is illustrated. The operating ellipses are not entirely overlapping. This is due to the difference in the cavitation number. This variance can be explained by the difference in engine speed that was also shown in figure C.18.

This study aims to determine whether the HIL setup can be used to improve numerical models. In this research, a Kalman filter and deadband are added to the APC strategy. The Kalman uncertainties are scaled. However, the effect of this scaling is unknown. The uncertainties are scaled according to the following equations.

$$q_{MS} = q_{FS} \lambda^{0.5} \quad (C.11)$$

$$r_{MS} = r_{FS} \lambda^{-0.5} \quad (C.12)$$

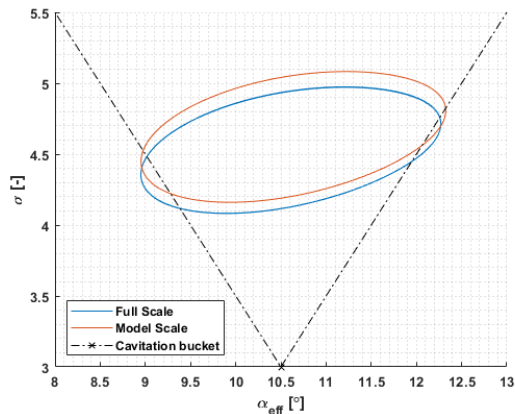


Figure C.19: Cavitation bucket

These scaling effects are chosen after an empirical study performed with these uncertainties. The results showed that if the process uncertainty increases and measurement uncertainty decreases, the Kalman filter becomes faster. A faster filter is required to compensate for the time scaling effects.

In figure C.20, the estimated and filtered inflow due to the Kalman filter is illustrated. The estimated inflow is almost similar, and the effect of the Kalman filter is also very comparable. Thus, the scaling is applied correctly. But more importantly, the HIL setup can show the differences in the control strategies.

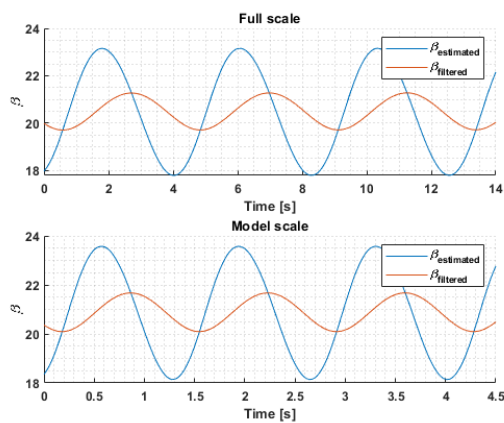


Figure C.20: Inflow with Kalman filter

It can be concluded that the dynamic behaviour in full and model scales are comparable at constant speed. Other control- and engine parameters are shown in table C.3. The differences are minor, which confirms that the HIL setup can be used to determine the dynamic behaviour of a propulsion plant at a constant speed.

Table C.3: Difference in waves between full- and model scale simulations

	Difference
n_{virt} [rpm]	0%
Pitch [deg]	1.8%
α_{eff}	1.0%
Engine speed [rpm]	1.0%
Fuel rack [mm]	2.6%
Air excess ratio [-]	2.5%
Exhaust valve temp [K]	1.2%
bsfc [g/kWh]	0.8%

5. Preparation of HIL experiments

For the preparations of the HIL experiments, the limitations of the hardware are studied. This is relevant because if the components react differently, the dynamic behaviour can be significantly influenced. For example, it is noticed that there is a backlash of five degrees in the blades. The APC strategy with filter and deadband operates within one degree pitch angle, and due to the backlash, the control actions in pitch changes cannot be observed. The second issue is the low sample rate of the pitch. This becomes an issue at higher wave frequencies to simulate lower sea states. In that case, the sample rate is under the Nyquist frequency, and this results in aliasing. The simulations show that this results in an unstable propulsion system. Another limitation is the acceleration of the towing car. It has no Froude similarity with a full-scale free sailing ship. Therefore, it is not possible to perform acceleration runs with the HIL setup.

5.1 Discussion

Due to the earlier mentioned limitations, no HIL experiments are performed. The backlash, sample rate and acceleration challenges should be solved to get reliable results that can be used to improve numerical models. However, more must be done before HIL experiments can be used to improve numerical models. Several studies used a propeller open water HIL setup to study the effects of ventilation (Smogeli [2006], Huijgens [2021]).). Though, it can be argued whether the results can be scaled to full scale. In the model scale, it can be assumed that air is incompressible. However, in full scale, this assumption does not hold (Savio et al. [2013]). Thus, further research must be performed before propeller ventilation can be studied with the HIL setup.

In a standard towing tank, it is impossible to see the effects of cavitation due to the unscaled environmental pressure. However, the setup can be placed inside the new cavitation tunnel of the TU Delft to study the cavitation behaviour combined with the

APC strategy. Nevertheless, the simulation of waves is complex in the cavitation tunnel. An alternative would be to use the setup in the Depressurised Wave Basin of MARIN in the Netherlands. In this towing tank, it is possible to simulate the dynamic behaviour of the entire propulsion plant and observe the cavitation behaviour. Though, a challenge would be to operate the setup wirelessly. This is required to control the setup in the depressurised basin.

Currently, there is a significant difference between the modelled and measured values during a turn, as is concluded by Schulten [2005]. Furthermore, Coraddu et al. [2013] reported that there are relative slow wake speed fluctuations in turns. Therefore, Geertsma [2019] expects that APC can maintain a constant angle of attack during these turns. Placing the propeller under an angle makes it possible to simulate oblique inflow and determine with a HIL experiment if this expectation holds. Oblique inflow is also relevant for ships that have a wind-assisted propulsion system. The results of such experiments can give new insights in improving the numerical models and control strategies. However, the applied angle is limited due to the forces that the strut of the setup will experience when it is moving forward.

However, even if new studies show that the dynamic interaction of propulsion plants during oblique inflow and ventilation can be simulated with HIL, it can be questioned whether it replaces full-scale trials. First, full- and model scale simulation showed that tuning works. However, differences in the sample rate and measurement/noise ratio of actual sensors could lead to inaccurate inflow estimation. Thus, tuning must be performed during a full-scale trial. Secondly, existing propulsion plants have different system delays that can influence the performance of the control strategy. An example of such a delay is the time it takes for the hydraulic system to build up the pressure to actuate the pitch. This can only be tested during full-scale trials.

6. Conclusions and recommendations

The shipping industry is forced to reduce exhaust gas emissions and radiated underwater noise. The latter is extra important for navy ships because they must operate during submarine or mine threats. A method to reduce emissions and noise is by improving the control strategies. Testing new strategies can be done with numerical models. However, these often do not take all the hydrodynamic phenomena into account. These are taken into account in the towing tank, however, with scaling effects. The open water HIL experiments can combine the benefits of both methods. These experiments can be used to determine

the interaction between the propeller hydrodynamics and the mechanical and electrical dynamics of the propulsor.

In this work, several simulations have been performed to determine whether HIL can be used to improve control strategies and numerical models. First, full-scale simulations are performed to determine whether pitch actuation reductions can be realised in the APC strategy. Secondly, models scale simulations are executed. The outcomes between full- and model scale are compared to assess the HIL setup's applicability to investigate propulsion plant dynamics. Finally, the experiments are prepared. However, due to physical constraints, the experiments are not performed. Nevertheless, an assessment is made whether HIL experiments could be used to improve control strategies and numerical models of a ship's propulsion plant.

The conclusions of the full-scale simulation study conclude:

- Adding a Kalman filter and deadband to the APC strategy reduces the pitch actuations during acceleration and constant speed in irregular waves.
- Reducing pitch actuations results in approximately 25 per cent more operating time outside the cavitation bucket. However, the cavitation behaviour is still significantly better than with the traditional combinator curve control strategy.
- The other measures of performance for virtual shaft speed, air excess ratio, fuel consumption and over- and underspeed are not influenced by the Kalman filter in combination with the deadband.

This leads to the following recommendations:

- To increase the time between overhauls, APC should be combined with a Kalman filter and deadband.
- Ships that need to be extra quiet during specific periods, such as navy frigates, should be able to switch off the filter and deadband.

The conclusions of the preparations for HIL experiments with scaled simulations are:

- Due to correctly applying Froude scaling in the propulsion plant model, it is possible to simulate the dynamic behaviour with the open water HIL setup.
- As a result of the backlash in the blades of the scaled CPP and the low sample rate of the pitch, it is impossible to perform useful experiments with novel control strategies that control the inflow.

- Froude unsimilarity in the towing car's acceleration makes it impossible to simulate the dynamic behaviour during an acceleration.

These conclusions lead to the following recommendations concerning the HIL setup:

- The CPP's pitch sample rate must be increased to at least the Nyquist frequency of the waves used in the towing tank. Also, the backlash needs to be reduced to less than one degree. Without solving these technical issues, performing HIL experiments has little added value.
- We recommend investigating applying a variable speed drive with accurate control of acceleration speed on the towing car. This is to accurately control the acceleration of the towing car at Froude similarity.

The conclusions concerning the methodology:

- Full-scale simulations can be used to prove that improvements in the control strategies are effective.
- The propeller's behaviour and the pitch control strategy can be investigated with the HIL setup by performing experiments with oblique inflow. Similarly, the behaviour of propeller and pitch control during propeller ventilation can be investigated. However, for the latter, additional research is required.

Leading to the following recommendations:

- For tuning the control strategy, a full-scale trial is required. In an actual system, the sample rate and noise of the actual thrust sensor are different. Therefore, the tuning parameters require other settings.
- To validate the APC strategy with Kalman filter and deadband, full-scale trials are required. First, the simulations demonstrated that it has the potential to work. However, a demonstration with the open water HIL setup is not possible. Second, extra delays in an existing propulsion system can result in other control strategy performance.

This research proposed to add a Kalman filter and deadband to the APC strategy to reduce pitch actuations. A trade-off is that the propeller cavitates 25 per cent more. However, the other control objectives of the dynamic performance of the propulsion plant are hardly influenced. By correctly implementing scale effects, it is possible to study the dynamic behaviour of the plant with the open water HIL setup. Still, in waves, HIL experiments are expected to provide little extra information compared to numerical models. Nevertheless, oblique inflow can be forced in controlled conditions and give new insights to improve numerical models and control strategies, thus investigating the behaviour in turns. These improvements can lead to emission and noise reduction to decrease the environmental impact and prevent detection of naval vessels under threat.

References

- IMO. Energy efficiency and the reduction of ghg emissions from ships. <http://www.imo.org/en/MediaCentre/HotTopics/GHG/Pages/default.aspx>, July 2020. [Online; accessed 7-October-2020].
- A. Vrijdag. *Control of Propeller Cavitation in Operational Conditions*. PhD thesis, Delft University of Technology, 2009.
- L.J.G. Huijgens. *Hardware in the Loop Emulation of Ship Propulsion Systems at Model Scale*. PhD thesis, Delft University of Technology, 2021.
- P.J.M. Schulten. *The interaction between diesel engines, ship and propellers during manoeuvring*. PhD thesis, Delft University of Technology, 2005.
- R.D. Geertsma. *Autonomous control for adaptive ships: with hybrid propulsion and power generation*. PhD thesis, Delft University of Technology, 2019.
- F.M. White. Potential flow and computational fluid dynamics. In *Fluid Mechanics*, pages 521–600. John Wiley, 2008.
- K. Niklas and H. Pruszko. Full-scale cfd simulations for the determination of ship resistance as a rational, alternative method to towing tank experiments. *Ocean Engineering*, 190:106435, 2019.
- A.M Kozłowska, Ø.Ø. Dalheim, L. Savio, and S. Steen. Time domain modeling of propeller forces due to ventilation in static and dynamic conditions. *Journal of Marine Science and Engineering*, 8, 2020. ISSN 20771312. doi: 10.3390/JMSE8010031.
- J.M.J. Journee and W. Massie. *Introduction in offshore hydromechanics (OT3600)*. 2001.
- T.J.C. van Terwisga, D.J. Noble, R. van't Veer, F. Assenberg, and B. McNeice. Effect of operational conditions on the cavitation inception speed of naval propellers. 2004.
- Calculation of marine propellers*. URL <https://rules.dnvgl.com/docs/pdf/DNVGL/CG/2015-12/DNVGL-CG-0039.pdf>.
- Arthur Vrijdag, D Stapersma, and T Van Terwisga. Control of propeller cavitation in operational conditions. *Journal of Marine Engineering & Technology*, 9(1):15–26, 2010.
- L. Pivano, Ø.N. Smogeli, T.A. Johansen, and T.I. Fossen. Experimental validation of a marine propeller thrust estimation scheme. *Modeling, Identification and Control*, 28:105–112, 2007. ISSN 03327353. doi: 10.4173/mic.2007.4.2.
- Simon D. Levy. The extended kalman filter: An interactive tutorial for non-experts. <https://simondlevy.academic.wlu.edu/kalman-tutorial/>. [Online; accessed 4-August-2021].
- Alex Becker. Kalman filter in one dimension. <https://www.kalmanfilter.net/kalman1d.html>. [Online; accessed 4-August-2021].
- TU Delft, 2019. URL <https://www.tudelft.nl/3me/onderzoek/cohesieprojecten/windturbines-als-inspiratie-voor-de-scheepvaart>. [Online; accessed 15-March-2021].
- T. Schulze, M. Wiedemeier, and H. Schuette. Crank angle-based diesel engine modeling for hardware-in-the-loop applications with in-cylinder pressure sensors. *SAE Transactions*, pages 834–850, 2007.
- F. Xia, S.Y. Lee, J. Andert, A. Kampmeier, T. Scheel, M. Ehrly, R. Tharmakulasingam, Y. Takahashi, and T. Kumagai. Crank-angle resolved real-time engine modelling. *SAE International Journal of Engines*, 11(6):1385–1398, 2018.

- Jasper Grevink. Lecture notes in mt44006 future marine propulsion systems, July 2020.
- M. Godjevac. *Wear and friction in a controllable pitch propeller*. [s.n.], 2009. ISBN 9789088911361.
- ITTC. Free running model tests. In *Recommend Procedures and Guidelines*, 2015.
- K. Tanizawa, Y. Kitagawa, K. Hirata, and M. Fukazawa. Development of an experimental methodology for a self-propulsion test with a marine diesel engine simulator and a controllable pitch propeller. *International Journal of Offshore and Polar Engineering*, 24:142–148, 2014. URL <http://www.isope.org/publications>.
- Y. Kitagawa, O. Bondarenko, Y. Tsukada, T. Fukuda, and K. Tanizawa. An application of the tank test with a model ship for design of ship propulsion plant system. *Marine Engineering*, 53(3):355–361, 2018.
- L. Savio, S.s Spence, K. Koushan, and S. Steen. Full scale and model scale propeller ventilation behind ship. In *Third International Symposium on Marine Propulsors, smp*, volume 13, 2013.
- Marin set to open its new depressurised wave basin. <https://www.marin.nl/publications/marin-set-to-open-its-new-depressurised-wave-basin>, December 2011. [Online; accessed 23-July-2021].
- ITTC. Open water test. In *Recommend Procedures and Guidelines*, 2014a.
- G. Kuiper. The wageningen propeller series. Technical report, Marin, 1992.
- M. Brown, A. Sánchez-Caja, J.G. Adalid, S. Black, M.P. Sobrino, P. Duerr, S. Schroeder, and I. Saisto. Improving propeller efficiency through tip loading. In *30th Symposium on Naval Hydrodynamics, Hobart, Tasmania, Australia*, 2014.
- S. Helma, H. Streckwall, and J. Richter. The effect of propeller scaling methodology on the performance prediction. *Journal of Marine Science and Engineering*, 6(2):60, 2018.
- E.M. Lewandowski. *The dynamics of marine craft: maneuvering and seakeeping*, volume 22. World scientific, 2004.
- R. Wereldsma. Experiments on vibrating propeller models. *International Shipbuilding Progress*, 12(130):227–234, 1965.
- L.C. Burrill and W. Robson. Virtual mass and moment of inertia of propellers (determination of entrained water effects, for use in connexion with torsional and axial vibration calculations). 1962.
- D.M. MacPherson, V.R. Puleo, and M.B. Packard. Estimation of entrained water added mass properties for vibration analysis. *SNAME New England Section*, 2007.
- J. Dang, H.J.J. Van den Boom, and J. Th Ligtelijn. The wageningen c-and d-series propellers. 2013.
- D. Stapersma. *Diesel engines, Volume 1: Performance analysis*. 2010a.
- H.D. Sapra. *Combined gas engine-solid oxide fuel cell systems for marine power generation*. PhD thesis, 2020.
- ITTC. Ittc performance prediction method. In *Recommend Procedures and Guidelines*, 2017.
- Hans J Klein Woud and Douwe Stapersma. Design of propulsion and electric power generations systems. *Published by IMarEST, The Institute of Marine Engineering, Science and Technology*. ISBN: 1-902536-47-9, 2003.
- Sayed Mohsen Vazirizade. *An intelligent integrated method for reliability estimation of offshore structures wave loading applied in time domain*. PhD thesis, The University of Arizona, 2019.
- M Ueno, Y Tsukada, and K Tanizawa. Estimation and prediction of effective inflow velocity to propeller in waves. *Journal of Marine Science and Technology (Japan)*, 18:339–348, 9 2013. ISSN 09484280. doi: 10.1007/s00773-013-0211-8.
- N. Smogeli. *Control of Marine Propellers From Normal to Extreme Conditions*. PhD thesis, 2006.
- A. Coraddu, G. Dubbioso, S. Mauro, and M. Viviani. Analysis of twin screw ships' asymmetric propeller behaviour by means of free running model tests. *Ocean Engineering*, 68:47–64, 2013.

Nomenclature

Abbreviations

APC	Adaptive Pitch Control
bsfc	Brake specific fuel consumption [g/kWh]
CPP	Controllable Pitch Propeller
DWB	Depressurised Wave Basin
EM	Electric Motor
FMPS	Oil distribution unit
MARIN	Maritime Research Institute Netherlands
MOP	Measures of Performance
MPC	Model Predictive Control
MPC	Model Predictive Control
MVFP	Mean Value First Principle
OD unit	Oil distribution unit
OPV	Ocean-going Patrol Vessel
PMSM	Permanent Magnet Synchronous Motor

Greek Symbols

α_i	Shock free entry angle onto the leading edge of the propeller profile [deg]
α_{eff}	Effective angle of attack [deg]
α_{wk}	Angle of the vertical wave moment at the propeller centre [rad]
β	Hydrodynamic pitch angle [rad]
β_j	Shape factor of wave spectrum
ϵ_n	Random phase angle [rad]
η	Efficiency [-]
γ	Peakedness parameter
λ	Air Excess Ratio [-]
λ	Geometric scale factor
ν	Kinematic viscosity [m^2/s]
ω	wave radial frequency [rad/s]
ω_{wv}	Wave frequency [rad/s]

ρ	Density [kg/m^3]
σ_f	Stoichiometric air-fuel ratio [K]
σ_n	Cavitation number [-]
τ_p	Time delay for pitch actuation [s]
τ_X	Time delay for fuel injection [s]
$\tau_{p,d}$	Time delay for filling the exhaust receiver [s]
θ	Pitch angle [rad]
θ_{red}	Pitch angle reduction [rad]
$H_{1/3}$	Significant wave height [m]
k_w	Wave number [$1/m$]
p_0	Atmospheric pressure [Pa]
p_v	Vapour pressure [Pa]
v_w	Relative wake speed [m/s]
z	Centerline of the propeller [m]
z	Height above the propeller shaft [m]

Roman Symbols

$\frac{A_e}{A_0}$	Expanded area ratio
\hat{x}_k	State estimation
a, b, c	Seiliger parameters for isochoric, isobaric and isothermal combustion
c_1	Vrijdag coefficient
c_p	Specific heat at constant pressure [J/KgK]
c_v	Specific heat at constant volume [J/KgK]
$c_{0.7}$	Chord length at 0.7R
D	Diameter [m]
Fr	Froude number [-]
g	standard gravity [m/s^2]
g_k	Kalman gain
h^L	Lower heating value of fuel at ISO conditions [kJ/kg]
I	Moment of inertia [kg/m^2]
i	Current [A]

List of Figures

1.1	Structure master thesis	3
1.2	Schematic representation of combining three studies	4
2.1	Ocean-going patrol vessel	7
2.2	HIL setup [Huijgens [2021]]	7
2.3	Scheme for the MATLAB Simulink model	8
2.4	Scheme Open Water HIL Simulink model	8
2.5	Cavitation bucket	9
2.6	Adaptive pitch control	10
2.7	Inflow estimation	11
2.8	Kalman filter	12
2.9	Open water HIL setup (Huijgens [2021])	13
2.10	Servo motor of hardware CPP	14
3.1	Layout CPP unit [19]	17
3.2	Pitch with Kalman filter off and on	18
3.3	Pitch with Kalman filter off and on zoomed in	18
3.4	Effective angle of attack the Kalman filter on and off	19
3.5	Cavitation bucket with Kalman filter on and off	19
3.6	Virtual shaft speed with the Kalman filter on and off	19
3.7	Engine speed with the Kalman filter on and off	20
3.8	Air excess ratio with Kalman filter on and off	20
3.9	Exhaust valve temperature with and without the Kalman filter	20
3.10	Specific fuel consumption with the Kalman filter on and off	21
3.11	Brake specific fuel consumption in engine envelope [Geertsma [2019]]	21
3.12	Ship speed the Kalman filter on and off	21
3.13	Effect of the process uncertainty on the number of actuations	22
3.14	Effect of the process uncertainty on the seconds out of the bucket during acceleration	22
3.15	Effect of the measurement uncertainty on the number of actuations	23
3.16	Effect of the measurement uncertainty on the seconds out of the bucket during acceleration	23
3.17	Pitch actuations with tuned Kalman filter	23
3.18	Cavitation bucket with tuned Kalman filter	23
3.19	Pitch actuations with deadband in APC	24
3.20	Cavitation bucket with deadband	24
3.21	Air excess ratio with deadband in APC	24
3.22	Exhaust valve temperature with deadband in APC	24
3.23	Engine speed with deadband in APC	25
3.24	Virtual shaft speed with deadband in APC	25
3.25	Specific fuel consumption with deadband in APC	25
3.26	Ship speed with deadband in APC	25
3.27	Pitch with the Kalman filter and deadband	26
3.28	Pitch with the Kalman filter and deadband zoomed in	26
3.29	Cavitation with the Kalman filter and deadband	27
3.30	Air excess ratio with the Kalman filter and deadband	27
3.31	Exhaust valve temperature with the Kalman filter and deadband	27
3.32	Engine speed with the Kalman filter and deadband	27
3.33	Virtual shaft speed with the Kalman filter and deadband	27
3.34	Specific fuel consumption with the Kalman filter and deadband	27
3.35	Ship speed with the Kalman filter and deadband	28

3.36	Virtual shaft speed with gain schedule on and off	29
3.37	Gain scheduling	30
3.38	Engine speed with gain schedule on and off	30
3.39	Ship speed with gain scheduling on and off	30
3.40	Specific fuel consumption with gain schedule on and off	30
3.41	Fuelrack with gain scheduling on and off	30
3.42	Exhaust valve temperature with gain schedule on and off	30
3.43	Wave speed in regular waves	31
3.44	Wave speed in irregular waves	31
3.45	virtual shaft speed in irregular waves with the Kalman filter on and off	32
3.46	Pitch in irregular waves with the Kalman filter on and off	32
3.47	Cavitation bucket in irregular waves with Kalman filter on and off	32
3.48	specific fuel consumption in irregular waves with the Kalman filter on and off	34
3.49	Exhaust valve temperature in irregular waves with the Kalman filter on and off	34
3.50	Air excess ratio in irregular waves with the Kalman filter on and off	34
3.51	Engine speed in irregular waves with the Kalman filter on and off	34
4.1	Wavespeed at full and model scale with Froude similarity	37
4.2	Virtual shaft speed	37
4.3	Propeller speed	37
4.4	Engine speed	37
4.5	Fuelrack	38
4.6	Brake specific fuel consumption	38
4.7	Air excess ratio	38
4.8	Exhaust valve temperature	38
4.9	Cavitation bucket	38
4.10	Inflow with Kalman filter	38
4.11	Ship speed during acceleration at FS and MS	40
4.12	Virtual shaft speed during acceleration at FS and MS	40
4.13	Engine speed during acceleration at FS and MS	40
4.14	Cavitation bucket during acceleration at FS and MS	40
4.15	Virtual shaft speed due to low sample rate	41
4.16	Engine speed due to low sample rate	41
4.17	Pitch due to low sample rate	41
4.18	Pitch due to backlash in hardware CPP	41
4.19	Cavitation bucket due to backlash in hardware CPP	41
A.1	Similarity (above) and dissimilarity (White [2008], p. 317)	50
A.2	Open water diagram with static effect (Huijgens [2021])	51
A.3	Velocity triangle (Vrijdag [2009])	54
A.4	Cavitation bucket	55
A.5	Specific fuel consumption (Geertsma [2019])	55
A.6	Open Water Diagram (Dang et al. [2013])	55
A.7	Representation of the diesel engine model (Geertsma [2019] p 69)	57
A.8	Seiliger process in PV diagram [35 p. 106-107]	58
A.9	Seiliger process in TS diagram [35 p. 106-107]	58
A.10	C4-40 open water diagram with K_T as a function of J plotted.	62
A.11	Optimal P/D ratio	62

List of Tables

1.1	Most relevant literature	2
3.1	Simulation Parameters of APC with Kalman filter	18
3.2	Significant wave height and frequency at different sea-states	22
3.3	Simulation parameters Kalman filter with deadband in regular waves	26
3.4	Actuations in regular waves at different sea states	28
3.5	Seconds out of bucket in regular waves at different sea states	28
3.6	Overview of control strategies on measures of performance	29
3.7	Simulation parameters irregular waves	31
3.8	Number of actuations in irregular waves	33
3.9	Seconds out of the cavitation bucket in irregular waves	33
4.1	Froude scaling	36
4.2	Difference free sailing and open water simulation without waves	36
4.3	Difference in waves between full- and model scale simulations	39
4.4	Simulation parameters for acceleration runs	39
A.1	Dimensionless parameters (White [2008], p. 311)	49
A.2	Scaling factors	51
A.3	Seiliger cycle equations	59
A.4	Intersections K_T as a function of J in open water diagram	62